UNIVERSITI SAINS MALAYSIA

Laporan Akhir Projek Penyelidikan Jangka Pendek

Development of Organic Semiconductor Thin Film

By
Assoc. Prof. Ir. Dr. Cheong Kuan Yew
Assoc. Prof. Chow Wen Shyang
Prof. Yeap Guan Yew

2013

International Conference on Science, Technology & Social Sciences (ICSTSS2012)
http://icstss.phg.my/2012/
email: icstss@pahang.uitm.edu.my

Universiti Teknologi MARA Cawangan Pahang
Lintasan Semarak, 26400 Bandar Tun Razak Jengka, Pahang, Malaysia.
Tel : 09-4602000 Fax : 09-4602455
http://pahang.uitm.edu.my

Date: 1st August 2013
Our reference: ICSTSS 100-UiTMKPH (PJI 9/10/2)

Pi Lin Tan
Universiti Sains Malaysia

Dear Prof./Assoc. Prof./Dr./Mr/Mdm,

APOLOGY FOR THE POSTPONEMENT IN PUBLICATION

The publication of the selected papers from the International Conference of Science, Technology and Social Sciences (ICSTSS 2012) have been postponed due to several issues related to the proposed indexed journal. Nonetheless, for your information, the issues have been resolved and the selected papers will now be included as chapters in book to be published by Springer.

However, for your information, this book will not be indexed in SCOPUS but most libraries in higher education institutions subscribed to Springer electronic databases. Hence, this would allow for a large and diverse audience. We understand the concern that the selected papers will not be published in an indexed journal. As such, we are sending this letter to seek your consent for your paper to be published as a chapter in a book.

On behalf of the organizing committee of the ICSTSS 2012 and Universiti Teknologi MARA Pahang, I would like to offer our apology for the delay in the publication of selected papers. It is hoped that you will agree to publish your paper that was presented at ICSTSS 2012 as a chapter in book to be published by Springer.

Enclosed is the consent for publication form which we would like you to fill and return to us as soon as possible.

Thank you.

Best regards,

Associate Professor Dr. Azhan Hashim @ Ismail
Chairman of ICSTSS 2012

Effects of Synthetic Porphyrin Concentration and Gap Distance between Electrodes on Electrical Properties of Organic Device

Pi Lin Tan[1, a], Guan Yeow Yeap[2,b], Wen Shyang Chow[3,c] and Kuan Yew Cheong[4,d, *]

[1,a; 3,c; 4,d] School of Materials and Mineral Resources Engineering, Universiti Sains Malaysia

[2,b] School of Chemical Sciences, Universiti Sains Malaysia

cheong@eng.usm.my

Keywords: Electrical Properties; Drop Casting; Organic Device; Porphyrin.

Abstract. OFET have attracted industries interest due to its vast variety of applications. Therefore, in this research the effect of various synthetic porphyrins concentration and gap distance towards the electrical properties were studied. Both 2, 3, 7, 8, 12, 13, 17, 18 – Octaethyl - 21H .23H - porphine Cu(II) (Cu-porphyrin) and 2, 3, 7, 8, 12, 13, 17, 18 – Octaethyl - 21H .23H - porphine (porphyrin) were diluted into chloroform with concentration of 0.1 mg/ml, 0.5 mg/ml, 1.0 mg/ml, 5.0 mg/ml and 10.0 mg/ml. These organic thin films were formed through drop casting method. The solution will drop casted on top of aluminum electrodes acting as source and drain. The aluminum source and drain were deposited on top of a glass substrate through thermal evaporation and the gap size of these source and drain were prepared through photolithography. The gap distance between source and drain varied from 150 μm to 700 μm. Surface of the drop casted devices were observed through scanning electron microscope and electrical properties were characterized by using current – voltage test. The present of central metal in porphyrin ring will greatly affect the redox and electron transfer of the porphyrins. Therefore, Cu-porphyrin showed higher electrical properties compare with metal-free porphyrin. Drying time plays an important factor for the arrangement of the organic macromolecule. Longer drying time will let the organic molecule to arrange themselves before the solution dry up. The results showed that Cu-porphyrin with concentration of 0.5 mg/ml has the highest electrical conductivity compared to the other concentrations due to the molecular packing of the organic thin film. Electrode distance did not bring much affect to the electrical properties of the device. Drop casting method has been selected because the amount of material needed for the device fabrication is lesser compare to the device fabricated using spin coating method.

Introduction

Organic semiconducting materials are being extensively studied for the fabrication of the organic semiconductor devices due to its low cost and high flexibility as compare with inorganic-based devices. Organic materials offered several advantages, such as inherent compatibility with plastic substrates, flexibility, and amenability to low-cost and low-temperature processing methods such as melt processing, printing, and solution deposition [1]. Therefore, organic devices would be an alternative to standard micro- and optoelectronic devices, such as diodes, transistors, LEDs, lasers and sensors [2]. Generally, organic semiconductors are classified into acene- and/or thiophene-fused aromatic compounds, oligothiophenes and their co-oligomers, polythiophenes, aromatic bisimides, metal phthalocyanines, fullerenes, and tetrathiafulvalene (TTF) derivatives [3]. In order to achieve good OFET performance organic semiconductor should possess large conjugated π-system, high purity chemical, good film forming properties and good intermolecular electronic overlap.

Porphyrins are one of the famous materials which have been widely used as dye materials and sensor applications. These macromolecules have a stable aromatic system. They tend to be stable and the redox chemistry is reversible under appropriate condition [4]. The core structures of the macromolecules have 11 π-bonds. Porphyrin materials outfit as one of the best candidates for organic transistor due to its strong π-π stacking and strong metal ligand coordination for the metalloporphyrin [5, 6]. Therefore, metal-free and metalloporphyrins have been selected for the fabrication of the organic devices. The effect on various solution concentrations and gap distance in between two electrodes towards the electrical properties of both porphyrins devices were study. There are various techniques used to deposit organic semiconductor on substrate in OFET. In this research work, drop-casting technique was used due to its economical, simplicity, and ease for up-scaling. This technique is also suitable for low solubility polymers. Drop casting technique which is a relatively slow drying process, able to reduce the materials consumption because the entire solution droplet evaporates to the final polymer film.

Experimental

All reagents used in this research were analytical grade. Both 2, 3, 7, 8, 12, 13, 17, 18 – Octaethyl - 21H .23H - porphine Cu(II) (Cu-porphyrin) and 2, 3, 7, 8, 12, 13, 17, 18 – Octaethyl - 21H .23H - porphine (porphyrin) were diluted in chloroform with concentration of 0.1 mg/ml, 0.5 mg/ml, 1.0 mg/ml, 5.0 mg/ml and 10.0 mg/ml. An aluminum source and drain with the thickness of 100 nm were deposited on top of the cleaned glass substrate through thermal evaporation and the gap distance of these metal electrodes were prepared through photolithography. Then, the porphyrin solutions were drop-casted on top of the aluminum electrodes, forming a layer of organic thin film. Gap distance of the aluminum source and drain were measured using optical microscope (OM). Scanning electron microscope (SEM) was used to analyze the surface morphology of the organic thin film. Finally, electrical properties of these organic devices were characterized using current-voltage (I-V) test.

Results and Discussions

Electrical Properties

Fig. 1 shows I-V test results on different concentration of Cu-porphyrin and porphyrin with gap distance of 630 μm and 160 μm respectively. Both solutions with the concentration of 0.5 mg/ml gave the highest current value at the voltage of 5V. However, the current values of porphyrin devices are much lower compared with the Cu-porphyrin devices.

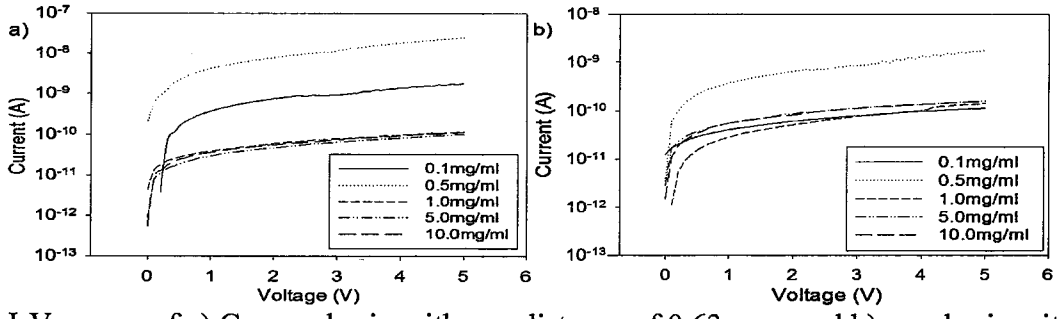

Fig.1 I-V curves of a) Cu-porphyrin with gap distance of 0.63 mm, and b) porphyrin with the gap size of 0.16 mm.

Fig.2 revealed the overall electrical results of Cu-porphyrin and porphyrin devices drop casted using 0.5 mg/ml solution with varying gap distances. The gap distance between source

and drain varied from 160 μm to 700 μm. The results proved that Cu-porphyrin with gap distance of 630 μm and porphyrin with gap distance of 160 μm, show the highest current value at 5V as to compare with the rest of the gap distances. Cu-porphyrin devices with larger gap distance (Fig.2a) showed a better electrical result. However, the current values of the electrical result for gap distance 0.16mm until 0.56mm are close compared to the electrical value for gap distance 0.63mm and 0.70mm. Drop casting method is not easy to fabricate a uniform thin film. Therefore, this incident happened. Fig. 2b with the 0.5 mg/ml porphyrin devices shows the devices with 0.16mm gap distance have much higher current value. The current value rest of the devices with different gap distance, from 0.25mm until 0.70mm remain almost the same. This also might due to the non-uniformity of the organic thin film. This proves that the gap distance of the device does not affect much towards the electrical properties of the device.

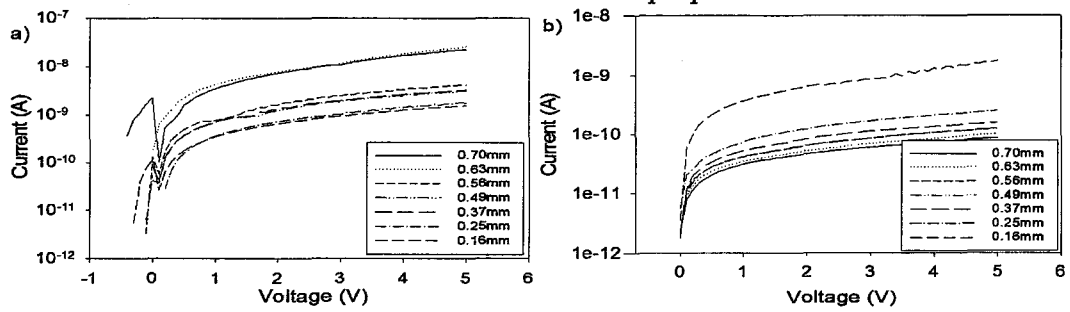

Fig. 2 I-V curves of a) 0.5 mg/ml Cu-porphyrin, and b) 0.5 mg/ml porphyrin

The current value for both Cu-porphyrin and porphyrin devices with the fixed gap distance of 630 μm and 160 μm respectively at the operating voltage of 5V are summarized at Table 1. From the table, the devices casted with Cu-porphyrin have higher conductivity compare to the devices casted with the solution of porphyrin. The current value drop as the drop casting solution concentration increase to above 0.5 mg/ml and the current value for both solutions remain almost the same as the drop casted solution with the concentration of 1.0 mg/ml to 10.0 mg/ml. This is caused by the arrangement of the organic molecules which have sufficient time to rearrange themselves accordingly and form as organic thin film with high degree of crsytallinity before the solution drying up [7].

Table 1 Current value of Cu-porphyrin and porphyrin at varying concentration with the specific gap distances and operating voltage of 5V.

Concentration (mg/ml) / Sample	0.1	0.5	1.0	5.0	10.0
	Current Value, I (A)				
Cu-porphyrin ***Gap distance = 630 μm**	$1.82\text{x}10^{-09}$	$2.53\text{x}10^{-08}$	$1.17\text{x}10^{-10}$	$1.01\text{x}10^{-10}$	$1.15\text{x}10^{-10}$
Porphyrin ***Gap distance = 160 μm**	$8.66\text{x}10^{-11}$	$1.75\text{x}10^{-9}$	$1.39\text{x}10^{-10}$	$1.55\text{x}10^{-10}$	$1.56\text{x}10^{-10}$

Fig.3 showing the bar charts of I-V test results for both porphyrin with varying organic concentration and gap distance at the voltage of 5V. As refer to Fig. 3a, Cu-porphyrin with the concentration of 0.1 and 0.5 mg/ml give a more significant value of current compared to the others concentration. The reason is the Cu-porphyrin has good intermolecule interaction where contact resistance was found higher with thicker film [8]. As a result, the current value decreased. However, the uppermost current value falls at the concentration of 0.5 mg/ml with the gap distance of 630 μm. Cu-porphyrin devices which casted with concentration of 0.1 mg/ml produced results which explained the effect of gap distance and current value at the early

stage. This proved that the larger the gap distance between source and drain, the higher the current value. However, the current values of the devices drop when the gap distance value greater than 490 μm. Based on research done by Gupta and Hong [9] using pentacene, the mobility drop when the thickness of the pentacene layer was above 35nm. Furthermore, Cu-porphyrin devices drop casted with the concentration of 0.5 mg/ml having constantly increasing current value with increasing gap distance up to 630 μm. The Cu-porphyrin devices with the concentration above 1.0 mg/ml shows low current value as compare to 0.1 mg/ml and 0.5 mg/ml. At low solution concentration, these macromolecules able arrange accordingly more freely and form a better crystallinity thin film. As portrayed in Fig. 3b, the highest current value is obtained for porphyrin devices drop casted with concentration of 0.5 mg/ml with the gap distance of 160 μm. In addition, porphyrin devices also contribute to the high current value when the devices are drop casted with the concentration of 5.0 mg/ml. As a comparison for both of these porphyrin drop casted devices, Cu-porphyrin devices exhibit a higher current value as compare to metal-free porphyrin, due to the metal-to-ligand charge transfer [10]. By referring to Fig.3, the gap distance does not contribute much effect towards the electrical properties of the organic devices, however, the concentration of the solutions play a major role to the electrical properties of the devices due to the crystal formation of the organic thin film. The reason is the lower the solution concentration, the longer the drying time and the organic molecules will have enough time to arrange themselves to form a better crystal thin film.

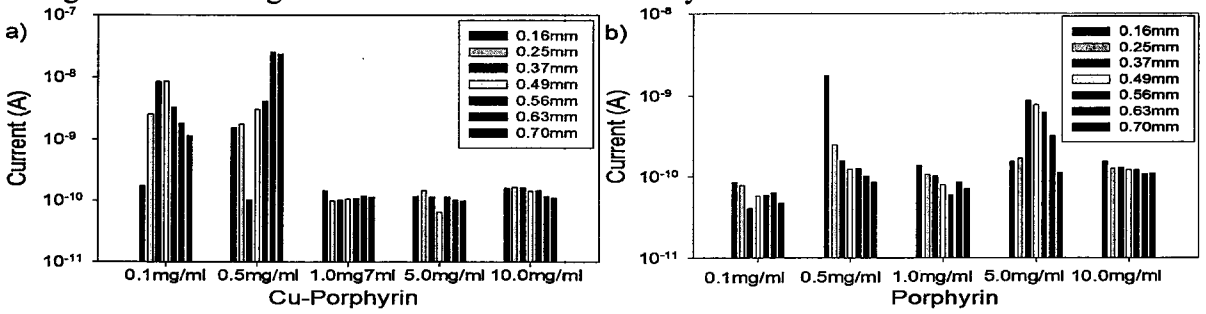

Fig. 3 Bar chart showing the I-V results for different concentration of a) Cu-Porphyrin and b) Porphyrin solution at 5 V.

Surface Morphology Using SEM

With refer to SEM image in Fig.4, the circular shape constituents are the Cu-porphyrin. The amount of the constituents increased proportionally with the concentration of the Cu-porphyrin thin film. The higher the concentration of the organic solution, the amount of constituents seen is more. From Fig. 4a, it shows that Cu-porphyrin is well coated on the surface of the glass substrate. Through observation using SEM, there are very few small rings shape constituents present, which identified as the crystal Cu-porphyrin, which formed during drop casting process. At low concentration, the droplet of the drop casting solution will have longer time to dry up as compare to the solution with higher concentration. This will further allow the organic materials to arrange themselves and form into a better quality of crystalline thin film [1, 11]. As the concentration increased from 0.1 mg/ml to 0.5 mg/ml, Fig. 4b shows that the amount of small crystal ring formation present on top of the glass substrate is a lot more and well dispersed compare with the crystal ring formation as shown in Fig. 4a. Therefore, Cu-porphyrin thin film form through 0.5 mg/ml solution concentration does show better electrical properties as compare to Cu-porphyrin thin film form through 0.1 mg/ml solution concentration. With refer to Fig. 4c, the flakes growing bigger as compare to the flakes show in Fig. 4b. The number of flakes reduces as the concentration of the drop casted solution increase to 1.0 mg/ml. This condition is more obvious when the drop casted solution concentration increase to 5.0 mg/ml

where the number of flakes present is lessen (Fig. 4c). Meanwhile, there are crystals which present in rod shape as concentration of the drop casting Cu-porphyrin solution increased. This happened due to many possible reasons such as strong electrostatic forces between the porphyrins molecules, hydrogen bonding, van der Waals, axial coordination, and other weak intermolecular interactions [12]. Fig.4a shows the current value of the organic device started to drop when the device are drop-casted at concentration higher than 0.5 mg/ml. This important finding proves that the performance of the device reduced due to poor thin film formation [13]. This indicates that the Cu-porphyrin have stronger interaction between molecules itself.

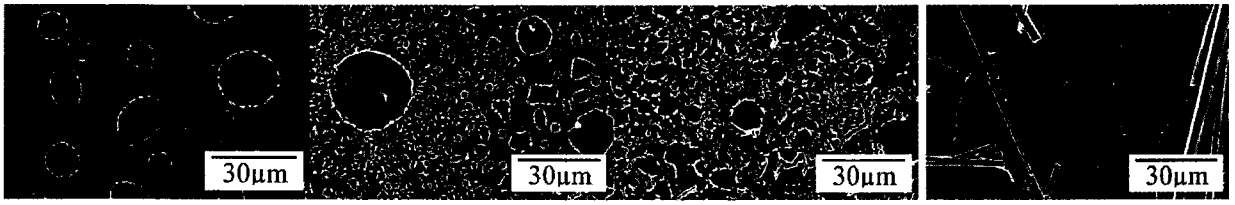

Fig.4 SEM image shows Cu- porphyrin with the concentration of a) 0.1 mg/ml; b) 0.5 mg/ml; c) 1.0 mg/ml and d) 5.0 mg/ml was dropped casted on top of a glass substrate.

Porphyrin has strong conjugated π-system which may cause this macromolecule to aggregate [14]. Fig. 5 indicates that the formation of these flakes become larger as the concentration of the drop casted solution increases. As the comparison between Fig. 5c and Fig. 4c, porphyrin tends to form a larger piece of crystal as compare with Cu-porphyrin. Therefore, it reveals that porphyrin conductivity keep on increasing as the concentration of the drop casted solution increase until reaching 5.0 mg/ml. However, Cu-porphyrin conductivity decreases as the drop casted solution increase to above 0.5 mg/ml. Cu-porphyrin devices have higher conductivity as a result of the present of copper atom at the centre of the porphyrin core structure. In order for these organic materials to have higher electrical conductivity, it must have better crystal packing and better alignment [15].

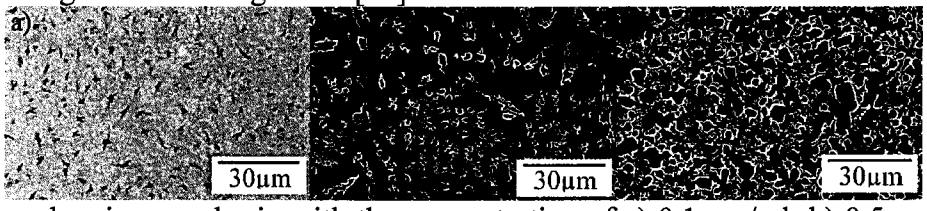

Fig.5 SEM image showing porphyrin with the concentration of a) 0.1 mg/ml; b) 0.5 mg/ml and c) 1.0 mg/ml was dropped casted on top of a glass substrate.

Conclusions

The effects of Cu in porphyrin thin film, concentration of the organic materials on surface morphology and leakage current have been studied. Cu-porphyrin and porphyrin at concentration of 0.5 mg/ml showed the highest current value at 5 V with gap distance of 630 μm and 160 μm, respectively. Current value for both Cu-porphyrin and porphyrin were 2.53×10^{-8} A and 1.75×10^{-9} A, correspondingly. Cu-porphyrin is a better choice to be used as the organic thin film because it enhanced the electrical properties of the device as compare to metal free porphyrin. The reason is Cu-poprhyrin thin film drop casted with low solution concentration is able to form a better crystal thin film due to the strong metal-ligand interaction in between the organic molecule and the metalloporphyrin will normally have better charge transfer as compare with metal-free porphyrin crystal formation of the Cu-porphyrin thin film.

References

[1] Kymissis, I, Organic Field Effect Transistors Theory, Fabrication and Characterization: Chapter 1, page 1, springer-New York City, 2008.

[2] Checcoli, P., Contea, G., Salvatori, S., Paolesse, R., Bolognesi, A., Berliocchi, M., Brunetti, F., D'Amico, A., Di Carlo, A., Lugli, P., Tetra-phenyl porphyrin based thin film transistors, Synthetic Metals 138, (2003), 261–266.

[3] Gao, X., Qiu, W., Liu, Y., Yu, G., Zhu, D., Organic field-effect transistors based on tetrathiafulvalene derivatives, Pure Appl. Chem., 80, 11, (2008), 2405–2423.

[4] Jurow, M., Schuckman, A.E., Batteas, J.D., Drain, C.M., Review: Porphyrins as molecular electronic components of functional devices, Coordination Chemistry Reviews, 254, 19–20, (2010), 2297–2310.

[5] Wang, X., Wen, Y., Luo, H., Yu, G., Li, X., Liu, Y., Wang, H., Donor-acceptor copolymer based on dioctylporphyrin: Synthesis and application in organic field-effect transistors, Polymer, 53, 9, (2012), 1864-1869.

[6] Zhang, Y., Cai, X., Bian, Y., Jiang, J., Organic Semiconductor of Phthalocyanine Compounds for Field Effect Transistors (FETs) in Structure and Bonding: Functional Phythalocyanine Molecular Materials, Springer-Verlag Berlin Heidelberg, 2010.

[7] Mittal, P., Kumar, B., Negi, Y.S., Kaushik, B.K., Singh, R.K., Channel length variation effect on performance parameters of organic field effect transistors, Microelectronics Journal, (August 2012), doi:10.1016/j.mejo.2012.07.016 Key: citeulike:11060691.

[8] Boudinet, D., Benwadih, M., Altazin, S., Gwoziecki, R., Verilhac, J.M, Coppard, R., Le Blevennec, G., Chartier, I., Horowitz, G., Influence of the semi-conductor layer thickness on electrical performance of staggered n- and p-channel organic thin-film transistors, Organic Electronics 11 (2010) 291–298.

[9] Gupta,D., and Hong, Y., Understanding the effect of semiconductor thickness on device characteristics in organic thin film transistors by way of two-dimensional simulations, Organic Electronics 11 (2010) 127–136.

[10] Maldotti, A., Amadelli, R., Bartocci, C., Carassiti, V., Polo, E., Varani, G., Photochemistry of Iron-porphyrin complexes. Biomimetics and catalysis, Coordination Chemistry Reviews, 125, 1–2, (1993), 143-154.

[11] Miyamoto, R., Yamauchi, S., Kobayashi, N., Osal, T., Ohba, Y., Iwaizumi, M., Interplanar interactions in the triplet dimers of Zn and metal free complexes of crowned porphyrin and phthalocyanine studied by time-resolved electron paramagnetic resonance, Coordination Chemistry ,Reviews, 132, (1994), 57-62.

[12] Lee, J.H., Lee, S.J., Microscopic crystalline rods from the self-assembly of mixed porphyrin building blocks, Inorganic Chemistry Communications, 14, (2011), 1014–1017.

[13] Amato, M.E., Licciardello, A., Torrisi, V., Ugo, L., Venditti, I., Russo, M.V., Nanostructured morphologies of complexes containing porphyrin bridges between Pt(II) acetylide tethers, Materials Science and Engineering C, 29, (2009), 1010–1017

[14] Gburek, B., Wagner, V., Influence of the semiconductor thickness on the charge carrier mobility in P3HT organic field-effect transistors in top-gate architecture on flexible substrates, Organic Electronics, 11, 5, (May 2010), 814–819.

[15] Ma, P., Chen, Y., Cai, X., Wang, H., Zhang, Y., Gao, Y., Jiang, J., Organic field effect transistors based on 5,10,15,20-tetrakis (4-pentyloxyphenyl) porphyrin single crystal, Synthetic Metals, 160, (2010), 510–515.

Subject: ECS Journals: MS #JSS-13-1909R1 Decision Letter

From: jennifer.bardwell@nrc.ca (jennifer.bardwell@nrc.ca)

To: cheong@eng.usm.my;

Cc: ckuanyew@yahoo.com;

Date: Tuesday, August 6, 2013 1:52 AM

Dear Dr. Cheong,

I am pleased to inform you that, based on our analysis and the reviewers' comments, your manuscript, referenced below, has been accepted for publication in Electronic Materials and Processing (SSS&T) section of the ECS Journal of Solid State Science and Technology.

"N-type Organic Field-effect Transistor Based on Fullerene with Natural Aloe Vera/SiO2 Nanoparticles as Gate Dielectric"

At the start of production, you will receive an e-mail message that will state in which issue your paper is expected to appear and will detail the production process. Your paper will be lightly copyedited and checked for conformity with ECS style.

When your page proofs are ready for your review, you will receive an e-mail message with instructions for downloading your page proofs. You will have only two business days to review the proofs and respond with any required corrections before the paper is finalized for publication.

ECS has recently eliminated page charges. Authors and their institutions are no longer expected to help meet publication costs through payment of page charges.

You can direct all forms and any questions pertaining to papers in the production process to: Andrea Guenzel, Journals Production Assistant, ECS, 65 South Main Street, Pennington, NJ 08534-2896. Phone (609) 737-1902 X109; Fax: (609) 730-0629; E-mail: andrea.guenzel@electrochem.org.

Thank you for your contribution to the Journal. If you have any questions, feel free to contact us at publications@electrochem.org.

Sincerely,

Jennifer A. Bardwell
Technical Editor
The Electrochemical Society Journals

2162-8769/2013/2(11)/P1/5/$31.00 © The Electrochemical Society

N-Type Organic Field-Effect Transistor Based on Fullerene with Natural Aloe Vera/SiO_2 Nanoparticles as Gate Dielectric

Li Qian Khor and Kuan Yew Cheong[z]

Electronic Materials Research Group, School of Materials and Minerals Resources Engineering, Universiti Sains Malaysia, Engineering Campus, Nibong Tebal, Penang 14300, Malaysia

This study reports on fullerene-based organic field-effect transistor (C_{60}-based OFET) with a combination of solution-processable natural Aloe vera blended with 1.5 wt% of SiO_2 nanoparticles as a natural gate dielectric. The natural gate dielectric is screen-printed on a glass substrate followed by thermally evaporation of a layer of C_{60} semiconductor to form a bottom-gate and top-contact OFET structure. Surface energy concept has been used to justify selection of the gate dielectric and semiconductor layers. The OFET operates under open air and exhibits an effective mobility and threshold voltage of 1.110 cm^2/V s and 0 V, respectively. After two weeks exposure in air, the parameters reduce but on/off current ratio and sub-threshold swing improve significantly.

Manuscript submitted June 21, 2013; revised manuscript received August 5, 2013. Published 00 0, 2013.

Organic field-effect transistors (OFETs) have attracted attention due to their ease of solution-processable at low temperature and low cost.[1–5] With these advantages, OFETs play an important role in applications such as electronic bar codes or active matrix elements for displays with minimum required mobility of 0.1 to 0.5 cm^2/V s[6–8] and gate voltage in the range of 20 to 80 V, which is higher than the threshold voltage of an OFET.[9] Threshold voltage reflects the minimum gate voltage applied to make the charge to be mobile in an OFET[10] and threshold voltage close to zero is generally preferable since large gate voltage is not required to switch on the device.[6] Besides the advantages mentioned above, organic electronics research began to investigate on natural materials due to their biodegradable, biocompatible and environmentally friendly properties. Various natural materials are being investigated and introduced as substrate, dielectric and semiconductor in organic electronic devices.[11] The natural materials which have been introduced as substrate are caramelized sugar, leather, silk,[12] hard gelatin, Ecoflex,[13] paper,[14,15] poly(lactide-co-glycolide) (PLGA),[16] nanocellulose paper,[17] and shellac.[18] Besides, nucleobases,[12] sugar, deoxyribonucleic (DNA),[18,19] natural silk fibroin,[20,21] and chicken albumen[19] are reported as dielectrics. While the vast majority of natural materials are substrate or dielectric, there are a few examples of natural semiconductors have been employed in organic electronics, such as carotenoids,[11,12] chlorophyll, hemin, phenazine, terpenoid molecules, indanthrene yellow G, indanthrene brilliant orange RF,[12] melanin,[19,22] indigo,[19] and tyrian purple.[23] As summary those natural materials have been reported to be useful in organic electronics.[11]

Recently, benchmark of n-type OFET is based on fullerenes (C_{60}) acting as an active semiconducting layer with the highest reported mobility up to 6 cm^2/V s.[24] The gate voltage and threshold voltage of the n-type OFETs are affected by the properties of semiconductor and dielectric layers which are depending on the choice of material, deposition technique, condition and treatment, electrodes (gate, source, and drain) material, interface between electrodes and semiconductor or dielectric layers.[10,25,26] In addition, mobility of the n-type OFETs is strongly depends on the gate dielectric material,[27] deposition methods of semiconductor and dielectric layers,[7] and interface between semiconductor and dielectric layers.[27]

n-type OFET based on C_{60} usually coupled with conventional synthetic dielectric materials, namely, benzocyclobutenes (BCB),[28] aluminum oxide/BCB (Al_2O_3/BCB),[29] parylene-C,[30] tantalum pentoxide (Ta_2O_5),[31] Al_2O_3,[32] polyvinyltoluene (PVT),[33] silicon dioxide/zirconium-silicon oxide/silicon dioxide (SiO_2/ZSO/SiO_2),[34] SiO_2/poly(methyl methacrylate) (PMMA),[35] polyimide,[36] and SiO_2.[37]

The reported mobility values of those OFETs are in the range of 6.6 × 10^{-7} to 6.0 cm^2/V s. The synthetic dielectrics mentioned above are deposited by spin coating with post thermal cured,[28] atomic layer deposition with post thermal cured,[29] vapor evaporation,[30] thermal growth,[38,39] and thermal evaporation[40] techniques. While C_{60} is deposited on those synthetic dielectric layer using hot wall epitaxy (HWE),[28] vacuum vapor deposition,[34,36] molecular beam deposition,[31] thermally evaporation,[30] drop casting,[40] and spin coating[42] techniques. Although hot wall epitaxy deposited C_{60} on BCB synthetic dielectric reveals the highest mobility (6.0 cm^2/V s), the technique employed to produce the BCB and C_{60} layer is suffering some disadvantages. The BCB layer on ITO/glass substrate is required to post-process at relatively high annealing temperature (250°C for at least 30 min with Ar gas or for 2 h in vacuum oven) and BCB has to heat to 250 or 300°C during deposition of C_{60}.[43] These processing conditions of BCB and C_{60} are strongly influencing mobility of the OFET.[44–46] Therefore, dielectric materials that are solution-processable at low temperatures must be developed in order to replace the conventional synthetic dielectric materials that need high deposition and/or post-deposition processing temperature.[47,48] Thus, there is a growing interest in developing an n-type OFET based on C_{60} with natural dielectric because of its low cost, solution deposition and low temperature process. Chang et al.[49] developed an OFET with chicken albumen as the natural dielectric that cured at 80 to 140 °C and deposited by spin coating technique with mobility of 0.13 cm^2/V s. As an alternative, commercially produced Aloe vera has also been investigated as a natural dielectric material for electronic application.[50] In that particular study, current-voltage characteristic and structural property of the dielectric layer has been reported but not the OFET characteristics. Referring to the encouraging results in Refs. 50 and 51, in this study, naturally extracted and lab-processed Aloe vera has being used as the gate dielectric of an n-type C_{60} OFET that is screen-printed on a glass substrate. In order to improve on the dielectric property and compatibility with C_{60} layer, silicon dioxide nanoparticles (SiO_2 NPs) has been incorporated in the natural Aloe vera layer. The characteristics of this combination either as a stand-alone dielectric or as an incorporated layer in an OFET have yet been reported. Therefore, in this study, the OFET characteristics of this combination have been reported using a test structure that has been produced via a simple and low processing temperature method.

Experimental

Bottom-gate and top-contact OFET was fabricated on a glass substrate. Mixture of extracted natural Aloe vera paste (20 g) from fresh leaves with 1.5 wt% of SiO_2 NPs, acquired commercially from Sigma Aldrich,[51] have been used as dielectric material. Glass substrates with 1 × 1-cm^2 area was cleaned using ethanol and de-ionized water in an ultrasonic bath and dried in an oven at 100 °C for an hour. Then, a 100-nm thick aluminum layer acting as gate electrode was evaporated (AUTO 306) on the glass substrate. The extracted natural Aloe vera with 1.5 wt% SiO_2 NPs, acting as the gate dielectric, was then screen printed on top of the aluminum. The screen printing mask was used so that the thickness of the printed dielectric layer can be uniform.

[z]E-mail: cheong@eng.usm.my

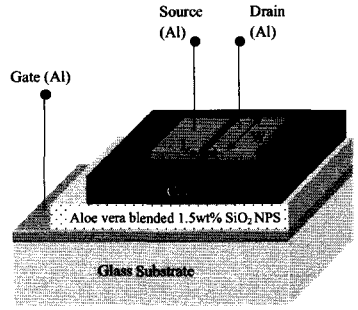

Figure 1. Schematic of the cross-sectional view of the test structure.

The printed dielectric was dried at room temperature for 30 min before the mask was removed. The sample was further dried at room temperature for another 24 h. The solidified natural Aloe vera with 1.5 wt% SiO_2 NPs on aluminum layer was additional dried in an oven at 40°C for 30 min in order to accomplish cross-linked reaction in the natural Aloe vera. After that, a 250-nm thick of C_{60} with 99.9% purity (Sigma-Aldrich) was thermally evaporated as received under high vacuum (4 × 10^{-5} mbar) onto the 226 ± 2 nm thick dielectric layer. Finally, an array of aluminum, with area of 0.64 mm^2 each, was thermally evaporated through a shadow mask on top of the semiconductor layer. The array of metal served as top-contact electrode of the device. The channel length (L) and width (W) were 0.01 mm and 0.79 mm, respectively. Schematic of the OFET with related dimensions are shown in Fig. 1. Output and transfer characteristics of the OFET were performed using a computer controlled Semiconductor Parameter Analyzer (Agilent 4156C) at room temperature and capacitance-voltage characteristic was measured by a LCR meter (Agilent 4282). The surface energy of dried natural Aloe vera layer and the similar layer with blended SiO_2 was determined by a two-liquid technique with deionized water as a polar solvent and diiodomethane (Sigma-Aldrich and 99.0% purity) as a non-polar solvent with the contact angle between the solid substrate and those liquid measured by a goniometer (Rame-hart 260-F4) and computed by a DROPimage software (Advanced v2.5). The thickness of dielectric layer was measured using a field-emission scanning electron microscope (ZEISS SUPRA 35VP) from a cross-sectional view of the sample. A series of measurements were carried out in the cross-section at 3 difference places for the same sample.

Results and Discussion

Previous work demonstrated that natural Aloe vera paste is a suitable natural material for dielectric application. This work further fabricated an OFET as test structure to investigate the workability of the natural material as gate dielectric. However, the study shows C_{60} and natural Aloe vera layers are incompatible due to their large different of surface energy ($\Delta\gamma = -23.6\%$); with C_{60} and natural Aloe vera layers respectively having surface energy of 43.8 mJ/m^2 and 57.3 mJ/m^2. Here, $\Delta\gamma = \gamma s - \gamma d$; where γs is the surface energy of C_{60} and γd is the surface energy of dielectric layer. To further enhance the compatibility of the natural Aloe vera and C_{60} layers, 1.5 wt% of SiO_2 NPs was blended into the natural Aloe vera paste. The surface energy of the blended dielectric layer has been reduced from 57.3 mJ/m^2 to 38.9 mJ/m^2. With the combination of C_{60} layer deposited on the blended dielectric, the magnitude of $\Delta\gamma(=+11.2\%)$ has been reduced more than 50% and the surface energy of blended dielectric layer is lower than that of C_{60}. The reduction of the surface energy is due to the interactions of natural Aloe vera molecules with SiO_2 NPs molecules. The addition of SiO_2 NPs tend to we intermolecular bond among the Aloe vera molecules[52,53] by the strong hydrogen bond between the Aloe vera molecules NPs molecules.[52] There are two advantages of this design. Fi predicted that the formation of C_{60} layer is following Volm mode with initially island of C_{60} being formed and later a co layer would be achieved with relatively thick dimension.[54] Th the organic semiconductor (C_{60}) layer, the higher the prob charges can be transported due to efficient connecting pat Hence, increases the mobility of an OFET.[55] It has been repo typical thickness of C_{60} in OFETs is in the range of 30 to with thicker the thickness; higher the mobility.[24,56,57] Thus thickness (250 nm) of C_{60} being used in this work is accep justifiable. Secondly, the molecular structures of C_{60} are b served without much distortion during the deposition as the force of those molecules within C_{60} is able to withhold the s together. If the cohesion force is extremely large, it is impo establish bondings between C_{60} and the blended dielectric In order to solve this adhesion issue, balance of force bet hesion and adhesion must be achieved. One of the indicator $\Delta\gamma$. It is preferable to have a positive value of $\Delta\gamma$ as what explained earlier. In order to achieve balance of force, the value of $\Delta\gamma$ must be as low as possible but not equal t lower than that.[50,61] This has been achieved by combining th (1.5 wt% of SiO_2 NPs) dielectric with C_{60} layers. As the l SiO_2 NPs in the dielectric is reducing from 1.5 wt% to 0 w nificant increment of γd has been recorded. It shifted $\Delta\gamma$ t values. In contrast, as the loading increases beyond 1.5 wt% γd is reducing monotonically. As a result, the $\Delta\gamma$ value incre itively. Besides, natural Aloe vera blended with 1.5 wt% of layer have displayed better dielectric properties; i.e., lowe current density and higher dielectric constant than natural without SiO_2 NPs.[51] Therefore, in this work, the optimur of 1.5 wt% of SiO_2 NPs has been used as the gate dielectr C_{60}-based OFET.

Previous research works on OFET device have reporte sult of effective mobility, threshold voltage, on/off current sub-threshold swing were affected when the device was ex atmospheric conditions.[7] To investigate the OFET performa mospheric conditions, in this work, the output and transfer c istics were measured twice. One measurement was done im after the OFET was fabricated and the other measurement wa the same test structure using similar measurement set up af exposure to atmospheric condition for 14 days. During the the device was kept in a clean container to prevent contamin the device. The output characteristics of those two meas are shown in Fig. 2. Based on the results, the device sho

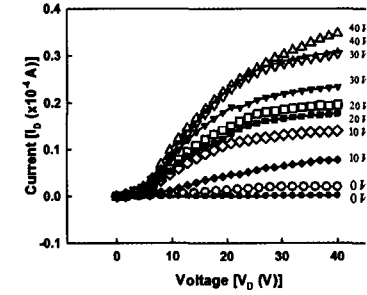

Figure 2. Output Characteristic of C_{60}-based OFET (open symbo measurement performed on as-fabricated test structure and clos indicates measurement obtained after 14th day).

Table I. Comparison of output current measured from as-fabricated OFET (1st day) and OFET exposure to open air for 14th days.

	Output current (A)			
Gate voltage	1st day	14th day	Different	Percent%
40 V	3.47×10^{-5}	3.09×10^{-5}	3.80×10^{-6}	11.0
30 V	3.04×10^{-5}	2.34×10^{-6}	2.81×10^{-5}	92.4
20 V	1.96×10^{-5}	1.78×10^{-5}	1.80×10^{-6}	9.2
10 V	1.40×10^{-5}	7.80×10^{-6}	6.20×10^{-6}	44.3
0 V	2.00×10^{-6}	1.04×10^{-7}	1.90×10^{-6}	95.0

output characteristics even though it was measured in open air without any encapsulation or passivation. The test structure measured at 14th day shows a minor shift with decreasing of current in a range of 9.3% to 94.8% with the increment of gate voltage from 0 V to 40 V (Table I) when compared to the measurement recorded on the as-fabricated test structure.

To further establish performance of the OFET, effective mobility (μ), threshold voltage (V_T), on/off current ratio (I_{on}/I_{off}), and sub-threshold swing (S) in the saturation regime of the transfer characteristics (Figs. 3 and 4) from the two measurements were extracted. Extrapolation method on the SQRT(I_D)-V_G curves (Fig. 3 and 4) has been used to extract the threshold voltage. This method consists of finding the gate-voltage axis from the point of maximum slope of the SQRT(I_D)-V_G curves. Effective mobility of the OFET was calculated by fitting the data into Equation 1,

$$I_D = 1/2(W/L)\mu C(V_G - V_T)^2 \quad [1]$$

where I_D is the drain current, V_G is the gate voltage, and C is the capacitance per unit area.[7] Capacitance of the dielectric was measured from a capacitor with an Al/natural Aloe vera blended with 1.5 wt% of SiO_2 NPs/Al structure, and found to be ~6.86 pF/cm^2 at 1.2 kHz (Fig. 5). In addition, dielectric constant (k) value was calculated by fitting the data into Equation 2,

$$C = (k\,\varepsilon_o A)/t \quad [2]$$

where ε_o is the electric constant (8.854×10^{-12} Fm^{-1}), A is the area of the electrode (4.9×10^{-8} m^2) and t is the thickness of the dielectric layer. The extracted parameters of the OFET with two measurements performed at different time are summarized in Table II.

The effective mobility measured on as-fabricated test structure is 1.110 cm^2/V s but after 14th days the mobility has dropped approximately 40% to 0.669 cm^2/V s. But these values are still higher than that being reported previously which used albumen as gate dielectric (0.13 cm^2/V s).49 Albumen sample has lower mobility, this may due to the k value of albumen sample (k = ~5.3–6.1)[49] which is higher than natural Aloe vera samples (k = 3.6). High-k dielectric layer may enhance charge carrier localization in semiconductor layer;[62–66] in contrast low-k value in dielectric may reduce charge carrier localization in semiconductor layer, i.e., at the interface between layers of organic dielectric and semiconductor interface and may lead to high mobility.[62,67–69] Although the contact resistance is one of the factors which may affect the mobility of the device, in this work, the resistance is considered as a constant. This is because throughout this study, the samples did not undergo any post-deposition treatment to reduce resistance of the contact. The reason is to avoid any additional effect, in particular using relatively high temperature treatment in certain ambient to improve the contact resistance that may change the quality of dielectric and semiconductor layers. Besides, the threshold voltage has been increased from 0 V to 7 V after 14th days of exposure. The value measured from as-fabricated test structure is comparable to the value reported in Ref. 49 (1.5 V). The values of threshold voltage and effective mobility are degraded over time due to increment of electron being trapped in either C_{60} or interface of C_{60} and dielectric; as the test structure is being exposure to open air, moisture or oxygen molecules can be easily diffused.[60] The oxygen molecules from the moisture act as traps that decreased the mobility and as electron acceptors that increased the threshold voltage.[70] Moreover, a large number of experiments have found that oxygen molecules which act as electron traps/electron acceptors thereby directly degraded the mobility of the samples.[71–73] With this trapping of electron, values of current on/off ratio and sub-threshold swing are actually improved over time. The former parameter increases an order of magnitude, which is preferable for organic memory application.[74] The much reduction of sub-threshold swing value indicates the reduction of interface trap density between C_{60} and dielectric.[7] With these, it has been demonstrated that natural Aloe vera blended with SiO_2 NPs have huge potential to be used as gate dielectric in OFET.

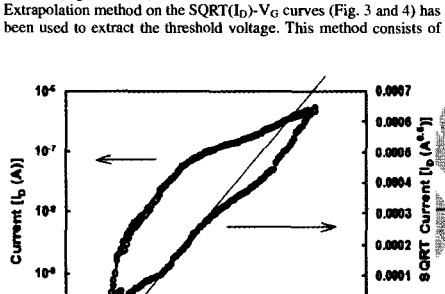

Figure 3. Transfer characteristic of C_{60}-based OFET with V_{DS} = 40 V, measured on as-fabricated test structure.

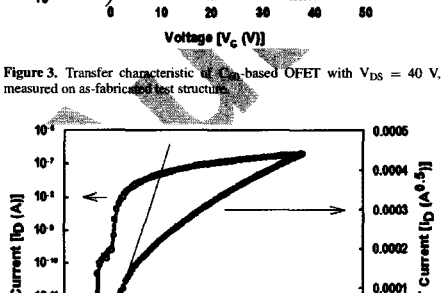

Figure 4. Transfer characteristic of C_{60}-based OFET with V_{DS} = 40 V, measured at 14th day.

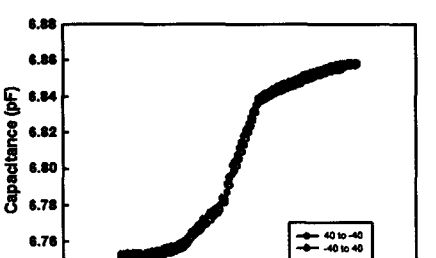

Figure 5. Capacitance (C) measured at 1.2 kHz, sweeping gate voltage from 40 V to −40 V and then from −40 V to 40 V.

Table II. Summary of the electrical parameters measured from as-fabricated OFET (1st day) and OFET exposure to open air for 14th days.

Properties	1st day	14th day
Effective mobility, μ (cm^2/V s)	1.110	0.669
Threshold voltage, V_T (V)	0	7
Current on/off ratio, $I_{on/off}$	10^3	10^4
Sub-threshold swing, S (V/decade)	4.56	1.31

Conclusions

This work had utilized natural Aloe vera blended with 1.5 wt% of SiO_2 NPs as a dielectric layer in C_{60}-based n-type OFETs. The blended dielectric layer was screen-printed on a glass substrate followed by thermally deposition of C_{60} as a semiconductor layer with bottom-gate and top-contact structure. The OFET characteristics had been studied at atmospheric condition. The design of C_{60} and blended dielectric layers in the OFET had been justified using surface energy concept. The produced OFET revealed an effective mobility of 1.110 cm^2/V s with zero threshold voltage. After 14 days of exposure in an open air, the parameters reduced but on/off current ratio and sub-threshold swing had improved significantly.

Acknowledgment

The authors thank the research grant provided by Universiti Sains Malaysia through USM Short Term grant (grant No. 60311034), USM Research grant (Individual) (814135) and RU-PRGS (grant No. 8035003). L.Q.Khor acknowledge the financial support given by the Ministry of Higher Education Malaysia under the MyMaster scholarship program.

References

1. J. Veres, S. Ogier, G. Lloyd, and D. de Leeuw, *Chemi. Materi.*, **16**, 4543 (2004).
2. A. Maliakal, in *Organic Field-Effect Transistors*, CRC Press (2007).
3. M. F. Chang, P. T. Lee, S. P. McAlister, and A. Chin, *Electron Device Lett.*, **30**, 133 (2009).
4. Y. Xu, M. Berggren, R. Gwoziecki, R. Coppard, T. Minari, C. Liu, K. Tsukagoshi, J. Chwalek, R. Balestra, and G. Ghibaudo, *J. Appl. Phys.*, **110**, 104513 (2011).
5. P. B. Shea, J. Kanicki, and N. Ono, *J. Appl. Phys.*, **98**, 014503 (2005).
6. D. I. James, J. Smith, M. Heeney, T. D. Anthopoulos, A. Salleo, and I. McCulloch, in *Organic Electronics II*, p. 1–26, Wiley-VCH Verlag GmbH & Co. KGaA (2012).
7. F. M. Li, A. Nathan, Y. Wu, and B. S. Ong, *Organic thin film transistor integration*, Wiley-VCH Verlag GmbH & Co. KGaA, Germany (2011).
8. M. O'Neill and S. M. Kelly, in *Liquid crystals beyond displays: Chemistry, physics, and applications*, Q. Li, ed., p. 303–340, John Wiley & Sons, Inc., Canada (2012).
9. K. Kuribara, H. Wang, N. Uchiyama, K. Fukuda, T. Yokota, U. Zschieschang, C. Jaye, D. Fischer, H. Klauk, T. Yamamoto, K. Takimiya, M. Ikeda, H. Kuwabara, T. Sekitani, Y. Loo, and T. Someya, *Nat. Commun.*, **3** 723 (2012).
10. R. Fornari, in *Comprehensive semiconductor science and technology*, P. Bhattacharya, R. Fornari, and H. Kamimura, eds., Vol. 4, Elsevier, USA (2011).
11. M. Irimia-Vladu, E. Głowacki, N. S. Sariciftci, and S. Bauer, in *Small Organic Molecules on Surfaces*, H. Sitter, C. Draxl, and M. Ramsey, eds., Vol. 173, p. 295–318, Springer Berlin Heidelberg (2013).
12. M. Irimia-Vladu, N. S. Sariciftci, and S. Bauer, *J. Mater. Chem.*, **21**, 1350 (2011).
13. M. Ying, A. P. Bonifas, N. Lu, Y. Su, R. Li, H. Cheng, A. Ameen, Y. Huang, and J. A. Rogers, *Nanotechnol.*, **23**, 344004 (2012).
14. D. Tobjörk and R. Österbacka, *Adv. Mater.*, **23**, 1935 (2011).
15. C. J. Bettinger and Z. Bao, *Polym. Int.*, **59**, 563 (2010).
16. C. J. Bettinger and Z. Bao, *Adv. Mater.*, **22**, 651 (2010).
17. G. Zheng, Y. Cui, E. Karabulut, L. Wågberg, H. Zhu, and L. Hu, *MRS B* 320 (2013).
18. M. Irimia-Vladu, E. D. Głowacki, G. Schwabegger, L. Leonat, H. Z H. Sitter, S. Bauer, and N. S. Sariciftci, *Green Chem.* (2013).
19. M. Muskovich and C. J. Bettinger, *Adv. Healthc. Mater.*, **1**, 248 (2012).
20. C. Wang, C. Hsieh, and J. Hwang, *Adv. Mater.*, **23**, 1630 (2011).
21. R. Capelli, J. J. Amsden, G. Generali, S. Toffanin, V. Benfenati, M D. L. Kaplan, F. G. Omenetto, and R. Zamboni, *Org. Electron.*, **12**, 1146
22. C. J. Bettinger and Z. Bao, *Polym. Int.*, **59**, 563 (2010).
23. E. D. Głowacki, G. Voss, L. Leonat, M. Irimia-Vladu, S. Bauer, and N. S *Israel J. Chem.*, **52**, 540 (2012).
24. M. Ullah, D. M. Taylor, R. Schwodiauer, H. Sitter, S. Bauer, N. S. Sar T. B. Singh, *J. Appl. Phys.*, **106**, 114505 (2009).
25. S. Lee, G. Jo, S. Kang, W. Park, Y. H. Kahng, D. Kim, B. H. Lee, and T *Appl. Phys.*, **51**, 02BK09 (2012).
26. C. S. S. Sangeeth, P. Stadler, S. Schaur, N. S. Sariciftci, and R. Menon, *108**, 113703 (2010).
27. S. D. Brotherton, *Introduction to thin film transistors*, p. 339–403, Spring tional Publishing, Switzerland (2013).
28. G. J. Matt, T. B. Singh, N. S. Sariciftci, A. M. Ramil, and H. Sitter, *Appl. **88**, 263516 (2006).
29. X. H. Zhang and B. Kippelen, *Appl. Phys. Lett.*, **93**, 143305 (2008).
30. A. Nigam, G. Schwabegger, M. Irimia, R. Ahmad, I. I. Fishchuk, A. K C. Simbrunner, H. Sitter, M. Premaratne, and V. R. Rao, *Appl. Phys.* 083305 (2012).
31. K. Ueno, S. Abe, R. Onoki, and K. Saiki, *J. Appl. Phys.*, **98**, 114503 (20
32. K. Itaka, M. Yamashiro, J. Yamaguchi, M. Haemori, S. Yaginuma, Y. M. Kondo, and H. Koinuma, *Adv. Mater.*, **18**, 1713 (2006).
33. M. Ahles, O. Cakmak, M. Tekin, A. Kara, H. Y. Guney, E. Arici, and N. S *Org. Electron.*, **12**, 497 (2011).
34. M. Kitamura, Y. Kuzumoto, M. Kamura, S. Aomori, and Y. Arakawa, *Lett.*, **91**, 183514 (2007).
35. C. Peng, T. Mei, and X. Hu, *Org. Electron.*, **12**, 1304 (2011).
36. Y. Kobayashi, T. Nagano, Y. Haruyama, E. Kuwahara, T. Takayanagi, K A. Fujiwara, *Appl. Phys. Lett.*, **87**, 143506 (2005).
37. T. Maruyama, M. Yahiro, and C. Adachi, *Appl. Phys. Lett.*, **91**, 103505
38. A. Konishi, E. Shikoh, Y. Kubozono, and A. Fujiwara, *Appl. Phys. Lett.*, (2008).
39. G. Schwabegger, M. Ullah, M. IrimiaVladu, M. Baumgartner, Y. Kanbur, P. Stadler, S. Bauer, N. S. Sariciftci, and H. Sitter, *Synth. Met.*, **161**, 2058
40. S. Olthof, S. Singh, S. K. Mohapatra, S. Barlow, S. R. Marder, B. Kip A. Kahn, *Appl. Phys. Lett.*, **101**, 253303 (2012).
41. W. Kang, M. Kitamura, and W. Arakawa, *Appl. Phys. Express*, **4**, 121602
42. P. H. Wöbkenberg, D. D. C. Bradley, D. Kronholm, J. C. D. M. de Leeuw, M. Cölle, and T. D. Anthopoulos, *Synth. Met.*, **158**, 468
43. Th. B. Singh, N. Marjanović, G. J. Matt, S. Günes, N. S. A. Montaigne Ramil, A. Andreev, H. Sitter, R. Schwödiauer, and S. Ba *Res. Soc. Symp. Proc.*, **871E**, 14.9.1 (2005).
44. T. D. Anthopoulos, B. Singh, N. Marjanovic, N. S. Sariciftci, A. M. Ram M. Colle, and D. M. de Leeuw, *Appl. Phys. Lett.*, **89**, 213504 (2006).
45. T. B. Singh, N. S. Sariciftci, H. Yang, L. Yang, B. Plochberger, and H. *Phys. Lett.*, **90**, 213512 (2007).
46. L. You, D. Hopper, and C. Streck. Advanced Micro Devices, Inc. (Sunn United States, 2000.
47. T. B. Singh and N. S. Sariciftci, *Annu. Rev. Mater. Res.*, **36**, 199 (2006).
48. G. Horowitz, *Adv. Mater.*, **10**, 365 (1998).
49. J. Chang, C. Wang, C. Huang, T. Tsai, T. Guo, and T. Wen, *Adv. Mater* (2011).
50. L. Q. Khor and K. Y. Cheong, *J. Mater. Sci. Mater. Electron.*, **24**, 2646 (
51. L. Q. Khor and K. Y. Cheong, *in "The 5th AUN/SEED-Net Regional on Materials & The 5th Regional Conference on Natural Resources rials (RCM5 & RCNRM5)"*, Parkroyal Penang Resort Hotel, Penang 2013.
52. H. Tang, H. Xiong, S. Tang, and P. Zou, *J. Appl. Polym. Sci.*, **113**, 34 (2
53. V. M. Gun'ko, P. Pissis, A. Spanoudaki, V. I. Zarko, Y. M. L. S. Andriyko, E. V. Goncharuk, R. Leboda, J. Skubiszewska-Zięba, V. I and Y. G. Ptushinskii, *J. Colloid and Interface Sci.*, **312**, 201 (2007).
54. J. A. Venables, *Introduction to surface and thin film processes*, The Pres of the University of Cambridge, UK (2000).
55. S. Y. Yang, K. Shin, and C. E. Park, *Adv. Funct. Mater.*, **15**, 1806 (2005)
56. S. Y. Yang, K. Shin, S. H. Kim, H. Jeon, J. H. Kang, H. Yang, and C. E. *Phys. Chem. B*, **110**, 20302 (2006).
57. X. H. Zhang, B. Domercq, and B. Kippelen, *Appl. Phys. Lett.*, **91**, 0921
58. C. Melzer and H. Seggern, in *Organic Electronics*, T. Grasser, G. Melle eds., Vol. 223, p. 189–212, Springer Berlin Heidelberg (2010).
59. Q. Qi, A. Yu, L. Wang, and C. Jiang, *J. Nanosci. Nanotechnol.*, **10**, 710
60. J. Gao, K. Asadi, J. B. Xu, and J. An, *Appl. Phys. Lett.*, **94**, 093302 (200
61. Y. Wang, O. Acton, G. Ting, T. Weidner, H. Ma, D. G. Castner, and *Appl. Phys. Lett.*, **95**, 243302 (2009).
62. H. S. Tan, N. Mathews, T. Cahyadi, F. R. Zhu, and S. G. Mhaisalkar, *Lett.*, **94**, 263303 (2009).
63. H. Houili, J. D. Picon, L. Zuppiroli, and M. N. Bussac, *J. Appl. Phys.*, (2006).
64. A. L. Deman and J. Tardy, *Mater. Sci. Eng. C*, **26**, 421 (2006).
65. D. Duarte, D. Sharma, B. Cobb, and A. Dodabalapur, *Appl. Phys. Lett.*, (2011).

66. H. Sakai, K. Konno, and H. Murata, *Appl. Phys. Lett.*, **94**, 073304 (2009).
67. Y. Kanbur, M. IrimiaVladu, E. D. Glowacki, G. Voss, M. Baumgartner, G. Schwabegger, L. Leonat, M. Ullah, H. Sarica, S. ErtenEla, R. Schwödiauer, H. Sitter, Z. Küçükyavuz, S. Bauer, and N. S. Sariciftci, *Org. Electron.*, **13**, 919 (2012).
68. D. I. James, J. Smith, M. Heeney, T. D. Anthopoulos, A. Salleo, and L. McCulloch, in *Organic Electronics II: More Materials and Applications*, p. 1–26, Wiley-VCH Verlag GmbH & Co. KGaA (2012).
69. B. Stadlober, M. Zirkl, M. Beutl, G. Leising, S. BauerGogonea, and S. Bauer, *Appl. Phys. Lett.*, **86**, 242902 (2005).
70. T. Sakanoue, M. Yahiro, C. Adachi, K. Takimiya, and A. Toshimitsu, *J. Appl. Phys.*, **103**, 094509 (2008).
71. S. Ono, N. Minder, Z. Chen, A. Facchetti, and A. F. Morpurgo, *Appl. Phys. Lett.*, **97**, 143307 (2010).
72. Rashmi A. K. Kapoor, U. Kumar, V. R. Balakrishnan, and P. K. Basu, *Pramana - J. Phys.*, **68**, 489 (2007).
73. W. T. Chen, L. Shih Yi, K. Shih Chin, Z. Hsiao Wen, T. Chuang Chuang, L. Jian Hong, C. H. Fang, and C. C. Lee, *Electron Device Lett.*, **32**, 1552 (2011).
74. W. Chen, H. Li, N. Li, Q. Xu, J. Lu, and L. Wang, *Dyes and Pigment.*, **95**, 365 (2012).

Queries

Q1: AU: Please provide a digital object identifier (doi) for Ref(s) 15, 22, and 43. For additional information on doi's please select t http://www.doi.org/. If a doi is not available, no other information is needed from you.
Q2: AU: Please verify the page no. and volume no. in Ref. 50.

FAKULTÄT AM
PROF. DR. RUPERT SCHREINER

HOCHSCHULE
REGENSBURG
UNIVERSITY
OF APPLIED
SCIENCES

HOCHSCHULE REGENSBURG I POSTFACH 12 03 27 I 93025 REGENSBURG

Herrn
Tan Pi Lin
8c, Lorong 7, Tanan Bukit Mas,

34000 Taiping,
Perak, Malaysia

Tel: (+49) 941 1277
Fax: (+49) 941 1473
Raum: T114
E-Mail: rupert.schreiner@hs-regensburg.de

Ihr Zeichen, Ihre Nachricht vom	Unser Zeichen, unsere Nachricht vom	Tel 0941/943-1277 Fax 0941/943-1252	Regensburg, 14.06.12

Bestätigung zur Vorlage bei der Ausländerbehörde

Sehr geehrter Herr Tan Pi Lin,

Hiermit bestätigen wir Ihnen, dass wir Sie an der Hochschule Regensburg im Labor Mikrosensorik als **wissenschaftlicher Mitarbeiter** (Gehaltsstufe E13) **in Teilzeit (50%)** befristet im Zeitraum vom **23.07.2012 bis zum 31.12.2012** beschäftigen werden.

Monatlich wird Ihnen das reguläre **Bruttogehalt** der Gehaltsstufe E13, 50% (öffentlicher Dienst, Land Bayern) bezahlt (derzeit monatlich brutto: **1593,50€**). Von Seiten der Hochschule (Akademisches Auslandsamt) wird Ihnen eine **Studentenwohnung bereitgestellt (zwischen 200€ bis max. 300€/Monat)**. Die Kosten dafür sind von Ihnen zu tragen.

Tätigkeitsbeschreibung:

Herr Tan ist Doktorand an unserer Partneruni USM in Malaysia auf dem Gebiet der organischen Elektronik. Er wird während seines Gastaufenthalts bei uns an der Vorbereitung des Applikationszentrums "Optoelektronik-Technologie" mitarbeiten und sein Know-How auf dem Gebiet der organischen Halbleiter (für OLED) mit einbringen.

Mit freundlichen Grüßen,

Prof. Dr. Rupert Schreiner

UNIVERSITI SAINS MALAYSIA

Pusat Pengajian Kejuruteraan Bahan & Sumber Mineral

School Of Materials & Minerals Resources Engineering

Kampus Kejuruteraan
(Engineering Campus)
Universiti Sains Malaysia
14300 Nibong Tebal
Pulau Pinang, Malaysia
Tel : 604 - 5995999 samb. 6101, 6104, 6106, 6186
Faks: 604 - 594 1011
www.eng.usm.my

26th March 2013

Dr. Guenter Gruber
Embassy of the Federal Republic of Germany
26th Floor Menara Tan&Tan
207, Jalan Tun Razak
50400 Kuala Lumpur
Malaysia

Dear Dr. Guenter Gruber,

Verification of Applicant for Attachment at University of Regensburg

With reference to the above matter, I would like to confirm that Mr. Tan Pi Lin is a postgraduate student at Universiti Sains Malaysia under my supervision. He is currently in his 4th year of PhD. I would like to propose the applicant and send him to Hochschule Regensburg University of Applied Sciences, Germany for extension of his attachment. The duration of this attachment is from 1st May 2013 until 30th September 2013. The research scope is on organic electronic.

Enclosed are memorandum of understanding.

Thank you.

Sincerely,

Assoc Prof Ir Dr Cheong Kuan Yew
School of Materials & Mineral Resources Engineering
Engineering Campus
Universiti Sains Malaysia
14300 Nibong Tebal
Penang , Malaysia
Tel: +604-599 5259
Mobile: +6012-515 3540
Fax : 604 – 5941011

Verified by,

Profesor Hanafi B. Ismail,
Dean,
School of Materials & Mineral Resources Engineering
Engineering Campus
Universiti Sains Malaysia
14300 Nibong Tebal
Penang, Malaysia.
Tel: 04-599 6113
Fax : 604 - 5941011

ASSOC. PROF. IR. DR. CHEONG KUAN YEW
Universiti Sains Malaysia
Engineering Campus
School of Materials & Mineral Resources Engineering
14300 Nibong Tebal

UNIVERSITI SAINS MALAYSIA

Pejabat Pengurusan Dan Kreativiti Penyelidikan
Research Creativity and Management Office

Canselori,

Universiti Sains Malaysia
Aras 6, Bangunan Canselori
11800, USM Pulau Pinang
T : (6)04-653 3108/3178/3988/5019
F : (6)04-656 6466/8470
: (6)04-653 2350
L : www.research.usm.my

Tarikh : 06 Januari 2012

Encik Ismail Jamaluddin
Ketua Penolong Bendahari
Jabatan Bendahari
Universiti Sains Malaysia
Kampus Kejuruteraan
Seri Ampangan 14300 Nibong Tebal
PULAU PINANG

Tuan,

CEK PROJEK PENYELIDIKAN PEMBIAYAAN AGENSI LUAR – PROJEK BARU

- **Penaja : MALAYSIAN TORAY SCIENCE FOUNDATION (MTSF)**
- **Tajuk : *'Investigation of the Interaction between Synthetic Porphyrin as An Organic Film and Flexible Substrate'***
- **Pelajar : ENCIK TAN PI LIN**

Dengan segala hormatnya perkara di atas dirujuk.

2. Bersama ini disampaikan cek Citibank Berhad Penang **No. 767340** berjumlah **RM20,000.00** bertarikh 22 November 2011 untuk bayaran bagi projek penyelidikan Encik Tan Pi Lin daripada Pusat Pengajian Kejuruteraan Bahan & Sumber Mineral yang berjaya mendapat geran Malaysia Toray Science Foundation (MTSF) untuk tahun 2011 di atas tajuk ***'Investigation of the Interaction between Synthetic Porphyrin as an Organic Film and Flexible Substrate'.***

3. Selanjutnya kerjasama tuan dipohon untuk mengeluar resit untuk disampaikan kepada pihak penaja.

Sekian.

"BERKHIDMAT UNTUK NEGARA"
'Memastikan Kelestarian Hari Esok'

b/p
(AMRA OTHMAN)
Penolong Pendaftar
Unit Pengurusan Geran & Pembangunan Penyelidikan
E-mel: rcmo@usm.my

s.k. Dekan
Pusat Pengajian Kej. Bahan & Sumber Mineral

Prof. Madya Ir. Dr. Cheong Kuan Yew
Penyelia
Pusat Pengajian Kej. Bahan & Sumber Mineral

Encik Tan Pi Lin
Pelajar

Untuk makluman tuan-tuan

UNIVERSITI SAINS MALAYSIA

INSTITUT PENGAJIAN SISWAZAH | INSTITUTE OF POSTGRADUATE STUDIES

Rujukan Kami : IPS12/MIN/022
Tarikh : 24 Julai 2012

Universiti Sains Malaysia
11800 USM Pulau Pinang
www.ips.usm.my

Lim Zhe Xi
10 Lintang Sungai Burung Satu
11000, Balik Pulau
Pulau Pinang

Tuan,

Tawaran Kemasukan Untuk Mengikuti Pengajian Siswazah di Universiti Sains Malaysia

Sukacita dimaklumkan bahawa Universiti telah meluluskan kemasukan tuan sebagai calon pengajian siswazah. Butiran pencalonan tuan adalah seperti berikut :-

Ijazah	:	Sarjana Sains (Kejuruteraan Bahan)
Pusat Pengajian/ Pusat/ Unit	:	Pusat Pengajian Kejuruteraan Bahan & Sumber Mineral
Kampus	:	Kampus Kejuruteraan, Pulau Pinang
Mod Pengajian	:	Penyelidikan
Bidang Penyelidikan	:	Bahan Elektronik
Tajuk Penyelidikan	:	Fabrication and Characterization of Organic-Based Memory Device
Status Pencalonan	:	Penuh Masa
Tempoh Pencalonan	:	Min : 12 bulan/ 2 semester Mak : 36 bulan/ 6 semester
Tarikh Luput Tawaran	:	24 Julai 2013.
Syarat Tawaran	:	-
Penyelia Utama (PU)	:	Prof. Madya Ir. Dr. Cheong Kuan Yew
Penyelia Bersama (PB1)	:	-
Penyelia Bersama (PB2)	:	-
Penyelia Bersama (PB3)	:	-
Penyelia Lapangan (PL)	:	-

Untuk maklumat lanjut tentang prosedur pendaftaran, sila rujuk **Panduan Pendaftaran Pelajar** yang disertakan.

Yang menjalankan tugas,

(NUR HUSNA MANSOR)
Penolong Pendaftar

s.k Dekan, Pusat Pengajian Kejuruteraan Bahan & Sumber Mineral
(PU) Prof. Madya Ir. Dr. Cheong Kuan Yew
-
-
-
-

Development of Organic Semiconductor Thin Film

A Final Research Report
Submitted to

Research Creativity and Management Office
Universiti Sains Malaysia

by

Assoc. Prof. Ir. Dr. Cheong Kuan Yew (Principle Researcher)
Assoc. Prof. Dr. Chow Wen Shyang
Prof. Dr. Yeap Guan Yew

In the fulfillment of the requirements of

Research University (Individual) Grant
Universiti Sains Malaysia
(Grant No: 1001/PBAHAN/814135)

August 2013

ACKNOWLEDGEMENT

I would like to take this opportunity to express my appreciation and sincere gratitude to all those who have devoted their time in making this project a success. My heartiest thank to all my postgraduate students who have contributed to the success of this project.

I would like to extend my most sincere gratitude to all staffs in USM that give me valuable assistance for completion this project. Last but no least, I would like to acknowledge the support and facilities given by the School of Materials & Mineral Resources Engineering, School of Chemical Science, USM and the financial support provided by USM Research University (Individual) Grant.

Assoc. Prof. Ir. Dr. Cheong Kuan Yew
Assoc. Prof. Dr. Chow Wen Shyang
Prof. Dr. Yeap Guan Yew

CONTENTS

CHAPTER 3: METHODOLOGY

LIST OF TABLES

LIST OF FIGURES

LIST OF ABBREVIATIONS

AMOLED	Active Matrix OLED
EA	Electron Affinity
ETL	Electrons Transport Layer
HOMO	Highest Occupied Molecular Orbital
HTL	Holes Transport Layer
IP	Ionization Potential
ITO	Indium-Tin-Oxide
LCD	Liquid Crystal Display
LED	Light Emitting Diode
LE-OFET	Light Emitting Organic Field Effect Transistor
LUMO	Lowest Unoccupied Molecular Orbital
MCMB	MesocarbonMicrobead
MEH-PPV	Poly[2-methoxy-5-(2'-ethyl-hexyloxy)-1,4-phenylene vinylene]
OFET	Organic Field Effect Transistor
OLED	Organic Light Emittind Diode
OPV	Organic Photovoltaic
PA	Polyacetylene
PAN	Polyaniline
PLED	Polymer Light Emitting Diode
PMOLED	Passive Matrix OLED
PPP	Polyparaphenylene
PPV	Poly(p-phenylenevinylene)
RMS	Root-Mean-Square
SMOLED	Small Molecule Organic LED
SWNT	Single-walled Nanotube
TCB	1,2,3-trichlorobenzene

Development of Organic Semiconductor Thin Film

ABSTRACT

In this study, three types of organic materials have been investigated with respect to their electrical, structural, and chemical properties. The three materials were porphyrin, poly[2-methoxy-5-(2'-ethylhexyloxy)-1,4-phenylenevinylene] (MEH-PPV), and liquid crystal dimers bis{2-alkyl-(S)-(+)-2-(6-[4-4-decyloxyphenylazo)-benzoyloxy]-2-naphthyl)propinate} (azo). In order to understand their performance, fullerene (C60) material has been used as a benchmark. The materials were deposited on glass or Si substrate, fabricating it into capacitor, memory, or transistor (OFET) structure for electrical testing. The effect of various synthetic porphyrins concentration and gap distance towards the electrical properties were studied. Both 2, 3, 7, 8, 12, 13, 17, 18 – Octaethyl - 21H .23H - porphine Cu(II) (Cu-porphyrin) and 2, 3, 7, 8, 12, 13, 17, 18 – Octaethyl - 21H .23H - porphine (porphyrin) were diluted into chloroform with concentration of 0.1 - 10.0 mg/ml. These organic thin films were formed through drop casting method. The gap distances between two electrodes varied from 150 to 700 μm. The present of central metal in porphyrin ring greatly affected redox and electron transfer of it. Therefore, Cu-porphyrin showed better electrical properties. Drying time played an important factor for the arrangement of the organic macromolecule. Longer drying time may let the organic molecule to arrange before the solution dry up. The results showed that Cu-porphyrin with concentration of 0.5 mg/ml has the highest electrical conductivity due to better molecular packing. Electrode distance did not bring much effect to the electrical properties. MEH-PPV powder was dissolved by chlorobenzene in four concentrations (6 to 12 mg/ml). Different weight percentage of aluminum (Al) and silver (Ag) nanoparticles (0.025 to 0.10 wt%) were incorporated into 12 mg/ml concentration of MEH-PPV to form composites layers. 12 mg/ml concentration of MEH-PPV is chosen due to its good electrical properties. Results indicated that MEH-PPV with Ag nanoparticles gave a better enhancement on the electrical performance because the dispersion of Ag nanoparticles was more uniform. Liquid crystal dimers azo were being investigated in terms of their thermal and physical properties. azo with spacer 7 and 9 (7 azo and 9 azo) had been selected for electrical transporting characteristic because of better crystallization formation. However, the results did not show an output characteristic and transfer characteristics of an OFET device, but showing a dielectric characteristic. azo material was not a semiconductor material but a dielectric material. 9 azo was more suitable to act as dielectric materials than 7 azo because of the length of the spacer which plays an important role in determining the arrangement of these macromolecules. C60-based OFET with a combination of solution-processable natural Aloe vera blended with 1.5 wt% of SiO_2 nanoparticles as a natural gate dielectric. The natural gate dielectric was screen-printed on a glass substrate followed by thermally evaporation of a layer of C60 semiconductor to form a bottom-gate and top-contact OFET structure. Surface energy concept has been used to justify selection of the gate dielectric and semiconductor layers. The OFET operates under open air and exhibits an effective mobility and threshold voltage of 1.110 cm2/Vs and 0 V, respectively. After two weeks exposure in air, the parameters reduce but on/off current ratio and sub-threshold swing improve significantly. All of the three materials being investigated did not performed as good as C60.

CHAPTER 1

INTRODUCTION

1.1 Introduction

Organic semiconductor technology has gainedan increasing research interest due to its great promise for large area, low-end, lightweight, and flexible electronics applications (Li et al., 2011). Due to their ease of processing and unique physical (i.e., electrical, optical, thermal, and magnetic) properties, organic semiconductors can bring great opportunities for broad-impact applications requiring large-area coverage, mechanical flexibility, low-temperature processing, and low cost. Hence, organic semiconductors have appeal for many devices including transistors, diodes, sensors, solar cells, and organic light emitting diode (OLED) (Li et al., 2011). Figure 1.1 shows the broad range of products and technologies inspired by organic electronics.

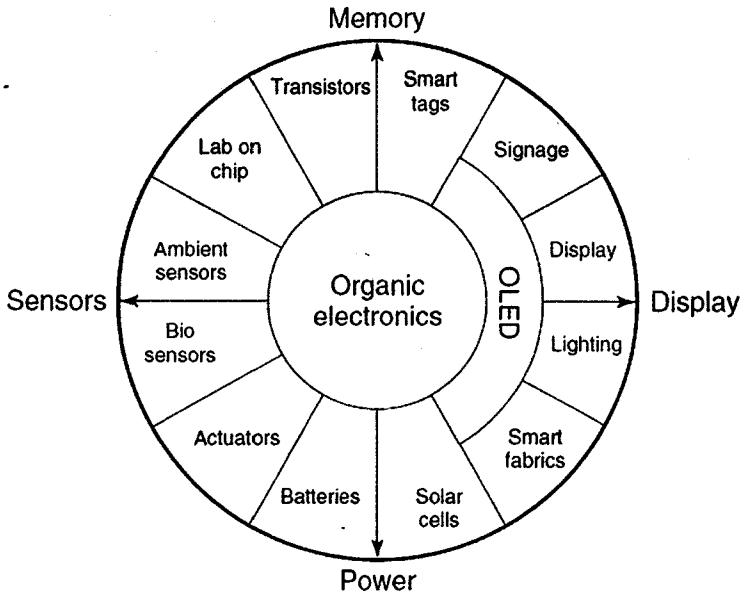

Figure 1.1: A broad range of products and technologies inspired by organic electronics (Li etal., 2011).

Before the discovery of electrically conductive properties, polymers were widely considered and used as electrical insulators because of their good insulating properties they exhibited. In 1977, the discovery of the first highly conductive polymer, chemically and electrochemically doped polyacetylene (P-type), was reported (Cui et al., 2008). The polyacetylene film was oxidatively doped with iodine vapors to induce metal-like conductivities (Wiederrecht et al., 2010). The discovery of doped polyacetylene has opened an entire new field for polymers and organic materials in applications as both conductors and semiconductors (Cui et al., 2008).

Most polymers are large band-gap insulators. In polymers, carbon is the main building unit. The carbon-carbon bonds are primarily single bonds (sp_3 hybridization). Since all of the four valance electrons form covalent bonds with neighboring carbon atoms, it is a saturated compound (Kline et al., 2008). On the other hand, conjugated polymers have alternating single and double bonds (sp_2 hybridization). This bond alternation structure results in delocalized π-electrons that give conjugated polymers their semiconducting or metallic properties (Kline et al., 2008). The conducting nature of conjugated polymers (doped polyacetylene) was discovered by Heeger, MacDiarmid and Shirakawa in 1977 (Kline et al., 2008).

Beside the functionality, conjugated polymers are interested because they are solution processible (Robinson et al., 2007). This allows techniques such as spin-coating, screen printing and ink jet printing that are easily adapted to large substrates to be used. The ease of processing and also the desirable mechanical properties make conjugated polymers quite attractive for a wide variety of applications including light

emitting diode (LED) and photovoltaic cells (Arnautov et al., 2004). Over the past 15 years, solutions and suspensions of conjugated polymers have been developed to the point where they are manufacturable, as shown by the products such as the organic light emitting diodes (OLEDs) used in Philips' electric razor (Kline et al., 2008).There are two types of OLED technologies available in the market: active matrix OLED (AMOLED) and passive matrix OLED (PMOLED) (Colegrove et al., 2010). Figure 1.2 shows the OLED shipment and forecast report in the past 11 years.

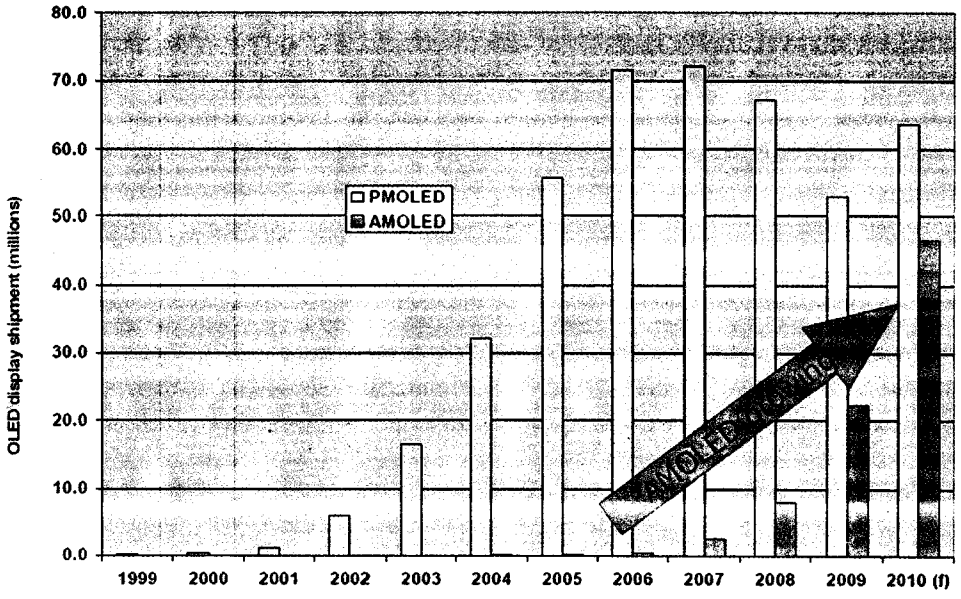

Figure 1.2: The OLED shipment and forecast report in the past 11 years (Colegrove, 2010).

In the manufacturing of OLEDs, polymer light emitting diodes (PLEDs) were developed. In 1990, PLEDs were first reported using poly(phenylenevinylene) (PPV) as the light emitting materials (Arnautov et al., 2004). PPV comprises of alternating benzene and vinylene units (Murray et al., 2000). Within the class of PPV, poly[2-methoxy-5-(2'-ethyl-hexyloxy)-1,4-phenylene vinylene] (MEH-PPV) exhibits characteristics that make it suitable for device fabrication (Arnautov et al., 2004). The

asymmetric alkoxy side chains allow MEH-PPV to be soluble in common organic solvents and hence, can be used in different processing techniques such as dip-coating, spin and drop-casting (Arnautov et al., 2004).

Since there have been considerable advances in polymer design and devices, polymer light emitting diodes (PLEDs) are widely considered for commercialization in displays. The advantages that PLEDs have over liquid crystal displays are that PLEDs do not require a backlight and need fewer or no filters (Hermona et al., 2007). They have faster response times which are an advantage for video with an 180° viewing angle may be printed and can be made on flexible substrates (Hermona et al., 2007). However, to improve the lifetime of PLEDs remains a challenge in this field (Hermona et al., 2007).

To enhance the performance of the devices, several studies have been carried out on composites made with polymers and nanoparticles. Carter et al. (1997) reported that the incorporation of TiO_2 and SiO_2 nanoparticles inside MEH-PPV result an increase in current and luminance output. Yang et al. (2007) also reported that by adding in TiO_2 and SiO_2 nanoparticles into MEH-PPV, the composites show a higher stability in the emission characteristics compared to bare polymer film. Beside oxide nanoparticles, Lee[a] et al. (2009) reported that the electron mobility inside the MEH-PPV can be enhanced by adding in fullerence.

Besides oxide nanoparticles, metal nanoparticles dispersed in conjugated polymers have also attracted many interests from researchers. The adding of metal nanoparticles into the polymer leads to improvement in electrical conductivity of the

composite layer (Chin et al., 2008). This is because metal nanoparticles can provide more electron transmitting / conducting points due to their high free surface area (Mariatti et al., 2010). Hence, percolation threshold of the devices can be reached easily with a small amount of metal nanoparticles is incorporated (Mariatti et al., 2010).

In this study, MEH-PPV is chosen as the organic material because it is readily soluble in aromatic solvent such as toluene or chlorobenzene. Different weight percentage (wt%) of Aluminum (Al) and Silver (Ag) nanoparticles are incorporated into the MEH-PPV matrix. The mixture will be spin-coated on a glass substrate. The effect of type of nanoparticles used and their composition on the devices will be studied in terms of film morphology and electrical properties.

Another group of molecular based organic semiconductors is porphyrins, which is widely used as an active layer in an OFET. This is due to its synthetic versatility, thermal stability and large π-electron system that porphyrins have [El-Nahass, 2010]. The chemical structure of a general porphyrin molecule which contains four pyrrole linked via methine bridges [James, 1996, Cao, 2009].

These molecules tend to aggregate are due to the π–π interaction in between the organic molecules [Mallamace, 2000]. This π-π interaction will leads to the final morphology of the organic molecules arrangement [Li, 2009]. Porphyrins derivatives stand a crucial role in biological processes, such as photosynthesis (chlorophyll), oxygen transport and storage (heme) [Krishnamurthy, , 2007; Fuhrhop and Li, 2003]. These porphyrins molecules are important in the metabolism of living organisms [Jacobus and Raluca, 2010]. Such complexes are used in a variety of applications as models for biological electron transport [Magdalena, 2000, Yanov, 2007] and oxygen transport [Natale, 2009]. To utilize the concept of natural porphyrin, synthetic-type of porphyrin has been

produced and its richness of properties have benefited a lot of electronic applications [Kononenko, 2009].

Porphyrins molecules are tend to aggregate and form huge supramolecule. Typically, formation of this syhthetic supramolecular through aggregation will further enrich the properties of the porphyrins. Therefore, supramolecules porphyrins do enhance performance of the devices [Zhang, 2007]. In recent times, significant improvements of supramolecular chemistry concepts further upgraded porphyrin usability. Supramolecular chemistry gains advantage from van der Waals forces or hydrophobic effects, π-π interactions, hydrogen bonding and axial ligation via a nitrogen-based ligand to the metal center of the metalloporphyrin [El-Khouly, 2004]. These weak interactions may enhance the pathways leading molecules to self assemble into a variety of nanostructured motifs, like tubes, rods, sheets and so on [Grimsdale, 2005]. However, the detail investigation of the effect of nanostructure incorporated into synthetic metalloporphyrin on electrical properties has yet been fully understood and reported.

Beside synthetic metalloporphyrin, liquid crystal materials are also considered as one of the potential molecular based organic materials for electronic applications. This is a thermally and electrically aligned material that is in a state between liquid and solid forms [Ha, 2010, Ha, 2009, Ha and Ong, 2009, Ha, S.T. and Koh, 2010, Yeap, G.Y., 2009]. Most of these materials are used for display applications [Lin, J.T. 2011]. Rarely, it is employed as an active layer in OFET. Therefore, in this work, thermotropic liquid crystals will be synthesized and investigated . The use of thermotropic liquid crystals in this work is justified by its superb crystal structure as a function of temperature [Zaki , 2010]. An isotropic phase at high temperature (at the temperature above glass transition temperature of the organic materials) is formed and at low

temperature (below glass transition temperature of the organic materials) this organic liquid crystal materials will have an anisotropic properties. Hence, semiconducting properties of the active layer can be adjusted accordingly.

1.2 Problem Statement

In general, organic electronic devices are not expected to compete with silicon devices in high-end products. Compared to silicon technology, one of the limitations of organic semiconductor materials is their intrinsically lower mobility which will lead to lower conductivity (Li etal., 2011).In this project, MEH-PPV is used as the organic material. To improve the charge transport in MEH-PPV, Ltaief et al. (2009) had incorporated single-walled nanotubes (SWNTs) into MEH-PPV to form composites photovoltaic cells. This results an increase in the dark current density of the devices (Ltaief et al., 2009). Besides, Yang et al. (2004) reported that the power efficiency of MEH-PPV was enhanced by blendingionic solid electrolyte, such as polyethylene oxide into the active layer. This results in the optimized polymer morphology and the improved electrical conductivity (Yang et al., 2004). Furthermore, Wang et al. (2005) improved the photocurrent of MEH-PPV using iodine doping, changing the MEH-PPV from n-type conduction into p-type conduction (Wang et al., 2005). Recently, Kamarulzaman et al. (2011) reported that the addition of a type of carbon, mesocarbonmicrobead (MCMB) improved the conductivity of MEH-PPV by the order of 2.

Besides that, previous researchers also incorporated nanoparticles into organic materials to improve their conductivity. From the previous researches, types of nanoparticles incorporated will influence the conductivity of the organic semiconductor

devices. In this project, aluminum (Al) and silver (Ag) nanoparticles were used due to their good electrical conductivity. Ag nanoparticles have the highest conductivity (6.21×10^7 S/m) among all the metal nanoparticles (Tibtech.com, 2011). Even though the conductivity of Al nanoparticles is lower than Ag nanoparticles, the cost of Al nanoparticles is lower and their electrical conductivity (3.69×10^7 S/m) is still acceptable (Tibtech.com, 2011).

For the past few years, composite materials containing Al and Ag nanoparticles have attracted great interest due to their unique chemical and physical properties. Compared to Al nanoparticles, Ag nanoparticles are more commonly studied by previous researchers. In year 2007, Kim et al. reported that the incorporation of Ag nanoparticles into MEH-PPV will give an enhanced electrochromic coloration of the composite films (Kim et al., 2007). This indicates that Ag nanoparticles induced an absorption enhancement compared to MEH-PPV (Kim et al., 2007). In year 2010, Park et al. reported an enhancement in current density was achieved with PPV / Ag nanocomposites due to an increase in electron affinity with Ag nanoparticles content. Also, the incorporation of Ag nanoparticles will cause roughening of surface morphology (Park et al., 2007). In year 2011, Kymakis et al. studied the efficiency of organic photovoltaic devices (OPV) after blending Ag and Au (gold) nanoparticles at the interface between the active and buffer layer. The results have shown that the doping of these nanoparticles improved the power conversion efficiency to the extent of 20% (Kymakis et al., 2011). In the same year, Kochergin et al. (2011) reported the absorption enhancement in OPV by incorporating Al, Ag and Au nanoparticles in the active layer. The results have shown that Al nanoparticles yield greater enhancement than Ag or Au due to the higher plasma frequency of Al (Kochergin et al., 2011).

Most organic semiconductor thin films are composed of polycrystalline and amorphous phases. The hoping process between molecules in the disorder regions often limits charge carrier mobility. Hence, proper material preparation is important to tune the molecular structure of organic semiconductor (Li et al., 2011). During preparation, proper solvent is needed in order to obtain good morphology of polymer thin film which will affect the properties of the devices (Liu et al., 2001). Liu et al. (2001) found that aromatic solvents are more suitable to solvate conjugated polymer compared to non-aromatic solvents. Besides, the widely used spin-coating process will also lower the carrier mobilities compared to solution-cast deposition. Therefore, Sirringhaus et al. (2004) reported that better electrical properties of conjugated polymer can be achieved using higher boiling point solvents such as 1,2,3-trichlorobenzene (TCB). This is because solvent evaporation speed facilitates the growth of crystalline film and stronger the interchain (Sirringhaus et al., 2004).

The conjugated polymer-inorganic nanocomposites were prepared by mixing polymer or precursor solution and inorganic nanoparticles. By using this method, the inhomogenities related problem associated with nanoparticles agglomeration is shown (Yoon et al., 2004). Therefore, time period used for ultrasonic mixing should be controlled properly. Besides that, suitable speed of spin-coater should be selected to improve uniformity of MEH-PPV layer on glass substrate (Liu et al., 2001).

In this study, the Al electrodes will be thermal evaporated on MEH-PPV layer as cathode and this will cause problem which will lead to inaccuracy result. This is because the heat generated during the thermal evaporation process will destroy the

structure of the MEH-PPV layer. Thus, during the electrode coating process, the timing must be controlled well to avoid this problem.

Porphyrins are one of the famous materials which have been widely used as dye materials and sensor applications. These macromolecules have a stable aromatic system. They tend to be stable and the redox chemistry is reversible under appropriate condition [Jurow et al., 2010]. The core structures of the macromolecules have 11 π-bonds. Porphyrin materials outfit as one of the best candidates for organic transistor due to its strong π-π stacking and strong metal ligand coordination for the metalloporphyrin [Wang et al, 2012 and Zhang et al., 2010]. Therefore, metal-free and metalloporphyrins have been selected for the fabrication of the organic devices. The effect on various solution concentrations and gap distance in between two electrodes towards the electrical properties of both porphyrins devices were study. There are various techniques used to deposit organic semiconductor on substrate in OFET. In this research work, drop-casting technique was used due to its economical, simplicity, and ease for up-scaling. This technique is also suitable for low solubility polymers. Drop casting technique which is a relatively slow drying process, able to reduce the materials consumption because the entire solution droplet evaporates to the final polymer film.

organic field-effect transistors (OFETs) based on single crystals had been widely developed for fundamental studies to investigate intrinsic charge transport and are now growing interest not only in the academic world but also in the industrial sector. Basically, with the present of grain boundaries (Horowitz, 2001; Yogev, et al., 2010) and minimum densities of disorders (Tiao, et al., 2012), defects and impurities will slow down the charge transport which the spontaneous emergence of molecularly flat crystalline surface plays an essential role in realizing the high performance in the practical devices (Kwok, 2008; Kotani et al., 2006; Urien et al.,). An increase in the

diversity of molecular architectures which were known to exhibit liquid crystal behaviors has been studied. The research on supramolecular liquid crystals along with liquid crystal oligomers has gained much attention (Takeya, et al., 2007; Uno, et al., 2013; Ma, et al., 2010). One of the simplest forms of oligomers is liquid crystal dimer in which the main part of the molecule contains two rigid mesogenic units connected via a flexible spacer (Yeap, et al., 2013). Symmetrical dimers also known as 'twins' are becoming popular because of the significant dependence in their transitional properties, not only in the aspect ratio but also in the parity of the flexible spacers linking to mesogenic units and also on terminal spacers (Senthil, et al., 2006). Compounds which consists of two mesogenic units linked by a flexible spacer exhibit transitional behaviour whose dependence on the length and parity of the spacer and such compounds have been termed liquid crystal dimers which have proved useful as model compounds for the polymers (C.T., Imrie, and P.A., Henderson, 2002).

In this research, symmetrical liquid crystal dimers bis{2-alkyl-(S)-(+)-2-(6-[4-4-decyloxyphenylazo)-benzoyloxy]-2-naphthyl)propinate} has been synthesized and their electrical properties were investigated. These dimers possess two identical mesogenic units with each of them attached to the terminal end of a flexible spacer (–CnH2n; where n = 6–10). Azo are compounds bearing the functional group R-N=N-R', in which R and R' can be either aryl or alkyl. Aryl azo is the compound used in the research and they are usually thermally stable (Chen, et al., 2008; Zaki, 2000; Singh, et al., 2012; Joraid, et al., 2011). At the same time, these azo materials do exhibit reversible bipolar redox behavior. The electrical properties of the azo materials can be modified by adding the electron-donating such as amino group and electron-attracting such as nitro group into the conjugated system in order to enhance the electrical properties of the materials. Meanwhile, the electron-donating and crystal packing effects of an amino group are

enhanced by adding alkyl groups to the N-atom (Mallik, et al., 2007; Ackermann, et al., 2003).

1.3 Research Objectives

The objectives of this project are as follow:

- To fabricate test structures with MEH-PPV, Prophyrin, and AZO on glass substrates.
- To investigate effect of different weight percentage of aluminum (Al) and silver (Ag) nanoparticles on MEH-PPV.
- To examine effect of electrode distances on the organic materials.
- To determine the optimum concentration of organic materials in producing thin film via drop casting or spin-coating technique.

CHAPTER 2

LITERATURE REVIEW

2.1 Introduction

In this chapter, background of organic semiconductor, organic materials, organic light emitting diodes (OLEDs) and researcher's studies will be described. This chapter will also include the review studies on polymer light emitting diodes (PLEDs).

2.2 Organic Semiconductor

Organic semiconductor has attracted considerable interest of many researchers due to its good promising for large area, low-end, lightweight, and flexible electronic applications (Li et al., 2011). The unique features which give organic electronics a technological edge are simpler fabrication methods and their mechanically flexible (Li et al., 2011). In general, organic semiconductor is unlikely outperformed inorganic conductor or semiconductor (Wiederrecht et al., 2010). However, organic electronics fabrication can be done using relatively simple process such as evaporation, spin-coating and printing which does not require high-end clean room laboratories (Li et al., 2011). Due to the benefit from versatility of organic electronic technology, organic semiconductor can be appeal for broad range of devices including transistors, diodes, sensors, solar cells, and light emitting diodes (Li et al., 2011).

2.3 Organic Materials

There are two fundamental material classes for organic semiconductors, namely, small molecule and polymers (Khan et al., 2008). Both conjugated materials with a HOMO-LUMO energy gap ranging from 1.5 to 3.5 eV (Khan et al., 2008). In the intrinsic form, they have a negligible quantity of free carriers at room temperature due to the large band gap(Khan et al., 2008). In this study, the organic layer used is polymers. So, discussion will be focused on the conjugated polymers.

2.3.1 Conjugated Polymer

In our daily life, everyone is familiar with polymers as flexible and mechanically strong materials. In fact, some polymers can also conduct electricity and emit light (Friend[a] et al., 1999). These semiconducting polymers, which have been intriguing researchers for the past 20 years, are now poised to enter the market (Friend[a] et al., 1999). Before the discovery of electrically conductive properties, polymers were widely considered and been used as insulators. Following a breakthrough work by Heeger, MacDiarmid, and Shirakawa during the late 1970s, the study of conducting polymer has emerged as a thriving field within organic electronics (Wiederrecht et al., 2010). The discovery of first highly conductive polymer, chemically and electrochemically doped polyacetylene was reported in 1977. The polyacetylene film was oxidatively doped with iodine vapors to induce metal-like conductivities (Wiederrecht et al., 2010).

Most large band gap polymers are primarily single bonds (sp_3 hybridization). Meanwhile, conjugated polymers have alternating single and double bonds (sp_2 hybridization) (Kline et al., 2008). In this configuration, sp_2 hybridized bonds form three σ-bonds where excitation energies are very high (~8eV). The remaining p-orbitals of adjacent molecules form relatively weak π-bonds. The highest π-(bonding) orbital that is occupied by electrons is called the highest occupied molecular orbital (HOMO), while the lowest π*-(antibonding) orbital that is unoccupied by electrons is called the lowest unoccupied molecular orbital (LUMO). The Fermi-level lies in the energy gap between HOMO-LUMO (Khan et al., 2008). In 1990, electroluminescence was first discovered in a conjugated polymer, namely poly(p-phenylenevinylene) (PPV), by workers at Cambridge University (Scott et al., 2000).

Atomic orbital hybridization is designed to understand the nature of chemical bonds of conjugated polymer. In carbon-based molecules, the orbitals involved in the hybridization are the four outer valence orbitals, namely the 2s, $2p_x$, $2p_y$ and $2p_z$ orbitals. There are three types of sp^n hybridization: sp hybridization, sp^2 hybridization and sp^3 hybridization. Figure 2.1 shows a schematic illustration of the σ and π ($2p_y$ and $2p_z$) orbitals shown in acetylene (Barford, 2005).Among the four valence electrons of carbon, three of them formhybrid orbitals known as orbital that bond with the atom's three neighbors (Heflin et al., 2004). The remainingvalence electrons from each carbon form orbitals, which are delocalizedover the molecule (Heflin et al., 2004). The delocalized electron results in strong optical absorption, largepolarizability, and large conductivity (Heflin et al., 2004).

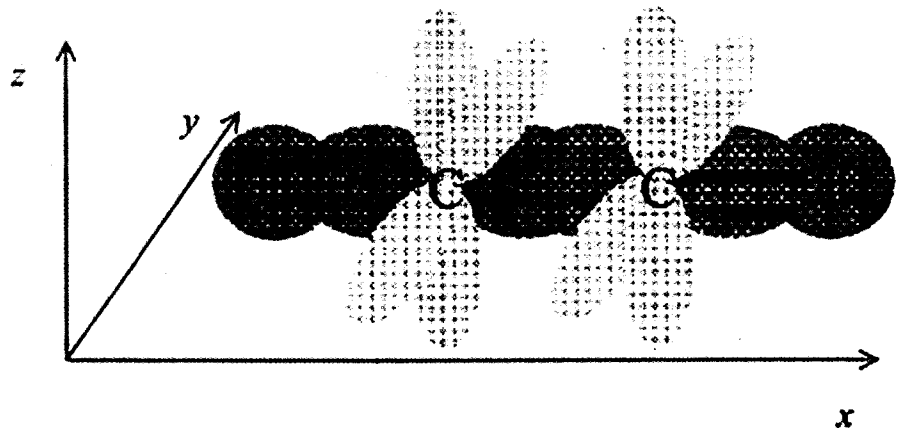

Figure 2.1: A schematic illustration of the σ and π ($2p_y$ and $2p_z$) orbitals shown in acetylene (Barford, 2005).

2.3.2 Structure of Conjugated Polymer

All conjugated polymer has the same signature in term of structure. Each atom along the backbone is involved in a π bond which is much weaker than the σ bonds that hold the atoms in the polymer chain together (Bredas et al., 1991). When placing the conjugated polymer side by side, these π bonds can delocalize over the atoms (Bredas et al., 1991). Polymers are not completely straight and flat over infinite distance (Bredas et al., 1991). Single (i.e. C-C) bonds, even when they are part of conjugated system, can rotate given the thermal energy available at room temperature (Bredas et al., 1991). Figure 2.2 shows structure of repeat unit of several conjugated polymer.

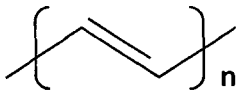

(a) Polyacetylene (PA)

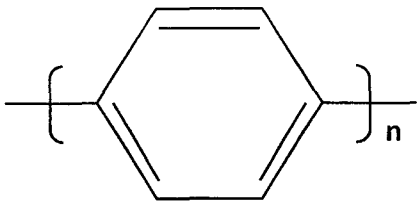

(b) Polyparaphenylene (PPP)

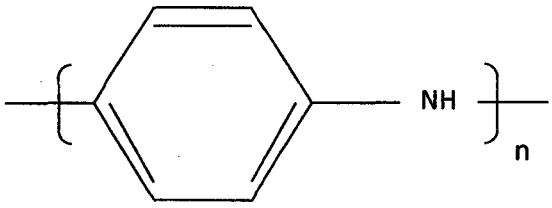

(c) Polyaniline (PAN)

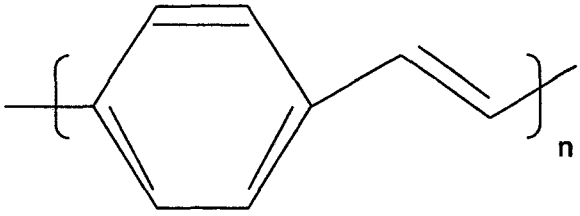

(d) Poly(p-phenylenevinylene) (PPV)

Figure 2.2: Structure of repeat unit of several conjugated polymers including their common abbreviation (Bredas et al., 1991).

2.3.3 Poly(p-phenylenevinylene) (PPV) and its derivatives

Conjugated polymer are nowadays used in several display applications, resulted from intensive research works over the last decade since the first report on polymer-based light emitting diodes (Yang et al., 2005). Among them, poly(p-phenylenevinylene) (PPV) and its derivatives have getting more attention because of their structure and their highly interesting electroluminescent properties (Yang et al., 2005). PPV composed of alternating benzene and vinylene units. The material is highly fluorescent and is bright yellow in color (Muray et al., 2000).

Since the discovery of electroluminescence of PPV in 1990, many derivatives of PPV have been synthesized and investigated (Scott et al., 2000). PPV itself is an insoluble polymer and therefore must be coated in a soluble unconjugated precursor form with subsequent thermal conversion. PPV can be used in single-layer devices because it can transport both electrons and holes (Scott et al., 2000).

Within the PPV-based polymers, the dialkoxy derivatives are particularly noteworthy (Scott et. al., 2000). Within the class of PPVs, poly[2-methoxy-5-(2'-ethylhexyloxy)-1,4-phenylenevinylene] (MEH-PPV) exhibits characteristics that make it favorable for device fabrication (Arnautov et al., 2004). MEH-PPV was introduced by the group at the University of California at Santa Barbara. The side-group substituents not only allow the polymer soluble in common organic solvent but they also alter the electrical and optical characteristics (Scott et al., 2000). The difference of structure between PPV and MEH-PPV is shown in Figure 2.3.

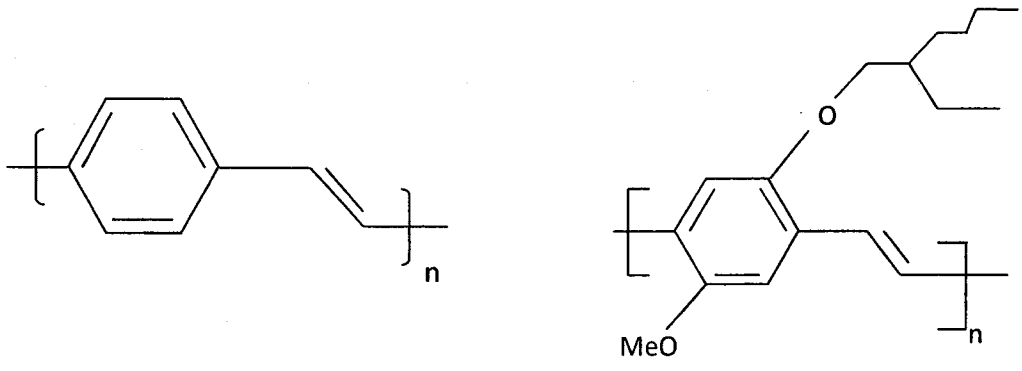

Figure 2.3: (a) Poly(p-phenylenevinylene) (PPV).

(b) Poly[2-methoxy-5-(2'-ethylhexyloxy)-1,4-phenylenevinylene] (MEH-PPV) (Arnautov et al., 2004).

2.4 Organic Light Emitting Diodes (OLEDs)

Organic light emitting diodes (OLEDs) are revolutionizing display technology by allowing low-cost, energy-saving, color flat panel displays with viewing properties comparable to conventional cathode ray tubes (Campbell et al., 2007). In the manufacturing of efficient OLEDs, both electroluminescent polymers and low molecular weight materials are being developed (Nguyen et al., 2008). In 1987, small molecule organic LEDs (SMOLEDs) with a two-organic-layer structure that used the small organic molecule tris-(8-hydroxyquinoline) aluminum (Alq) as the emissive layer was first reported. In 1990, polymer LEDs (PLEDs) using poly(p-phenylenevinylene) (PPV) in the devices were first reported (Campbell et al., 2007). The device physics of SMOLEDs is in general similar to that of PLEDs (Campbell et al., 2007). Table 2.1 shows the comparison between SMOLEDs and PLEDs.

Table 2.1: Comparison betweenSMOLEDs and PLEDs (Blochwitz, 2001).

LED/ Properties	SMOLEDs	PLEDs
Preparation	Vacuum sublimation	Spin Coating under atmosphere
Advantages	Control of purity & compatibility to CMOS technology	Cheap (patterning by printing)
Disadvantages	Expensive vacuum system needed	Impurity & solubility incompatibilities
LED operating voltage (for 100cd/m^2)	Higher	Lower
Lifetime	>10.000h	Comparable

2.4.1 Basic Operation Principle of Organic Light Emitting Diodes (OLEDs)

In conventional LEDs, light emission is created by the combination of charge carriers supplied by the semiconductor p-n junction (Nguyen et al., 2008). Figure 2.4 shows the band diagram of the junction (Nguyen et al., 2008). Under an applied electric field, the minority carriers are injected from one semiconductor to the other and recombine with the majority carriers to form radiation process (Nguyen et al., 2008). From example, the electron from n-region will diffuse into p-region and recombine with the hole in p-region to yield photon (Nguyen et al., 2008).

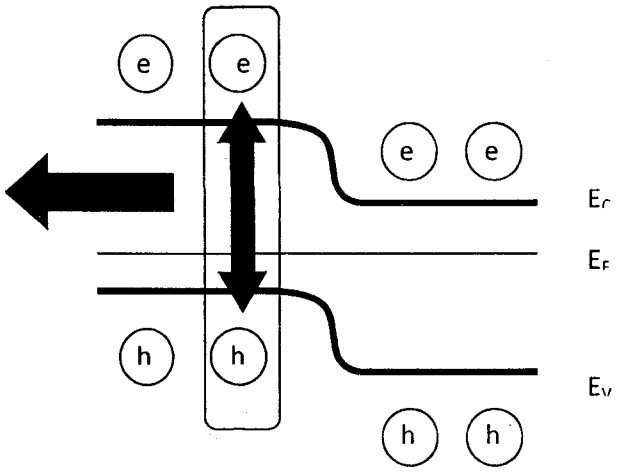

Figure 2.4: Energy diagram of an inorganic p-n junction and light emission process (Nguyen et al., 2008).

The light emission mechanism in OLEDs is similar to those in conventional LEDs. However, the characteristics and formation of recombining carriers in OLEDs are different compared to the conventional LEDs. Figure 2.5 shows the principle of single active layer OLED (Nguyen et al., 2008). This is because most of the small molecule or polymeric films used in OLEDs form disorder amorphous films without macroscopic crystal lattice (Brutting et al., 2000).

Principles of operation of OLEDs:

i. Injection

Electrons are injected from the cathode to the LUMO. Holes are injected from the anode to the HOMO (Khan et al., 2008). This mechanism is controlled by the characteristics of the interface formed between the electrode and the organic layer (Nguyen et al., 2008).

ii. Transport

Both carriers drift toward each other in the applied field. The transport mechanism will influence the carrier recombination because holes and electrons must be transported into close spaces for recombination where they can react to each other's (Nguyen et. al., 2008). The organic compounds must have sufficient mobility to transport the charge carriers to the recombination sites (Khan et al., 2008).

iii. Recombination

During recombination, the opposite signs of carriers will radiative decay to the equilibrium state (Nguyen et al., 2008). However, only a fraction of the recombination processes are radiative, the others produce phonons. This depends largely on the electronic structure of organic film and also the structure of the device (Nguyen et al., 2008).

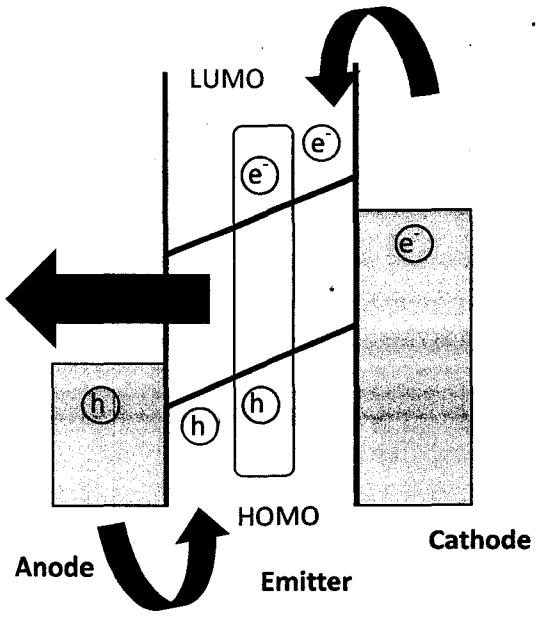

Figure 2.5: Energy diagram of an organic light emitting diode and light emission process (Nguyen et al., 2008).

2.4.2 Device Structure

The simplest structure of an OLED is a single organic layer sandwiched by two electrodes (Scott et al., 2000). In a single-layer device, the organic material must perform all these three functions: holes transport, electrons transport and emission (Scott et al., 2000). For efficient emission, the injection rates of holes from the anode into the HOMO must be almost equal to injection rates of electrons from the cathode into the LUMO (Scott et al., 2000). Otherwise, the charge carriers will just pass through the organic layer without recombination (Scott et al., 2000). For solution-processed PLEDs, a thin layer of semiconducting polymer film is typically sandwiched between two contact electrodes, as shown in Figure 2.6.

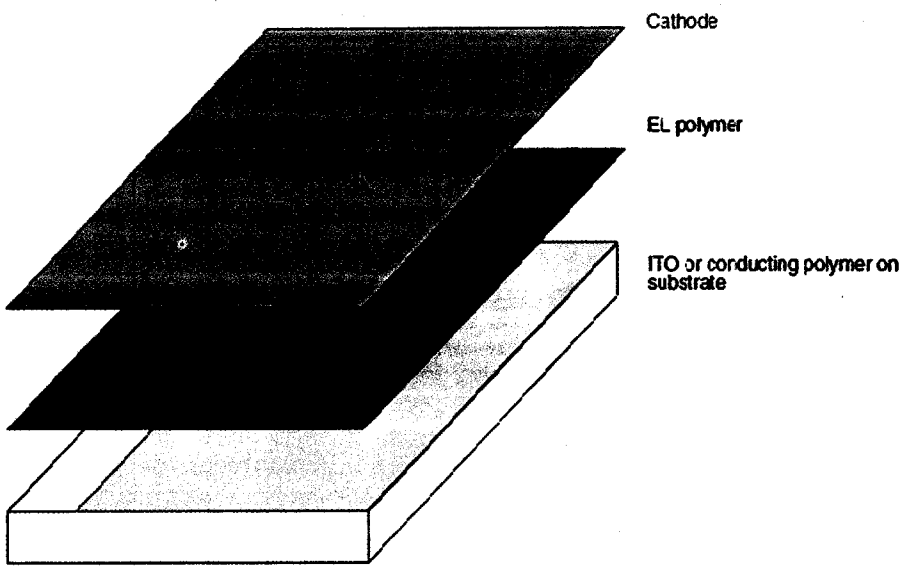

Figure 2.6: Single layer PLED in sandwich configuration (Li et. al., 2007).

To overcome the limitations imposed on a single material, multiple organic layers can be used. This has been done by Kodak group in the early 1980s (Scott et al., 2000). Material with good holes injection and transport can be located next to the anode, while material with good electrons injection and transport will be next to the cathode (Scott et al., 2000). The energy offsets on the interface between these two layers will act as a barrier for electrons entering the holes transport layer, and vice versa. This will prevent the loss of efficiency caused by passage of charge to the electrode without recombination (Scott et al., 2000). Also, due to the high density of charge carriers on each side of the organic interface, recombination will more likely to occur at the interface and far away from the electrode (Scott et al., 2000). This can reduce the probability of exciton quenching by dissociation at the electrode (Scott et al., 2000). Figure 2.7 shows the multilayer of SMOLED structure.

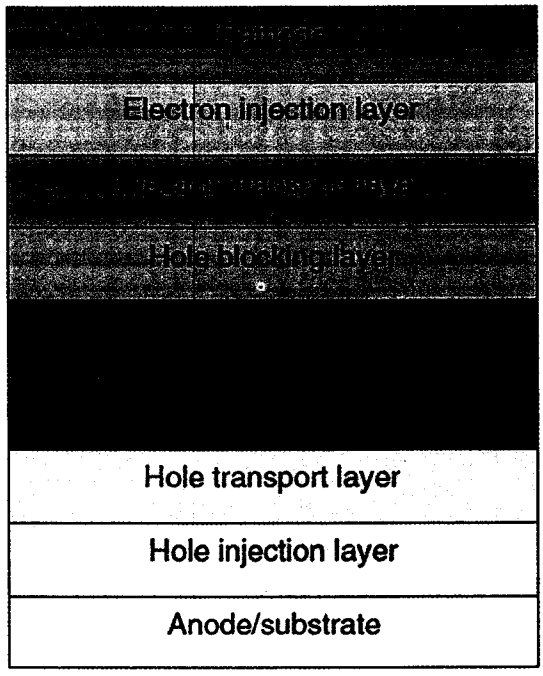

Figure 2.7: Multilayer structure of SMOLED (Li et al., 2007).

Trilayer structure offers the additional possibility of selecting the emissive material, independent of its transport properties (Scott et al., 2000). In the case of small molecules, the emitter is added as dopant in either the holes transport layer (HTL) or electrons transport layer (ETL), near the interface between them (Scott et al., 2000). The dopant may act as an electron trap in the ETL to capture and hold electron until a hole is injected nearby from HTL. In this case, the dopant will act as recombination center (Scott et al., 2000). Figure 2.8 shows the energy diagram of three if the devices in forward bias:

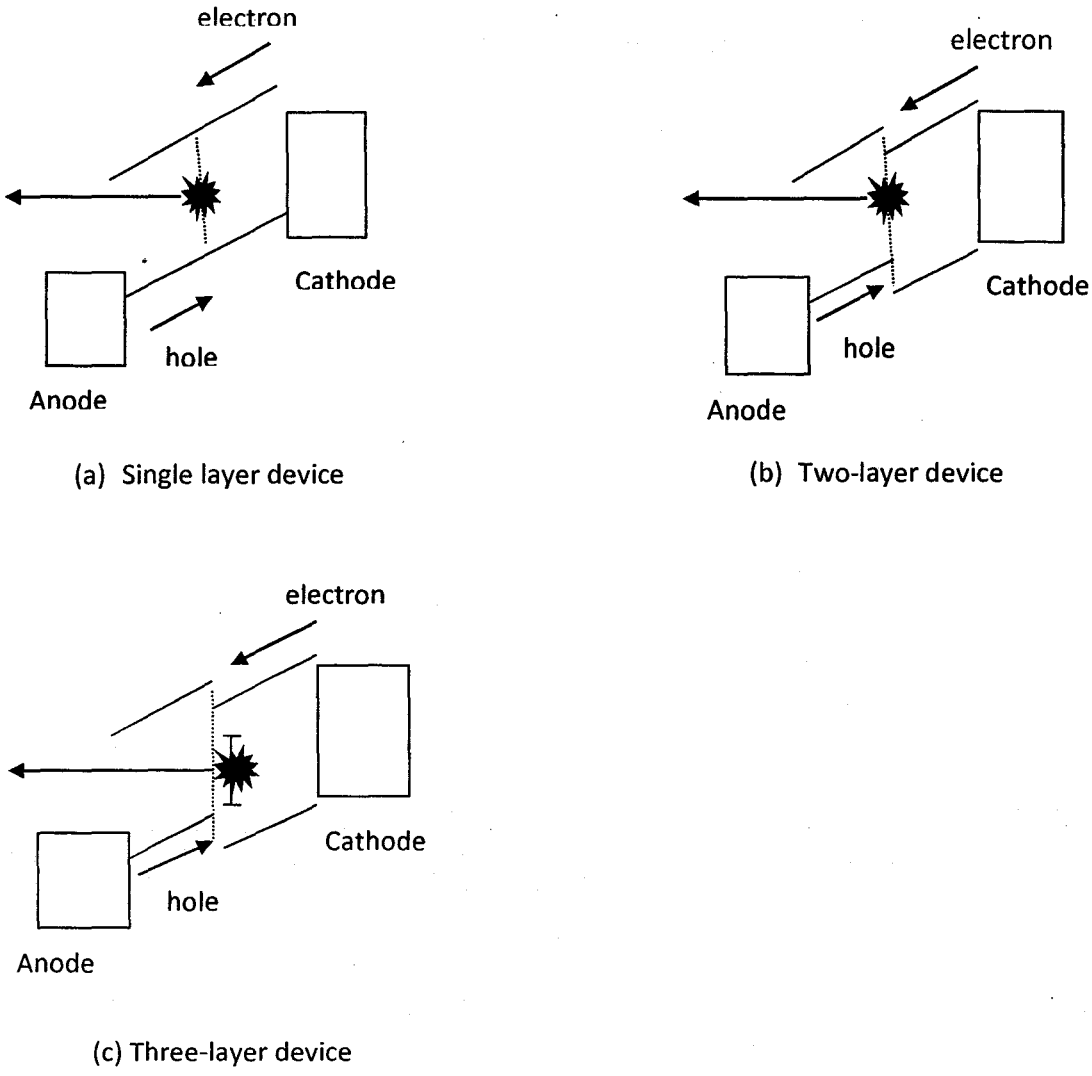

Figure 2.8: Energy level diagrams under forward bias (Scott et al., 2000).

2.4.3 Electrodesfor OLEDs

The materials used as the electrons and holes injecting electrodes play an important role in the overall performance of the device. To enable good injection of electrons and holes, the work function of the cathode must be sufficiently low while the anode sufficiently high (Scott et al., 2000). By far, the most prevalent material used for anode is indium-tin-oxide (ITO) due to its relatively high work function (4.5-5.1

eV)(Scott et al., 2000). As for cathode, the choice of material should be an electronegative metal since the functional requirement of the cathode is to inject electrons (Scott et al., 2000). Figure 2.9 shows a schematic energy level diagram for an ITO/PPV/Al LED, showing the ionization potential (IP) and electron affinity (EA) of PPV, the work functions of ITO and Al (Φ_{ITO} and Φ_{Al}), and the barriers to injection of electrons and holes (ΔE_e and ΔE_h).

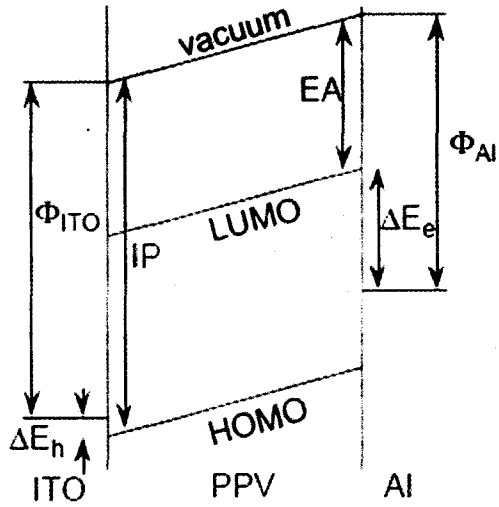

Figure 2.9: Schematic energy level diagram for an ITO/PPV/Al LED (Friend[b] et al., 1999).

2.4.4 Applications

(a) OLED Display

Liquid crystal displays (LCDs) have now been in the market for a number of years. However, recent improvements on organic light emitting diodes (OLEDs) become a new alternative to the flat panel display industry. OLEDs offer improved luminous efficiency, high brightness and wide viewing angle (Kazafi et al., 2005). In addition, OLEDs give lighter weight and consume less power than LCDs (Kazafi et al., 2005). Besides that, OLEDs do not require backlight (Kazafi et al., 2005). For OLEDs, display drivers are divided into two different addressing schemes: active matrix addressing and passive matrix addressing (Kazafi et al., 2005). Passive matrix displays apply a voltage directly across the lighting element, whereas active matrix displays use a data voltage to control a current through the LED (Kazafi et al., 2005). The main difference between both techniques relates to the fraction of time that a given pixel is allowed to emit light (Kazafi et al., 2005).

OLED technology has been used in commercial applications such as displays for mobile phones and portable digital media players, car radios and digital cameras among others (EDN, 2005).OLEDs have been used in most Motorola and Samsung color cell phones, as well as some HTC, LG and Sony Ericsson models (EDN, 2005).Samsung's latest AMOLED smartphones use their Super AMOLED trademark, with the Samsung Wave S8500 and Samsung i9000 Galaxy S being launched in June 2010. In January 2011 Samsung announced their Super AMOLED Plus displays, which feature 50% more sub-pixels, and also given improvements in contrast and outdoor readability over the 'original' Super AMOLED displays(Oled-info.com, 2010). Figure 2.10 shows the new AMOLED products in the market.

Samsung Galaxy S

(a) Mobile

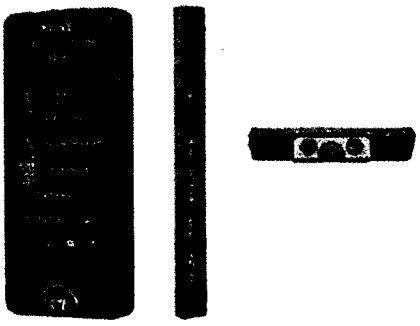

Sony

(b) Digital Media Player

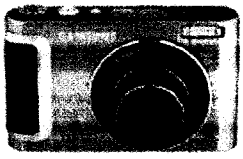

Samsung

(c) Digital Camera

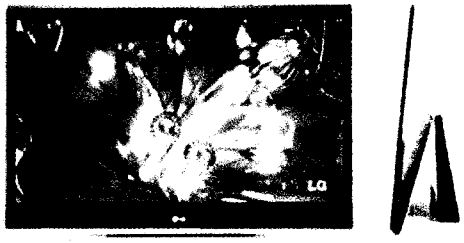

LG Display 15"

(d) TV Display

Figure 2.10: New AMOLED display products in the market (Colegrove, 2010).

(b) OLED Lighting

Today, OLEDs are used to make beautiful and efficient displays, but this technologyis also possible forcreation of white light panels for lighting. Unlike conventional lighting, OLEDs provide an area-lighting panel and feature good color temperature (Oled-info.com, 2009). Besides that, OLED panels are slimmer. This allows OLED lighting placed directly on ceilings rather than hanging them (Oled-display.net, 2012). In addition, the flexibility of OLED allowed it to be manufactured in various designs (Oled-display.net, 2012).In addition, OLED lighting is more stable than that of ordinary lighting. Compared to LED or conventional fluorescent lamps, OLED lighting is more comfortable for viewing (Oled-display.net, 2012). Figure 2.11 shows the OLED bulbs in a room.

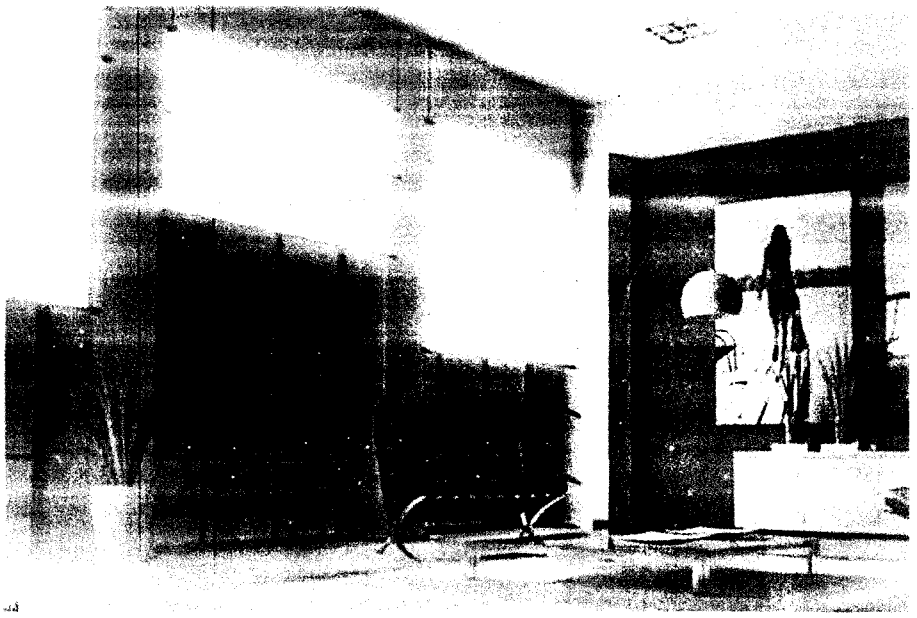

Figure 2.11: OLED bulbs in a room (Oled-display.net, 2012).

2.5 Researcher's Studies

In recent years, the interest of studying hybrid organic / inorganic nanostructures has been increasing due to possibility of combining the electrical properties of semiconductor organic polymers with the optical peculiarities of inorganic nanoparticles (Agostiano et al., 2004). Organic polymer / inorganic nanoparticles composites have been increasingly studied because of their enhanced optical and electrical properties (Kim et al., 2000). Nanomaterials exhibit special electrical, optical, and magnetic properties that differ from those of atoms and bulk. The unique properties of nanomaterials are caused by quantum-confinement or surface effects that become operative on that scale (Wen et al., 2007). However, the organic polymer-inorganic nanocomposites showed inhomogenities related with nanoparticles agglomeration, and therefore it was difficult to know accurately how the nanoparticles affected the conjugated polymer (Yoon et al., 2004).

Previous researches have studied the performance of organic polymer / inorganic nanoparticles composites for different kinds of devices such as polymer light emitting diodes (PLEDs), organic field effect transistors (OFETs), light emitting organic field effect transistors (LE-OFETs), solar cell, memory device, and diodes. Among these devices, PLEDs and solar cell are more commonly studied by researchers. Previous researchers have incorporated different nanoparticles into polymer matrices to study the interaction between the nanomaterials and matrix. The development of nanotechnology has gainedan increasing interest because nanomaterials exhibit special electrical, optical, and magnetic properties that differ from those of atoms and bulk (Wen et. al., 2007).

Solar cell or photo voltaic cell is the most common device used to study the effect of nanoparticles on the conjugated polymer. In solar cell, charge recombination of the photogenerated electron-hole pairs is the major bottleneck in the use of conjugated polymers. In order to overcome this limitation, organic polymers have been combined with oxide nanoparticles. In this blend, the organic polymers act as electron donor and the inorganic nanoparticles as electron acceptor (Agostiano et al., 2004). Besides that, previous researchers also mixed metallic nanoparticles with conjugated polymer in order to enhance the charge transport properties and the control of optical properties by selection of suitable size. The metallic nanoparticles will increase the electrical conductivity of composite layer which will lead to the enhancement of efficiency (Chin et al., 2008). Metallic nanoparticles also exhibit localized surface plasmon resonance (LSPR) property (Chin et al., 2008). This effect can create strong near-field electromagnetic fields and far-field propagating waves, which could be used for enhancement of light absorption of active layer (Qian et al., 2011). Also, nanoparticles of inorganic semiconductors are also incorporated as good electron acceptors from the polymers because they possess elevate carrier mobilities and high electron affinity which can favorably combine with low ionization potential of conjugated polymers (Cosma et al., 2008). The combining of organic polymers and nanoparticles enables the formation of percolation pathways for electron transport (Cosma et al., 2008).

PLEDs are also another common device used to study the effect of nanoparticles on the conjugated polymer. PLEDs were first reported in 1990 using poly(phenylenevinylene) (PPV) as the light emitting materials (Kim et al., 2000). Organic conjugated polymer such as PPV and its derivatives have shown many advantages for PLEDs because of their high fluorescence efficiency and their good

processibility (Park et al., 2007). In PLEDs, photoluminescence emission efficiency is a key factor (Zhang et al., 2001). Therefore, to improve the optical and electronic properties of PPV, a feasible way is to combine PPV with inorganic nanoparticles (Zhang et al., 2001). For example, the incorporation of SiO_2 nanoparticles into PPV can be used to tune the luminescent properties of PLEDs by adjusting the conjugated length of PPV (Zhang et al., 2001). However, the widespread adoption of conjugated polymer-based devices is limited by their short lifetime due to the rapid photo-oxidation of the films under ambient conditions (Park et al., 2002). In PLEDs, the conjugated polymers are inherently susceptible to oxygen and moisture (Yoon et al., 2004). Hence, understanding the effects of photo-oxidation in conjugated polymer films is necessary in order to optimize the performance of the devices (Park et al., 2002).

Previous researchers have also used organic field effect transistors (OFETs) devices to study the effect of nanoparticles on the conjugated polymer. Organic conjugated polymer usually exhibit high on/off ratios in OFETs but has lower mobilities (Cumings et al., 2011). In contrast, carbon-based materials such as graphene and carbon nanotubes (CNTs) exhibit very high mobility but usually have lower on/off ratio (Cumings et al., 2011). Therefore, previous researchers have developed composite thin-films containing both organic conjugated polymer and graphene flakes in order to enhance effective mobility in OFETs (Cumings et al., 2011). Besides that, previous researchers have also incorporated oxide nanoparticles such as ZnO nanoparticles into conjugated polymer in order to improve the mobility of the devices (Navan et. al., 2011).

Organic memory device is also another device that has gained the interest of many researchers. By incorporating the metallic nanoparticles into conjugated polymer,

the operating voltages of the device will be lowered and the write/erase times will become faster (Macbrook et al., 2008). Besides that, several reports on the use of nanoparticles embedded in conjugated polymer as an organic capacitor exhibit memory effect (Aw et al., 2011).

In addition, previous researchers have also studied the organic polymer / inorganic nanoparticles composites using LE-OFET. Compared to the other devices, nanofiber and LE-OFET are less studied by researchers. As for LE-OFET, it was reported that the concentration of the oxide nanoparticles added will affect the mobility of charge carriers (Aleshin et al., 2011).

2.5.1 The Incorporation of Nanoparticles

Previous researchers have incorporated varies kind of nanoparticles into conjugated polymer in order to study their effect on the performance of devices. Among the nanoparticles, oxide nanoaparticles are the earliest and most studied by previous researchers since year 1997. Started from year 2002, metallic nanoparticles have gained the attention of researchers. Besides oxide and metallic nanoparticles, carbon and semiconducting nanoparticles were also studied by previous researchers. However, both of these nanoparticles are not much explored by previous researchers. Table 2.2 shows the studies of effects of nanoparticles on the performance of organic devices.

Table 2.2: The Effects of Nanoparticles on the Performance of Organic Devices.

Author	Device	Nanoparticles	Results
Carter et al., 1997	PLEDs	Titanium Oxide (TiO_2) and Silicon Oxide (SiO_2)	▪ Incorporation of the nanoparticles inside MEH-PPV thin film results in order of magnitude increases in current and luminance output.
Agostiano et al., 2004	Solar Cell	Titanium Oxide (TiO_2)	▪ A significant fluorescence quenching of MEH-PPV / TiO_2nanorods hetero-junctions is observed. This shown an efficient transfer of the photogenerated electrons from the organic semiconductor to the nanocrystals.
Yang et al., 2007	PLEDs	Silicon Oxide (SiO_2) and Titanium Oxide (TiO_2)	▪ It is shown that the conjugation length of MEH-PPV is not affected by the presence of the particles. ▪ It also shown that the studied composites present a higher stability in emission characteristics compared to bare polymer films.
Cuong et al., 2008	Solar Cell	Zinc Oxide (ZnO)	▪ PL measurements show a remarkable blue shift in the luminescence spectra upon addition of the ZnO nanoparticles. ▪ Raman spectroscopy indicates that the conjugation length and the chemical structure of MEH-PPV are unaffected by the incorporation of ZnO nanoparticles up to 16 wt%.

Table 2.2(continued): The Effects of Nanoparticles on the Performance of Organic Devices.

Uthirakumar et al., 2008	PLEDs	Zinc Oxide (ZnO)	▪ By employing different ratio of ZnO composites with respect to fluorescent polymer, the PL emission efficiency showed a significant enhancement. ▪ The fabricated devices showed better improvement in stability and lifetime.
Wang et al., 2008	Solar Cell	Titanium Oxide (TiO_2)	▪ For PPV / TiO_2 composite prepared by direct mixing, there is severe aggregation of the TiO_2 nanoparticles. ▪ On the contrary, the composite prepared by sol-gel method shows a nanosized phase separation. This composite also show the improved photovoltaic performance.
Yang et al., 2010	Organic Field Effect Transistors (OFETs)	Titanium Oxide (TiO_2)	▪ From SEM and AFM images, it is shown that the surfaces of the TiO_2 nanoparticles are compatible with PVP, providing homogeneous polymer / nanoparticles blend. ▪ The leakage current of the composite also has been increased.
Aw et al., 2011	Memory Device	Zinc Oxide (ZnO)	▪ A capacitor-based organic memory device can be realized using a simple solution based fabrication technique. ▪ This device can be programmed and erased similar to a flash-memory.

Table 2.2(continued): The Effects of Nanoparticles on the Performance of Organic Devices.

Navan et al., 2011	Organic Field Effect Transistors (OFETs)	Zinc Oxide (ZnO)	▪ It has been reported that the mobility enhancement of p-type of organic transistors formed using P3HT when ZnO nanostructures are dispersed into it. ▪ OFET based on this structure show a mobility enhancement of more than 60%.
Yang et al., 2011	Solar Cell	Iron Oxide (Fe_3O_4)	▪ The power conversion efficiency (PCE) of the P3HT: PCBM / $Fe_3O_4$is enhanced by ~ 18%.
Lee et al., 2009	Solar Cell	Fullerene (C_{60})	▪ Charge transport was studied in composites of MEH-PPV and low concentration of fullerene (C_{60}) below the percolation threshold. ▪ The electron mobility showed a linear increase with the fullerene concentration while the hole mobility was insensitive.
Cuming et al., 2011	Organic Field Effect Transistors (OFETs)	Graphene	▪ Based on the result, it is shown that effective mobilities of polymer / graphene hybrid FETs can be significantly higher than that of a pure polymer FET. ▪ However, when the concentration of graphene was increased by 4 times, the effect mobility was reduced. This is because the high density graphene flakes in the organic semiconductor layer resulted in a more disorder film.

Table 2.2(continued): The Effects of Nanoparticles on the Performance of Organic Devices.

Cosma et al., 2008	Solar Cell	CdS	▪ The luminescence quenching of MEH-PPV was observed on both solution and thin film. ▪ Chronoamperometric measurements of dispersed heterojunctions showed higher photoactivity compared to the single component, due to presence of great number of interfaces which enhanced charge transfer.
Bredol et al., 2009	Solar Cell	ZnS	▪ The P3HT / ZnS composite devices showed a very high value for V_{oc} and short circuit current density, I_{sc}. ▪ However, some of the devices failed to operate or lower PCE due to the bad quality of the interface between active layer and aluminum electrode.
Kim et al., 2007	Solar Cell	Silver (Ag)	▪ The absorption maximum of MEH-PPV / Ag film was much higher than that of the MEH-PPV film, indicating that the Ag nanoparticles induced an absorption enhancement compared to MEH-PPV.
Wen et al., 2007	PLEDs	Gold (Au)	▪ Incorporating of Au nanoparticles into HY-PPV film enhances the electroluminescence efficiency of HY-PPV based PLED. ▪ Blue-shifts in the emission spectra and a decrease in capacitance of the emitting layer were observed.

Table 2.2(continued): The Effects of Nanoparticles on the Performance of Organic Devices.

Chin et al., 2008	Solar Cell	Gold (Au)	▪ From the result, it is shown that increase of the PCE is mainly attributed to the enhancement of photocurrent, both the fill factor and open circuit voltage of photovoltaic device were not sensitive to the concentration of gold nanoparticles. ▪ The enhanced absorption was observed in the 520-550 nm range, which brings improvements of the photocurrent and PCE for the devices.
Park et al., 2010	PLEDs	Silver (Ag)	▪ Incorporation of Ag nanoparticles in PPV resulted in an increase of current density, ▪ The UPS spectra show that Ag nanoparticles modify the electron energy band structure.
Kochergin et al., 2011	Solar Cell	Silver (Ag), Gold (Au) and Aluminum (Al)	▪ Based on the results, Al nanoparticles are more superior to Ag and Au nanoparticles in enhancing the light absorption in organic photovoltaic cell. Thus, Al nanoparticles bring more improvements in conversion efficiency of the devices. ▪ This is because the higher plasma frequency of Al ensures a better overlap between Plasmon resonance and absorption band of semiconductors.

2.5.2 Organic Solvent Used

In year 2001, Liu et al. reported that the photovoltaic devices fabricated with tetrahydrofuran (THF) or chloroform (non-aromatic solvents) have smaller photocurrents under same reverse bias as well as higher open circuit voltages compared to the devices fabricated with xylene, dichlorobenzene (DCB), or chlorobenzene (CB) (aromatic solvents) (Liu et. al., 2001). This is because salvation induced morphology effects will result in different arrangements (polymer conformations) of the polymer chains (Liu et. al., 2001). For aromatic solvents such as xylene, the solvent molecules tend to solvate the π-electron conjugated segments and result in a conformation which has better π-π stacking and subsequently better electrical conduction (Liu et. al., 2001). On the other hand, non-aromatic solvents such as THF will tend to solvate the non-conjugated segments of the polymer and result in a polymer conformation with a lower electrical conductivity (Liu et. al., 2001).

In this paper, spin coating is used to fabricate the MEH-PPV thin film on the glass substrate. Spin coating has been demonstrated to be an easy and low cost fabrication process for polymer electronic devices with good device performance (Sirringhaus et al., 2004). The widely used spin coating process will significantly lower mobilities as compared with solution-cast desposition. This is closely related to the limited time available for chain alignment forced by the rapid drying of solvent (Sirringhaus et al., 2004). In year 2004, Sirringhaus et al. found that, by using higher boiling point solvents such as 1,2,3-trichlorobenzene (TCB) instead of chloroform for spin coating, P3HT transistors with mobilities higher than $0.1 cm^2/(V\ s)$ and large on:off current ratio of 10^6 can be achieved (Sirringhaus et al., 2004). This is because slower solvent evaporation speed helps the growth of a highly crystalline film and the

interchain interactions become stronger. Thus, the electrical conductivities will be improved significantly (Sirringhaus et al., 2004).

2.5.3 Review Studies on Polymer Light Emitting Diodes (PLEDs)

In this paper, our work is more focusing on polymer light emitting diodes (PLEDs). In 1990, the Cambridge group of Friend had announced that they had achieved green-yellow EL using PPV in a single-layer structure (Bernius et al., 2000). PPV was used as a semiconducting layer sandwiched between metallic electrodes, as shown in Figure 2.12. In 1991, Heeger and co-workers at the University of California at Santa Barbara announced the EL application of a soluble derivative of PPV, namely MEH-PPV (Bernius et al., 2000). Compared to PPV, MEH-PPV offered the advantage of soluble in conjugated form in organic solvent due to its dialkoxy side chain (Friend[b] et al, 1999).

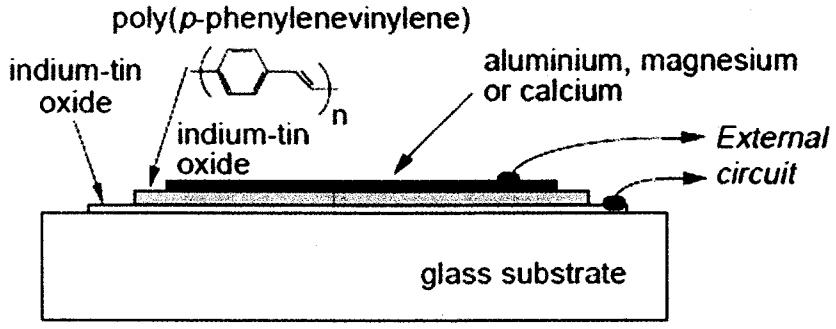

Figure 2.12: Device structure of a single layer polymer electroluminescent diode.

Various types of nanoparticles can be used to enhance the performance of PLEDs. Among them, oxide nanoparticles are more commonly employed. The polymer

composite light emitting device was first studied by Carter et al. in year 1997. Carter et al. (1997) reported that incorporating insulating oxide nanoparticles such as TiO_2 and SiO_2 nanoparticles into electroluminescent polymer resulted in increased current densities, radiances and power efficiencies in the devices, as shown in Figure 2.13.

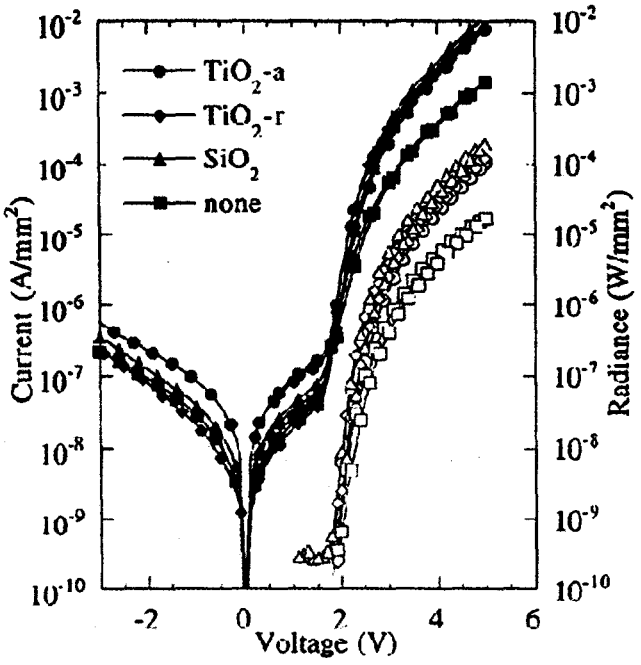

Figure 2.13: Current-voltage and radiance-voltage curves for 1:1 TiO_2 (anatase)/MEH-PPV (circles), 1:1 TiO_2 (rutile)/MEH-PPV (diamonds), 1:1 SiO_2/MEH-PPV (triangles) and for MEH-PPV film with no nanoparticles (square) (Carter et al., 1997).

In year 2008, Uthirakumar et al. reported that an incorporation of few weight percentage of zinc oxide (ZnO) into the fluorescent polymer showed better improvement in stability and lifetime of the devices. Based on the Thermogravimetric analysis (TGA)curves in Figure 2.14, the weight loss is decreased as the weight percentage of ZnO is increased (Uthirakumar et al., 2008).

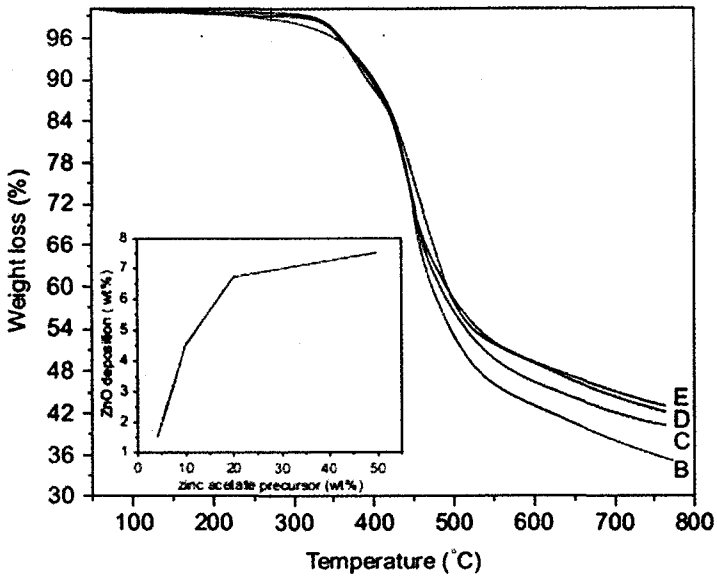

Figure 2.14: TGA curves of fluorescent polymer with different weight fractions of ZnO content. The values of the ZnO content are 1.5%, 4.5%, 6.7% and 7.5% for samples B, C, D, and E (Uthirakumar et al., 2008).

Meanwhile, size and dispersion of the nanoparticles in the conjugated polymer will also affect their performance. In year 2004, Yoon[a] et al. reported that PPV with 20nm SiO_2 nanoparticles produced higher current output than PPV with 5 nm SiO_2nanoparticles,as shown in Figure 2.15. Also in the same year, Yoon[b] et al. reported that the PPV/TiO_2nanocomposite prepared by the particulate sol processing had much better dispersion of nanoparticles than that prepared by the conventional processing. The composites with well-dispersed nanoparticles resulted in enhanced current density and radiance, as shown in Figure 2.16.

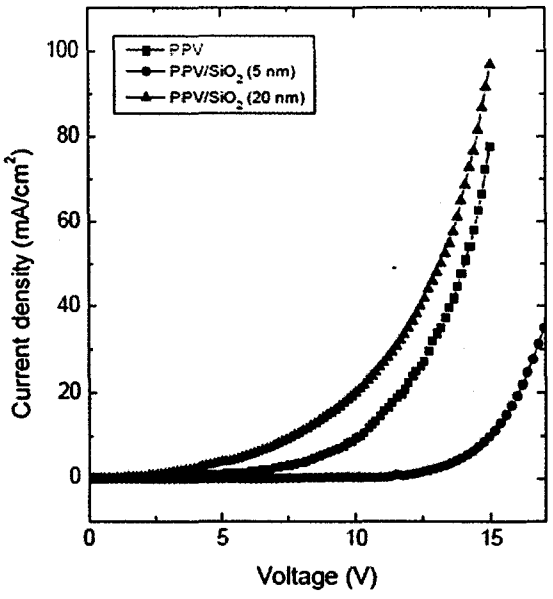

Figure 2.15: Current-voltage characteristics for PPV (squares), PPV/SiO_2 (5 nm) and PPV/SiO_2 (20 nm) (Yoon[a] et al., 2004).

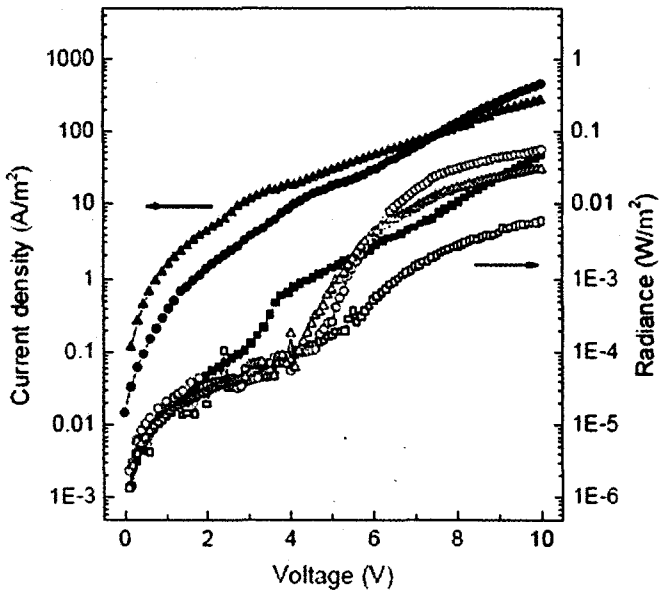

Figure 2.16: Current-voltage and radiance-voltage characteristics for PPV (squares), PPV/TiO_2nanopowder (circles), and PPV/TiO_2 particulate sol (triangles) (Yoon[b] et al., 2004).

Despite many studies have shown that incorporating oxide nanoparticles such as TiO_2 nanoparticles can enhanced the electrical and optical properties of PLEDs, there is a drawback too. In year 2012, Nguyen et al. reported that high concentration of ZnO nanoparticles in MEH-PPV showed a drastic decrease in lifetime compared to composite with low concentration, as shown in Figure 2.17. Therefore, composition of nanoparticles used is critical to the performance of devices.

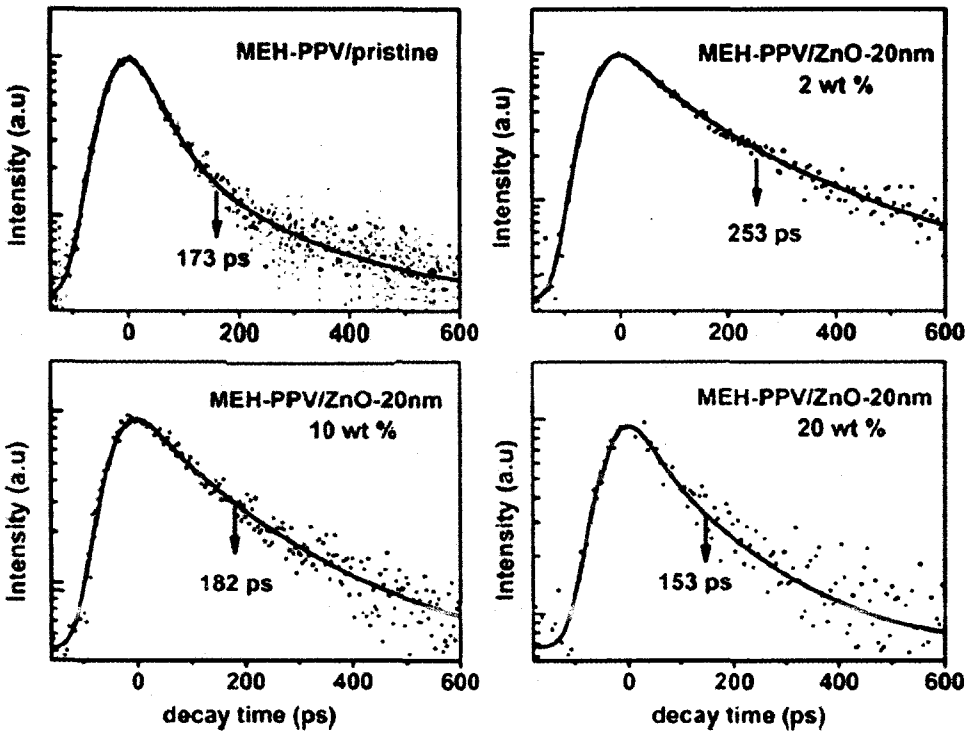

Figure 2.17: Time-resolved PL kinetics (excitation: 267nm) of (a) pristine MEH-PPV and composites containing (b) 2% (c) 10% (d) 20% ZnO 20nm nanoparticles (Nguyen et al., 2012).

Beside oxide nanoparticles, metal nanoparticles such as gold (Au) and silver (Ag) are also being adopted (Park et al., 2010). In year 2010, Park et al. reported that the incorporation of Ag nanoparticles into PPV can result in an enhancement of current density due to an increase in the electron affinity with Ag nanoparticles content, as

shown in Figure 2.18. Furthermore, roughening of the surface morphology was observed with incorporation of Ag nanoparticles (Park et al., 2010).

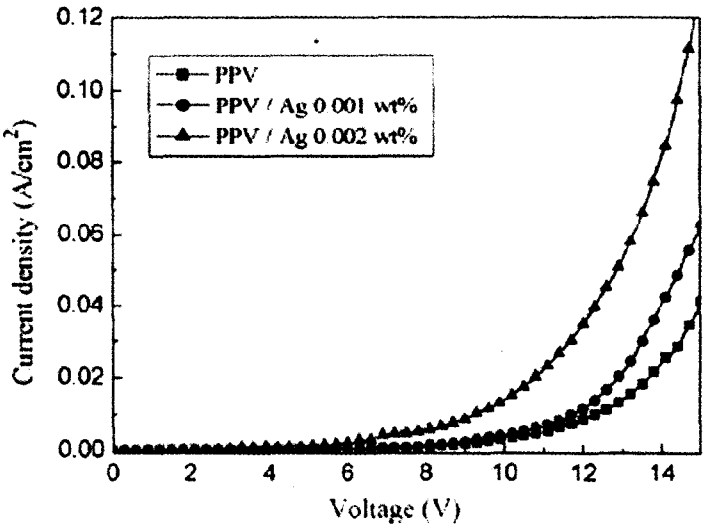

Figure 2.18: Current-voltage curves for the PPV and PPV/Ag nanocomposite films (Park et al., 2010).

CHAPTER 3

METHODOLOGY

3.0 Poly[2-methoxy-5-(2'-ethylhexyloxy)-1,4-phenylenevinylene] (MEH-PPV)

3.1 Introduction

In this chapter, materials, equipment and methodology used will be described. In this project, the experiment was divided into three parts. Table 3.1 shows the parts of the experiment and their description.

Table 3.1: Description of the parts of experiment.

No.	Experiment	Description
1	Dispersion of Nanoparticles	Different weight percentage of aluminum (Al) and silver (Ag) nanoparticles were spin-coated on glass substrate. The weight percentage of nanoparticles which has better dispersion on substrate will be selected for final device fabrication.
2	Concentration of MEH-PPV	Different concentrations of MEH-PPV solution were prepared and spin-coated on glass substrate. The concentration of MEH-PPV which has better electrical properties will be selected for final device fabrication.
3	Final Devices	In this part of experiment, the nanoparticles were incorporated into MEH-PPV solution to form the active layer. The concentrations of nanoparticles and MEH-PPV used were chosen based on the results of previous experiments.

Experimental setup such as substrate preparation, solution preparation, spin coat and electrode coating will be discussed. Samples with different parameters were prepared. The substrate used is glass, with dimension of 1 cm x 1 cm. Aluminum (Al) was thermal evaporated and coated on the glass as an anode. The active layer is formed from MEH-PPV with or without nanoparticles, which is spin-coated on the glass substrate. Lastly, the Al electrodes are coated on the layer as a cathode. Figure 3.1 shows the structure of samples fabricated.

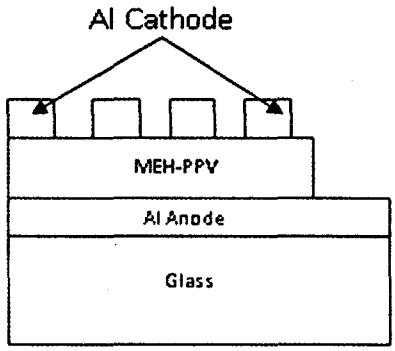

Figure 3.1: Structure of samples fabricated.

The raw material and samples were submitted to physical and electrical characterization. Physical characterizations include Scanning Electron Microscope (SEM), Energy Dispersive X-ray spectroscopy (EDX), Atomic Force Microscope (AFM) and Fourier Transform Infrared Spectroscopy (FTIR). Meanwhile, the electrical characterization carried out is Current-Voltage (I-V) characterization. Figure 3.2 shows simplified flow chart of the methodology of this project.

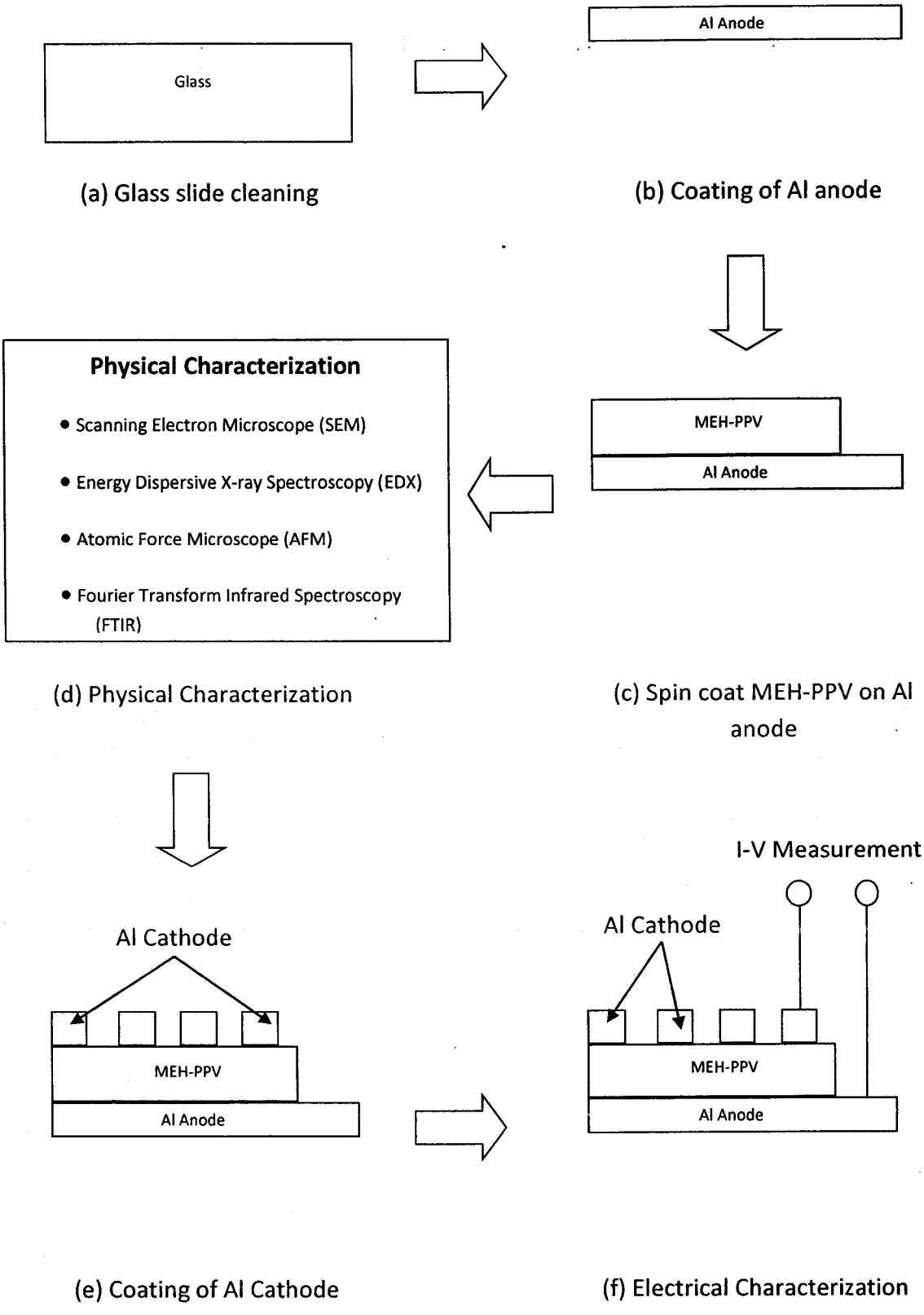

Figure 3.2: Simplified flow chart of sample fabrication.

3.2 Materials and Chemicals

Materials and chemicals used in this project are listed as below:

i. Superior quality microscope slides (25.4 x 76.2 mm (1" x 3"), 1 mm – 1.2 mm thick)

ii. J.T. Baker Acetone, 99-100% purity

iii. Ethanol, 95% purity

iv. Sigma Aldrich MEH-PPV powder

v. MTI Corporation Aluminum (Al) Nanopowder

vi. MTI Corporation Silver (Ag) Nanopowder

vii. BDH Chlorobenzene

viii. Ionized water

ix. Alfa AesarAluminum Wire (1 mm diameter), 99.99%

3.3 Equipment

Tools and equipments which are used in this project are listed as below:

i. Sartorius Weight Balance

ii. BRANSON 1510 Ultrasonic Cleaning Machine

iii. Cookson Electronics Equipment, SCS G3P-12 Spin Coater

iv. EDWARDS AUTO306 Thermal Evaporator

v. KEITHLEY 420-SCS Semiconductor Characterization System

vi. KHinD OT 2502 Oven

vii. Perkin Elmer Spectrum One FTIR System

viii. Nano Navi SPI 3800N AFM

ix. ZEISS SUPRA 35 VP SEM

x. ZEISS SUPRA 35 VP EDX

xi. Diamond Cutter

xii. Glass Beaker

xiii. Pipette

xiv. Wire Tape

xv. Tweezers

xvi. Aluminium Foils

3.4 Experimental Setup

3.4.1 Substrate Preparation

In this project, glass slides were used as substrate of the device. The glass was cut into dimension of 1 cm x 1 cm to be used as the substrate. Firstly, required dimension of glass slide was printed on a white paper. The glass is put on top of the paper and ruler was placed on top of glass. The ruler was aligned to the dimension of the printed paper. Diamond cutter was used to draw lines on the glass into required dimension by using ruler as a guide. To break the glass into required dimension, pressure was applied softly using hand.

After cutting, glass slides were cleaned prior to the next step. Solvent such as ethanol was used to remove the contaminants (e.g. oils and organic residues) from the surface of glass slides. Glass slides were placed in holder and put into a beaker. Then, ethanol was poured into the beaker until all the glass slides were immersed inside it. After that, the beaker was put into ultrasonic machine to perform ultrasonic bath for 30

minutes. After 30 minutes, the holder was removed from ethanol and placed in deionised water for another 10 minutes in ultrasonic bath. The glass slides were then dried by blowing them using air-gun. To ensure the glass slides had dried completely, they were baked in oven at temperature of 100°C for 1 hour.

3.4.2 Solution Preparation

In this project, chlorobenzene was used as the solvent. For the first part, different weight percentage of Aluminum (Al) nanoparticles and Silver (Ag) nanoparticles dispersed on glass substrate were prepared in order to determine dispersion of the nanoparticles on glass substrate. The weight percentage used for both of the nanoparticles were 0.025 wt%, 0.050 wt%, 0.10 wt%, 0.15 wt%, 0.20 wt% and 0.25 wt%. To calculate the weight of nanoparticles need in 1 ml of chlorobenzene for different weight percentage of solutions, the following equation 3.1 can be used.

$$\text{Weight Percentage (wt \%)} = \frac{\text{Weightofsolute}}{\text{Weightofsolution}} \times 100\% \text{ ---------- (3.1)}$$

Based on equation 3.1, weight of solute is the total weight of nanoparticles required. Weight of solution is the total weight of chlorobenzene and nanoparticles.

After the weight of nanoparticles required was determined, the nanoparticles were weighed using a balance. Firstly, the weight of small bottle was measured. Then, nanoparticles were added into the small bottle until the required weight was obtained. After that, 1 ml of chlorobenzene was measured using pipette and then added into the small bottles. Small bottles were placed in ultrasonic machine to perform

ultrasonication for 2 hours to disperse the nanoparticles. During the ultrasonication, ice was added into the medium of the ultrasonic machine to prevent oxidation of the nanoparticles. After 2 hours, the solutions were used for next step which is spin coating.

For the second part, chlorobenzene was used to dissolve MEH-PPV. Four solutions with different concentrations of MEH-PPV (4 mg/ml, 6 mg/ml, 8 mg/ml and 12 mg/ml) were prepared in order to investigate the effect of concentrations on performance of the devices. The weight of MEH-PPV powders required were 4 mg/ml, 6 mg/ml, 8 mg/ml and 12 mg/ml. To obtain these weights, the weight of small bottles was measured using a balance. Then, the MEH-PPV powders were poured into the small bottles until the required weights were obtained. After that, 1 ml of chlorobenzene was measured using pipette and then added into the small bottles. The small bottles were placed in ultrasonic machine for 2 hours. During ultrasonication, ice was also added in order to prevent the damage on the polymer from the heat generated by ultrasonic. After 2 hours, the solutions were used for the next step which is spin coating.

For the last part, aluminum (Al) and silver (Ag) nanoparticles need to be added into a solution of 12 mg/ml. The solutions were prepared by the similar procedure as mentioned above. When the solutions were prepared, they were mixed with Al and Ag with different weight percentage (0.025 wt%, 0.05 wt% and 0.10 wt%). After adding in the nanoparticles, the mixtures were placed in ultrasonic bath for 2 hours.

3.4.3 Spin Coating

Before spin coating was started, setting of spin coater needed to be performed. The setting of spinning speed is 1000 revolutions per minute (rpm) for 15 seconds followed by 2000 rpm for 60 seconds. The spinning speed was same for all of the samples. Motor of spin coater was turned on for 1 minute before spinning so that spin coater can be warmed up. Glass slide was placed at the center of spin coater. Then, solution was dropped on top of the glass slide. The solution need to cover whole surface of the glass slide. For sample that required masking, wire tape can be used to cover the masking area. After that, "Start" button was pressed to begin spinning. When spinning was completed, the sample coated was subjected to next steps.

3.4.4 Electrode Coating

Turbo evaporator was used to perform thermal evaporation of electrode. Anode was coated on the surface of glass substrate while cathode was coated on top of MEH-PPV active layer. The material used for electrode was Aluminum (Al). To obtain required thickness, 0.1 g Al wire was cut and weighed on a balance. The prepared Al wire was then washed with acetone followed by deionised water and then dried completely using air gun. After dried, the prepared Al wire was put onto a tungsten basket which acts as holder. Meanwhile, the sample stage was also washed with acetone to remove contaminants followed by Decon 90 to remove metallic residues. After the sample stage was dried, samples were attached on it using tape.

After the samples and Al wire were loaded into the evaporator, the dome of evaporator was covered and then pumped into vacuum condition. Pressure was pumped down to approximately 4 x 10^{-5}Torr. When reached required pressure, current was increased slowly to melt the Al wire. The melted Al wire will be evaporated and coated on the samples. Once the samples have been coated completely, the operation would stop and the vacuum was turned off. After the dome was opened, the samples were removed from the sample stage and kept in container.

3.5 Porphyrin and Cu- Porphyrin

All reagents used in this research were analytical grade. Both 2, 3, 7, 8, 12, 13, 17, 18 – Octaethyl - 21H .23H - porphine Cu(II) (Cu-porphyrin) and 2, 3, 7, 8, 12, 13, 17, 18 – Octaethyl - 21H .23H - porphine (porphyrin) were diluted in chloroform with concentration of 0.1 mg/ml, 0.5 mg/ml, 1.0 mg/ml, 5.0 mg/ml and 10.0 mg/ml. An aluminum source and drain with the thickness of 100 nm were deposited on top of the cleaned glass substrate through thermal evaporation and the gap distance of these metal electrodes were prepared through photolithography. Then, the porphyrin solutions were drop-casted on top of the aluminum electrodes, forming a layer of organic thin film. Gap distance of the aluminum source and drain were measured using optical microscope (OM). Scanning electron microscope (SEM) was used to analyze the surface morphology of the organic thin film. Finally, electrical properties of these organic devices were characterized using current-voltage (I-V) test.

3.6 bis{2-alkyl-(S)-(+)-2-(6-[4-4-decyloxyphenylazo)-benzoyloxy]-2-naphthyl)propinate} (azo)

i) Synthesis of Azo Materials:

All the chemicals were obtained from Sigma Aldrich Chemicals (St. Louis, MO, USA) and Merck (Darmstadt, Germany) except for (S)-(C)-2-(6-methoxy-2-naphthyl)propionic acid which was purchased from Tokyo Chemical Industry (Chuo, Tokyo, Japan). The synthesizing of azo materials of all intermediates 1–5 and corresponding dimers 6a–6e were carried out based on the procedures as shown in Fig.1.

A) Synthesis of 4-(4-hydroxyphenylazo)benzonitrile

4-Cyanoaniline was dissolved in a mixture of hydrochloric acid and water with the ratio of 1:1. The reaction mixture was cooled in a stirred ice bath and diazotized by slow addition of a solution of sodium nitrite in water at temperature below 5°C. 10% of sodium hydroxide solution was used to dissolve phenol and cooled to 5°C. The reaction mixture was stirred prior to the addition of cold diazonium salt solution. The mixture was kept in an ice bath. Upon reaction completion, the mixture was poured into water and acidified with aqueous hydrochloric acid, whereupon the orange colour product was obtained. The crude product was filtered and washed with water. The product was orange-red in colour and dried in vacuum oven at 60◦C for 24 h (yield 66%).

B) Synthesis of 4-(4-(7decyloxy) phenylazo)benzonitrile (2a)

4-(4-(7-decyloxy)phenylazo)benzonitrile was synthesized by suspension of 4-(4-hydroxyphenylazo) benzonitrile, anhydrous K_2CO_3 and KI in dry DMF. The reaction was carried out for 24 h at 90◦ C. 1-Bromodecane was added drop wise to the reaction mixture and was refluxed for 24 h. Upon completion of the reaction, the mixture was

filtered and washed with excess of DMF. The filtrate was poured into ice water, extracted using diethyl ether and dried with anhydrous sodium sulphate. The solvent was removed under vacuum and purified by column chromatography (silica gel, chloroform). An orange-coloured solid was obtained with 75% yield.

C) Synthesis of 4-(4-(7-decyloxy)phenylazo)benzoic acid (3a)

A mixture of 4-(4-(7-decyloxy) phenylazo) benzonitrile, potassium hydroxide and ethanol was refluxed for 4h. The reaction mixture was poured into water and acidified with aqueous hydrochloric acid. The crude product was filtered and washed with water. The crude product was recrystallized from ethanol (yield 95%).

D) Synthesis of bis{2-heptyl-(S)-(+)-2-(6-methoxy-2-naphthyl)- propionate}(4a)

(S)-(+)-2-(6-Methoxy-2-naphthyl) propionic acid, 1,6-hexanediol and DMAP were added in dry dichloromethane. Then, DCC was added before the mixture was stirred at room temperature for 3h. The precipitate formed was obtained by filtration. The solution was washed with 5% acetic acid, followed by saturated NaCl and water. The organic layer was dried over anhydrous $MgSO_4$ and filtered. The solvent was stripped out under reduced pressure. The product was purified by column chromatography using dichloromethane as eluent and recrystallised using ethanol where white solid were obtained (yield 92%). The similar procedure was used for the preparation of compounds 4a–4e.

E) Synthesis of bis{2-heptyl-(S)-(+)-2-(6-hydroxy-2-naphthyl)propionate}(5a)

Bis{2-hexyl-(S)-(+)-2-(6-methoxy-2-naphthyl)propionate} was dissolved in dry dichloromethane and cooled to -20°C. BBr_3 was added slowly under inert atmosphere under stirring condition. The reaction was monitored by TLC. Dichloromethane was

added upon completion of reaction. The solution was poured into ice-cold saturated NH_4Cl solution. The mixture was stirred and the organic layer was washed with saturated NaCl solution, water and dried over anhydrous $MgSO_4$ and filtered. The solvent was stripped out under reduced pressure. The product was purified by column chromatography using dichloromethane and ethylacetate (5:1) mixture which gave white solid (yield 81%). The similar procedure was adopted for the preparation of compounds 5b–5e.

F) Synthesis of bis{2-hexyl-(S)-(+)-2-(6-[4-4-deccyloxyphenylazo)benzoyloxy]-2-naphthyl)-propinate} (6a)

Compound 5a, 4-(4-(7-decyloxy) phenylazo) benzoic acid and DCC were added in dry dichloromethane. Next, DMAP was added and the mixture was stirred at room temperature for overnight before the precipitated materials were removed by filtration. The solvent was stripped out under reduced pressure. The product was purified by column chromatography using dichloromethane as eluent and recrystallised using ethanol which gave white solid (yield 86%). The similar procedure was adopted for the preparation of compounds 6b–6e. Purified compounds of 6a-6e were used for device application.

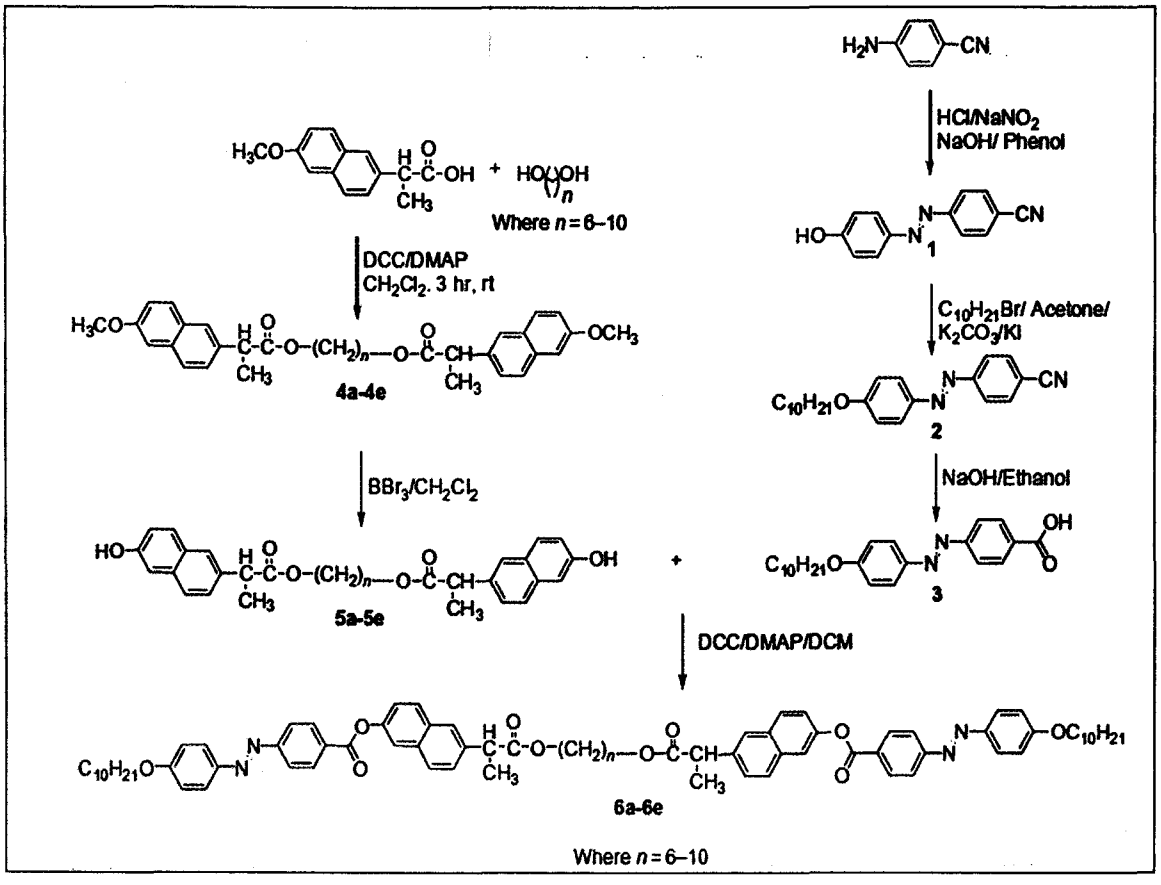

Figure 3.3: Synthetic scheme towards the formation of compounds 6a-6e

ii) Device Fabrication:

Bottom-gate and top-contact OFET was fabricated on a glass substrate as shown in Fig.2. Mixture of extracted natural Aloe vera paste (20 g) from fresh leaves with 1.5 wt% of SiO_2 NPs, acquired commercially from Sigma Aldrich, has been used as dielectric material. Besides, 1.0 mg of azo (7 azo and 9 azo) was dissolved in 1.0 ml chloroform and was used as a semiconductor material. Glass substrates with 1 x 1-cm^2 area were cleaned by using acetone, ethanol and de-ionized water in an ultrasonic bath. The glass substrates were further dried in an oven at 100°C for an hour. Then, 100-nm thick aluminum (Al) layer acting as gate electrode was evaporated (turbo thermal evaporator K950X) on the glass substrate. The extracted natural Aloe vera with 1.5 wt% SiO_2 NPs, acting as the gate dielectric, was then screen printed on top of the aluminum

layer. The screen printing mask was used so that the thickness of the printed dielectric layer will be uniformed. The printed dielectric was dried at room temperature for 30 min before the mask was removed. The samples were further dried at room temperature for another 24 h. The solidified natural Aloe vera blended with 1.5 wt% SiO_2 NPs on aluminum layer was additionally dried in an oven at 40°C for 30 min in order to accomplish the cross-linked reaction in the natural Aloe vera. After that, azo solution was dropped cast on top of the dielectric layer. The samples were placed on the hotplate for heat treatment at 100°C. The samples were then cooled down gradually to room temperature. Azo materials will melt when exposed to heat treatment process and form into crystal when cool it down slowly. Refer Table 1 for the phase transition temperatures and enthalpies for azo materials. Finally, an array of aluminum was thermally evaporated through a shadow mask on top of the semiconductor layer. The array of metal served as top-contact electrode of the device. The channel length (L) and width (W) was 1.7 mm and 2.5 mm, respectively. Output and transfer characteristics of the OFET were performed using a computer controlled Semiconductor Parameter Analyzer (Agilent 4156C) at room temperature.

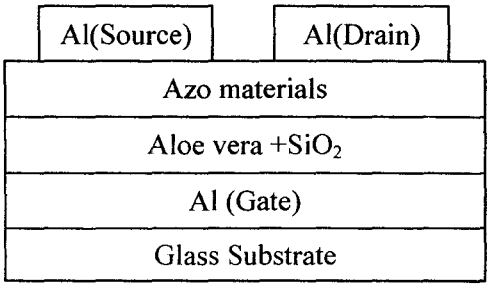

Figure 3.4: Bottom-gate and top-contact OFET

Table 3.2: Phase transition temperatures (°C) and enthalpies [J/g] for azo materials.

Compound	Phase sequence	
	Heating	Cooling
6 (6a)	Cr 107 [30.5] I	I 105 [0.9] N 94a SmA 84 [28.6] Cr
7 (6b)	Cr 105 [32.7] I	I 104 [0.8] N 96a SmA 82 [29.9] Cr
8 (6c)	Cr 103 [46.2] I	I 101 [0.8] N 95a SmA 82 [46.8] Cr
9 (6d)	Cr 104 [44.9] I	I 99 [0.7] N 91a SmA 81 [41.4] Cr
10 (6e)	Cr 103 [39.2] I	I 97 [1.1] N 88a SmA 79 [36.0] Cr

3.7 Fullerene (C60)

Bottom-gate and top-contact OFET was fabricated on a glass substrate. Mixture of extracted natural Aloe vera paste (20 g) from fresh leaves with 1.5 wt% of SiO_2 NPs, acquired commercially from Sigma Aldrich,[51] have been used as dielectric material. Glass substrates with 1 x 1-cm^2 area was cleaned using ethanol and de-ionized water in an ultrasonic bath and dried in an oven at 100°C for an hour. Then, a 100-nm thick aluminum layer acting as gate electrode was evaporated (AUTO 306) on the glass substrate. The extracted natural Aloe vera with 1.5 wt% SiO_2 NPs, acting as the gate dielectric, was then screen printed on top of the aluminum. The screen printing mask was used so that the thickness of the printed dielectric layer can be uniform. The printed dielectric was dried at room temperature for 30 min before the mask was removed. The sample was further dried at room temperature for another 24 h. The solidified natural Aloe vera with 1.5 wt% SiO_2 NPs on aluminum layer was additional dried in an oven at 40°C for 30 min in order to accomplish cross-linked reaction in the natural Aloe vera. After that, a 250-nm thick of C_{60} with 99.9% purity (Sigma-Aldrich) was thermally evaporated as received under high vacuum (4 x 10^{-5} mbar) onto the 226±2 nm thick

dielectric layer. Finally, an array of aluminum, with area of 0.64 mm^2 each, was thermally evaporated through a shadow mask on top of the semiconductor layer. The array of metal served as top-contact electrode of the device. The channel length (L) and width (W) were 0.01 mm and 0.79 mm, respectively. Schematic of the OFET with related dimensions are shown in Fig. 1. Output and transfer characteristics of the OFET were performed using a computer controlled Semiconductor Parameter Analyzer (Agilent 4156C) at room temperature and capacitance-voltage characteristic was measured by a LCR meter (Agilent 4282). The surface energy of dried natural Aloe vera layer and the similar layer with blended SiO_2 was determined by a two-liquid technique with deionized water as a polar solvent and diiodomethane (Sigma-Aldrich and 99.0% purity) as a non-polar solvent with the contact angle between the solid substrate and those liquid measured by a goniometer (Rame-hart 260-F4) and computed by a DROPimage software (Advanced v2.5). The thickness of dielectric layer was measured using a field-emission scanning electron microscope (ZEISS SUPRA 35VP) from a cross-sectional view of the sample. A series of measurements were carried out in the cross-section at 3 difference places for the same sample.

3.8 Physical Characterization

Raw material and substrate which were coated with MEH-PPV had undergone physical characterization such as SEM, EDX, AFM and FTIR.

3.8.1 Scanning Electron Microscope (SEM)

SEM is a type of electron microscopy which is used to investigate sample surface by scanning sample with a high-energy beam of electrons in raster scan pattern. The electrons interact with the atoms and producing signals which contain information about the sample's composition, surface topography and other properties. For the first

part, 12 samples with different weight percentage of Al and Ag nanoparticles (0.025 wt%, 0.050 wt%, 0.10 wt%, 0.15 wt%, 0.20 wt% and 0.25 wt%) were dispersed on glass substrate and subjected to SEM test. The magnifications used were 1 kX, 5 kX, 10 kX, 30 kX and 50 kX. For the second part, 4 samples with different concentration of MEH-PPV (6 mg/ml, 8 mg/ml, 10 mg/ml and 12 mg/ml) were spin-coated on glass substrate and subjected to undergo SEM test. The magnifications used were 500 X, 1 kX, 5 kX, 10 kX and 50 kX. For the last part, 6 samples of added with different weight percentage of Al and Ag (0.025 wt%, 0.050 wt% and 0.10 wt% respectively) were prepared to undergo SEM test. All of the samples were coated with platinum before they can be tested by SEM. Coating with platinum can prevent accumulation of charges on the samples so that clear images can be obtained.

3.8.2 Energy Dispersive X-ray Spectroscopy (EDX)

Energy dispersive X-ray spectroscopy is a relatively simple yet powerful technique used to identify the elemental composition of as little as a cubic micron of material. The equipment is attached to the SEM to allow for elemental information to be gathered about the specimen under investigation. This technique depends on the investigation of an interaction of some source of X-ray excitation and a sample. Each element has a unique atomic structure. Hence, all elements have their unique set of peaks on X-ray spectrum. By analyzing the X-ray spectrum, the elements can be identified.

In this project, 4 samples with different concentrations of MEH-PPV (6 mg/ml, 8 mg/ml, 10 mg/ml and 12 mg/ml) and 6 samples added with different weight percentage of Al and Ag (0.025 wt%, 0.050 wt% and 0.10 wt%) were prepared to under EDX analysis.

3.8.3 Atomic Force Microscope (AFM)

Atomic Force Microscope (AFM) is a very high-resolution type of scanning probe microscopy, with a resolution on the order of nanometer. AFM provides a 3D profile of the surface on a nanoscale, by measuring a sharp probe (<10 nm) and surface at very short distance (0.2 – 10 nm probe and sample separation). In this project, 8 samples were prepared to undergo AFM. These samples were glass slide, sample with 12 mg/mL of MEH-PPV, 6 samples added with different weight percentage of Al and Ag nanoparticles (0.025 wt%, 0.050 wt% and 0.10 wt%). The scanning ranges used for AFM were 5 μm and 10 μm.

3.8.4 Fourier Transform Infrared Spectroscopy (FTIR)

Fourier Transform Infrared Spectroscopy (FTIR) is a technique used to obtain an infrared spectrum of absorption, emission, photoconductivity or Raman scattering of a solid, liquid or gas. In FTIR, infrared (IR) radiation is passed through a sample. Some of the infrared radiation is absorbed by the sample and some of the IR is transmitted. The resulting spectrum represents molecular absorption and transmission creating a molecular fingerprint of the sample. The spectrum obtained can be used to identify unknown materials, determine the quality or consistency of a sample and amount if components in a mixture.

In this project, MEH-PPV powder, 4 samples with different concentrations of MEH-PPV (6 mg/ml, 8 mg/ml, 10 mg/ml and 12 mg/ml), 6 samples added with different weight percentage of Al and Ag nanoparticles (0.025 wt%, 0.050 wt% and 0.10 wt%) had prepared to undergo FTIR. FTIR was performed in transmission mode for all the samples. Scanning time used is 8 times. Minimum and maximum wavelengths used were 400 cm^{-1} and 4000 cm^{-1}.

3.9 Electrical Characterization

Samples with different parameters were subjected to undergo electrical characterization which is Current-Voltage (I-V) measurement. Current-voltage (I-V) measurement could be performed using Precision Semiconductor Parameter Analyzer (SPA). The SPA model used in I-V measurement was KEITHLEY 420-SCS Semiconductor Characterization System. Vacuum system had to be switched on to locate the probe station before measuring. Sample was placed on the stage and then the probe was adjusted to connect with the electrode of sample. It had to be very careful when connecting electrodes with probes because to avoid the probe damage on the sample. This step was aided using stereoscope. Setting for this machine was done before measuring. "Diode" was chosen as tested device. The anode was set to be SMU 1 and the cathode was set to be SMU 3. Sweep mode was used during measuring, starting from -10 volt (V) to 10V. Figure 3.3 shows the schematic diagram of testing setup.

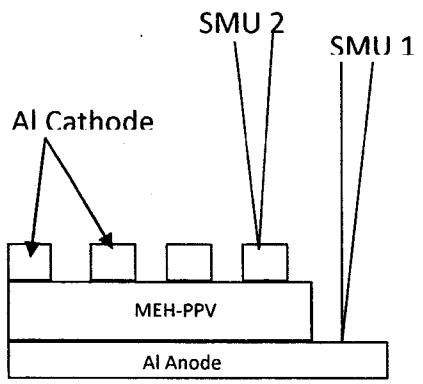

Figure 3.5: Schematic diagram of I-V testing setup.

CHAPTER 4

RESULTS & DISCUSSION

4.0 poly[2-methoxy-5-(2'-ethylhexyloxy)-1,4-phenylenevinylene] (MEH-PPV)

4.1 Introduction

This chapter comprises results of raw materials, physical and electrical characterization. The results were from Scanning Electron Microscopy (SEM), Energy Dispersive X-ray spectroscopy (EDX), Atomic Force Microscope (AFM), Fourier Transform Infrared Spectroscopy (FTIR) and Current-Voltage (I-V) characterization. The results obtained from these characterizations were discussed in this chapter.

4.2 Raw Material Characterization

In this project, SEM was used to characterize the Aluminum (Al) and Silver (Ag) nanoparticles. The magnification used was 50 kX. At this magnification, the shape of the nanoparticles can be observed. Figure 4.1 shows that Al nanoparticles are in spherical shape. However, Al nanoparticles are agglomerated into cluster form. Figure 4.2 shows that Ag nanoparticles are also in spherical shape.

Besides shape, the sizes of nanoparticles can also be determined using SEM. From Figure 4.1, the average size of Al nanoparticles is 66.27 nm. Meanwhile, from Figure 4.2, the average size of Ag nanoparticles is 52.87 nm. According to data sheet provided by supplier (MTI Corporation), Al nanoparticles should have smaller size (18

nm) compared to Ag nanoparticles (50 nm). However, this is in the other way round compared to the measurement taken from SEM. This indicates that Al nanoparticles have been agglomerated more severely due to their smaller particle size which leads to higher surface energy (Cao et al., 2012). Hence, the reduction of overall surface energy can be occurring through combining individual Al nanoparticles to form larger structure in order to reduce the overall surface area (Cao et al., 2012).

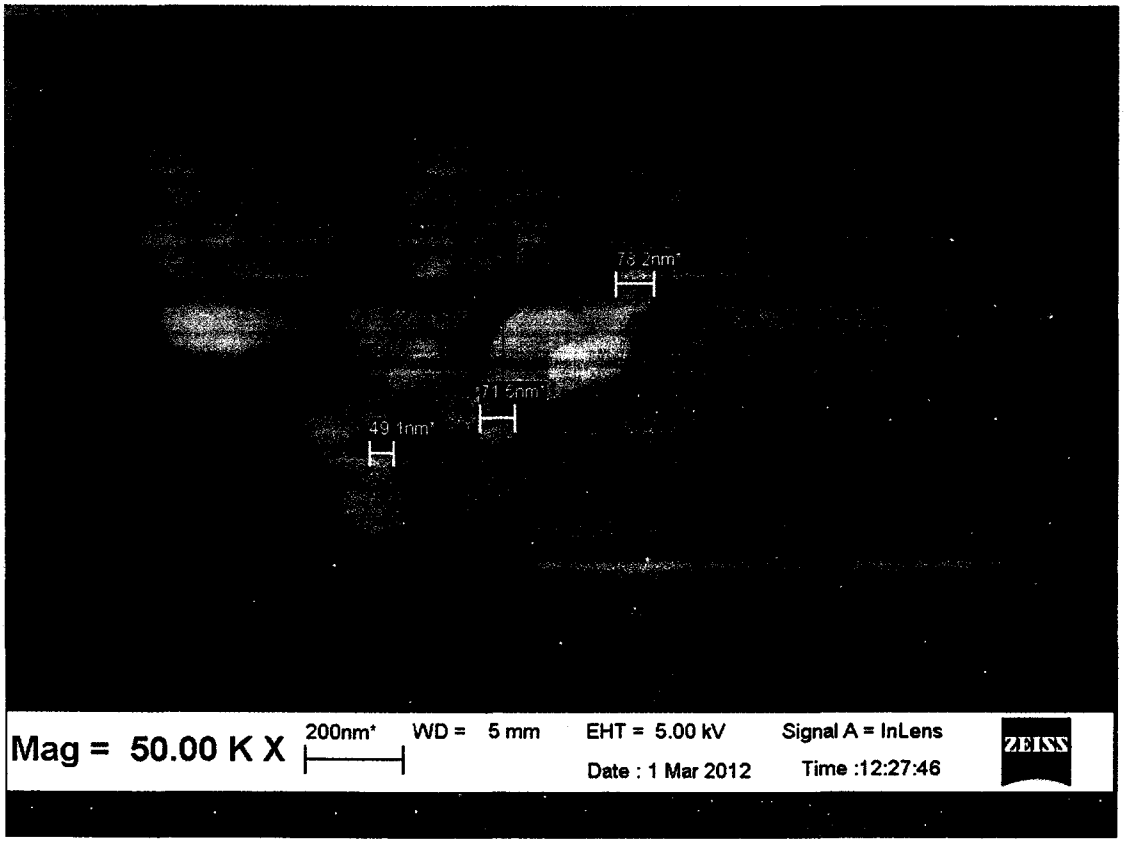

Figure 4.1: SEM image of Al nanoparticles at 50 kX magnification.

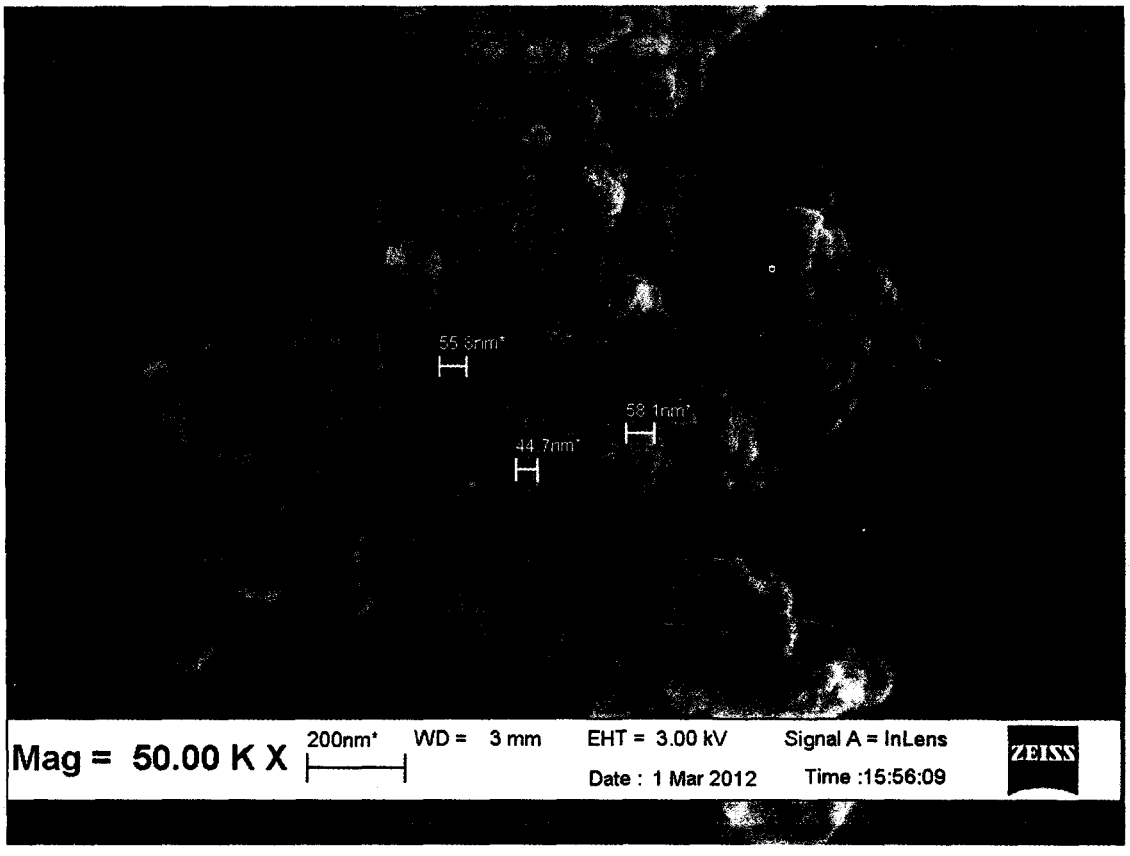

Figure 4.2: SEM image of Ag nanoparticles at 50 kX magnification.

4.3 Physical Characterization

Physical characterization is used to investigate the physical properties of samples such as surface morphology, surface roughness and chemical composition.

4.3.1 Analysis of SEM

For the first part of project, 12 samples with different weight percentage of Al and Ag nanoparticles (0.025 wt%, 0.050 wt%, 0.10 wt%, 0.15 wt%, 0.20 wt% and 0.25 wt%) which were dissolved in chlorobenzene were subjected to SEM test. The

magnification used was 1 kX. The purpose of characterize these samples is to investigate the dispersion of different weight percentage of Al and Ag nanoparticles on glass substrate.

Based on Figure 4.3, it is found that as the weight percentage of nanoparticles increased, the dispersion of nanoparticles has become more agglomerated. In general, nanoparticles possess a large fraction of surface atom per unit volume (Cao et al., 2012). Due to the huge surface area, nanoparticles possess a huge surface energy and thus, are thermodynamically unstable or metastable (Cao et al., 2012). This is because nanoparticles have very large surface energies that drive spontaneous room temperature agglomeration (Riman et al., 2009).

Based on Figure 4.3, the dispersion of 0.025 wt%, 0.050 wt% and 0.10 wt% Al nanoparticles on glass substrate are still acceptable and can be adapted to the last part of this project which is final device fabrication. For 0.15 wt%, 0.20 wt% and 0.25 wt% of Al samples, agglomeration has occurred badly and these samples are not suitable for final device fabrication. In order to compare between Al and Ag nanoparticles, the weight percentage of both nanoparticles selected for the last part of project should be the same. Hence, 0.025 wt %, 0.50 wt% and 0.10 wt% were also selected for Ag nanoparticles in final device fabrication.

Weight Percentage (wt%)	Al	Ag
0.025	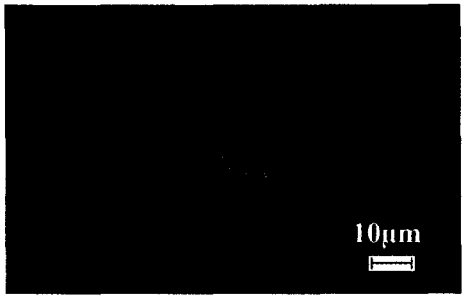	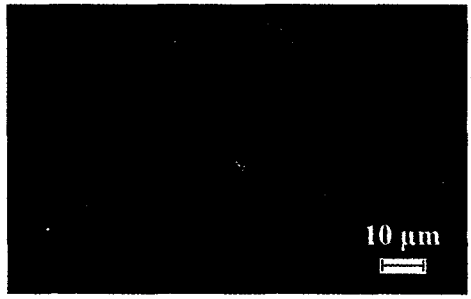
0.050	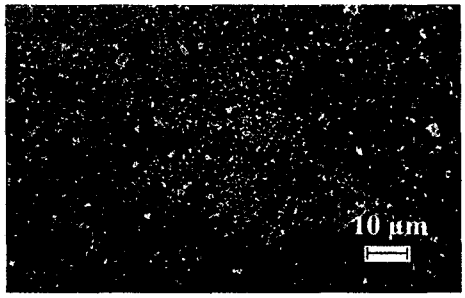	
0.10	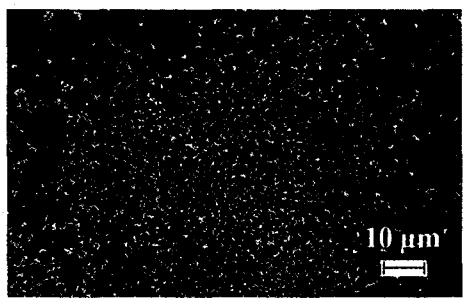	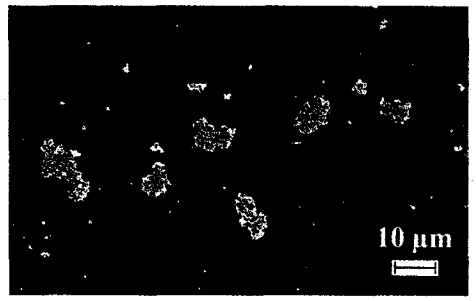

Figure 4.3: SEM images of different weight percentages of Al and Ag nanoparticles.

Weight Percentage (wt%)	Al	Ag
0.15		
0.20		
0.25		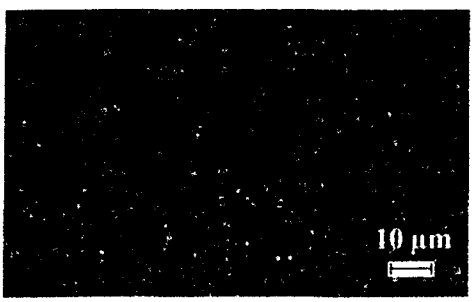

Figure 4.3(continued): SEM images of different weight percentage of Al and Ag nanoparticles.

For the second part of project, 4 samples with different concentration of MEH-PPV (6 mg/ml, 8 mg/ml, 10 mg/ml and 12 mg/ml) were spin-coated on glass and

subjected to SEM test. The magnifications used were 1 kX and 50 kX. The purpose of characterize these samples is to investigate the uniformity of the MEH-PPV layer on glass substrate. The uniform surface of MEH-PPV layer indicated that the film had covered the substrate completely.

Concentration (mg/ml)	**1 kX**	**50 kX**
6		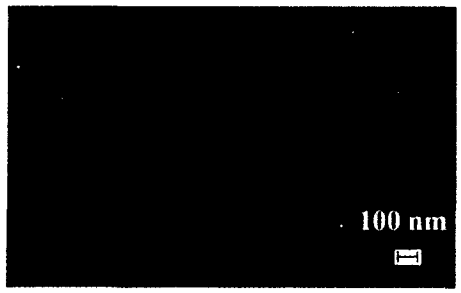
8	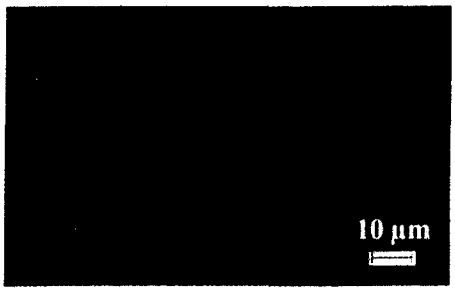	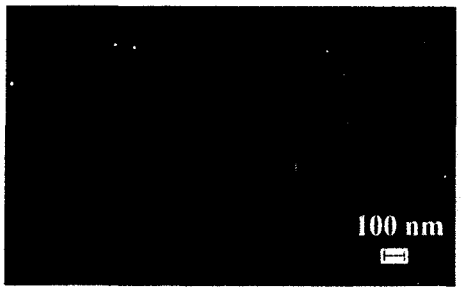

Figure 4.4: SEM images of different concentration of MEH-PPV.

Concentration (mg/ml)	1 kX	50 kX
10	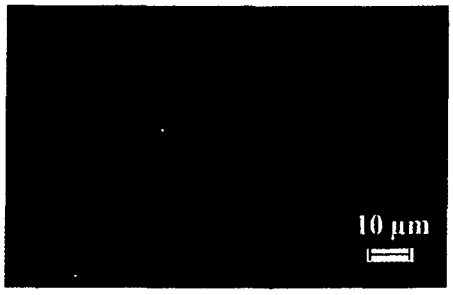	
12	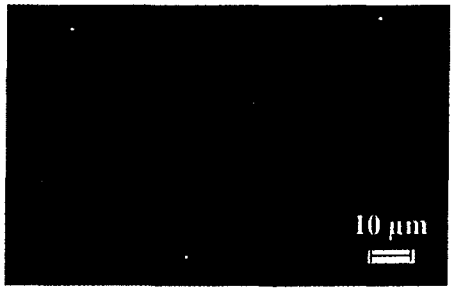	

Figure 4.4(continued): SEM images of different concentration of MEH-PPV.

For the last part of project, 6 samples with different percentage of Al and Ag nanoparticles (0.025 wt%, 0.050 wt% and 0.10 wt%) added into 12 mg/ ml concentration of MEH-PPV layer were subjected to SEM test. Compared to other concentration of MEH-PPV (6 mg/ml, 8 mg/ml and 10 mg/ml), 12 mg/ml concentration of MEH-PPV was chosen because it has shown the better electrical properties during the I-V measurement. The magnifications used were 1 kX and 50 kX. The purpose of this test is to check the dispersion of nanoparticles in the MEH-PPV matrix. Based on Figure 4.5 and 4.6, the dispersion of Al and Ag nanoparticles in MEH-PPV matrix are better compared to those dispersed without MEH-PPV matrix, as shown in Figure 4.3. This is because due to the hydrophobicity of Al and Ag nanoparticles surface, both of these particles can be dispersed successfully in the organic system such as polymer

matrix but it is more difficult to be dispersed in aqueous system (Cheng et al., 2006). Also, Al and Ag nanoparticles are not easy to be dispersed in aqueous system due to their high surface energy (Cheng et al., 2006). However, under high magnification (50 kX), agglomeration can still be observed. The cluster form of Al and Ag nanoparticles are measured.

Weight Percentage of Al (wt%)	1 kX	50 kX
0.025		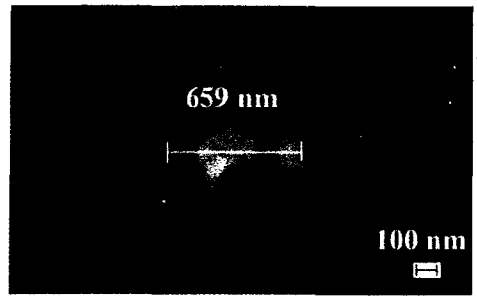
0.050		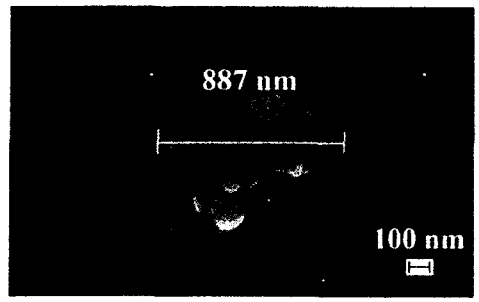
0.10		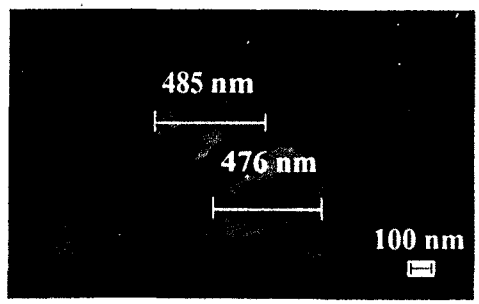

Figure 4.5: SEM images of different weight percentage of Al nanoparticles.

Weight Percentage of Ag (wt%)	1 kX	50 kX
0.025		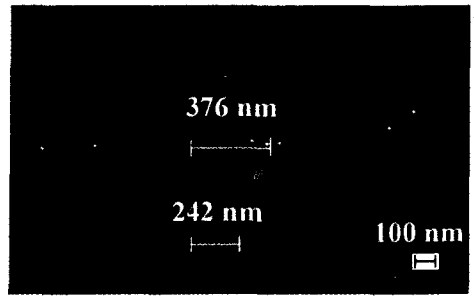
0.050		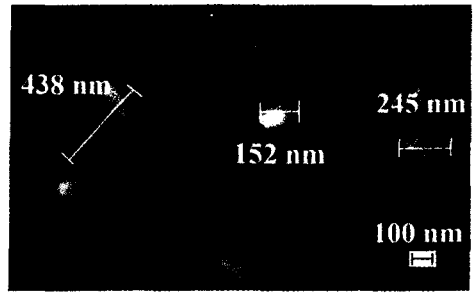
0.10		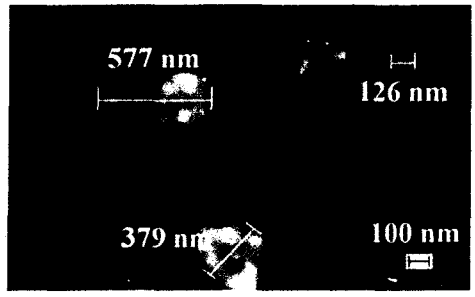

Figure 4.6: SEM images of different weight percentage of Ag nanoparticles.

4.3.2 Analysis of EDX

EDX is an analytical technique used for the elemental analysis or chemical characterization of a sample. The purpose of this analysis is to analyze the presence of elements on the samples. From the second part of project, 4 samples with different concentration of MEH-PPV (6 mg/ml, 8 mg/ml, 10 mg/ml and 12 mg/ml) were spin-coated on glass and sent to EDX analysis. Figure 4.7 shows EDX analysis of the samples mentioned above.

The results of EDX analysis showed in Figure 4.7 are summarized into Table 4.1. From Table 4.1, it is shown that carbon, oxygen, sodium and silicon were detected in the samples. Carbon and oxygen are the elements in MEH-PPV while sodium and silicon are elements in glass. Based on the results, the atomic percentage (at %) of carbon increased as the concentration of MEH-PPV increased from 6 mg/ml to 12 mg/ml. The reason is that the increases of concentration of MEH-PPV will results more carbon content in the samples as the backbone of MEH-PPV is composed of carbon atoms.

Table 4.1: Atomic percentage of elements in samples with different concentration of MEH-PPV.

Samples	Elements (At %)			
	C	O	Na	Si
6 mg/ml	26.01	39.83	6.49	27.67
8 mg/ml	27.90	38.50	6.64	26.96
10 mg/ml	33.15	37.65	3.38	25.82
12 mg/ml	41.62	31.84	4.61	21.94

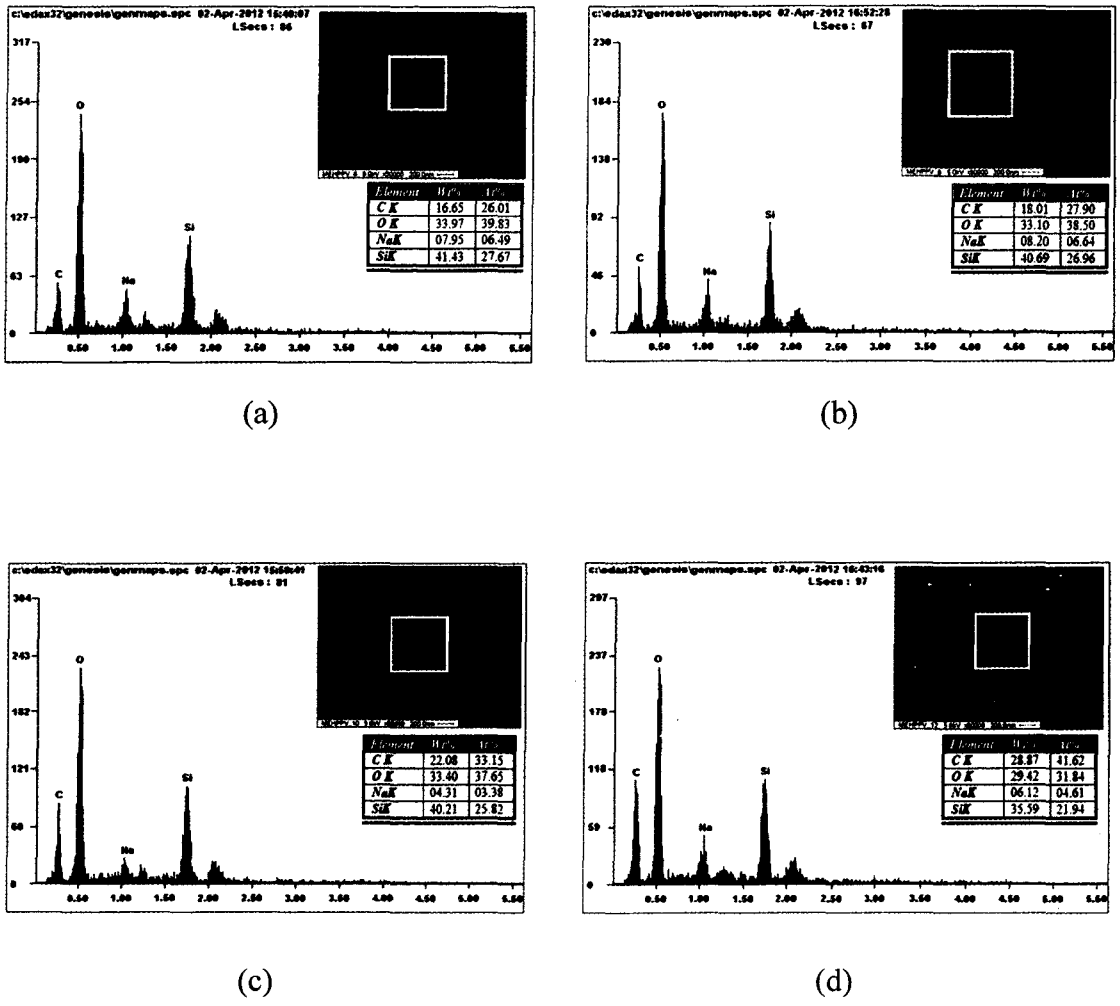

Figure 4.7: EDX analysis of samples with (a) 6 mg/ml (b) 8 mg/ml (c) 10 mg/ml (d) 12 mg/ml concentration of MEH-PPV.

From the last part of project, 6 samples with 12 mg/ml concentration of MEH-PPV mixed with different weight percentage of Al and Ag nanoparticles (0.025 wt%, 0.050 wt% and 0.10 wt%) were spin-coated on glass and characterized by EDX analysis. Figure 4.8 shows EDX analysis of samples with 12 mg/ml MEH-PPV mixed with different percentage of Al nanoparticles.

The results of EDX analysis in Figure 4.8 are summarized into Table 4.2. Based on the results, the atomic percentage of Al increased as the weight percentage of Al nanoparticles increased from 0.025 wt% to 0.050 wt%. This is because the increase of weight percentage of Al nanoparticles will result more Al content in the samples. Theoretically, sample contains 0.10wt% Al nanoparticles should have the highest atomic percentage of Al. However, this is not shown as the atomic percentage of Al decreased as the weight percentages of Al nanoparticles increased from 0.050 wt% to 0.10 wt%. This is because some of the Al nanoparticles were agglomerated and only one point of the sample was selected to undergo EDX analysis. Therefore, the results obtained were different with the theory.

Table 4.2: Atomic percentage of elements in samples with 12 mg/ml MEH-PPV mixed with different weight percentages of Al nanoparticles.

Samples	Elements (At %)				
	C	O	Mg	Al	Si
0.025 wt%	62.71	15.40	0.00	15.80	6.09
0.050 wt%	63.99	9.61	0.00	26.40	0.00
0.100 wt%	62.50	11.30	1.85	21.59	2.76

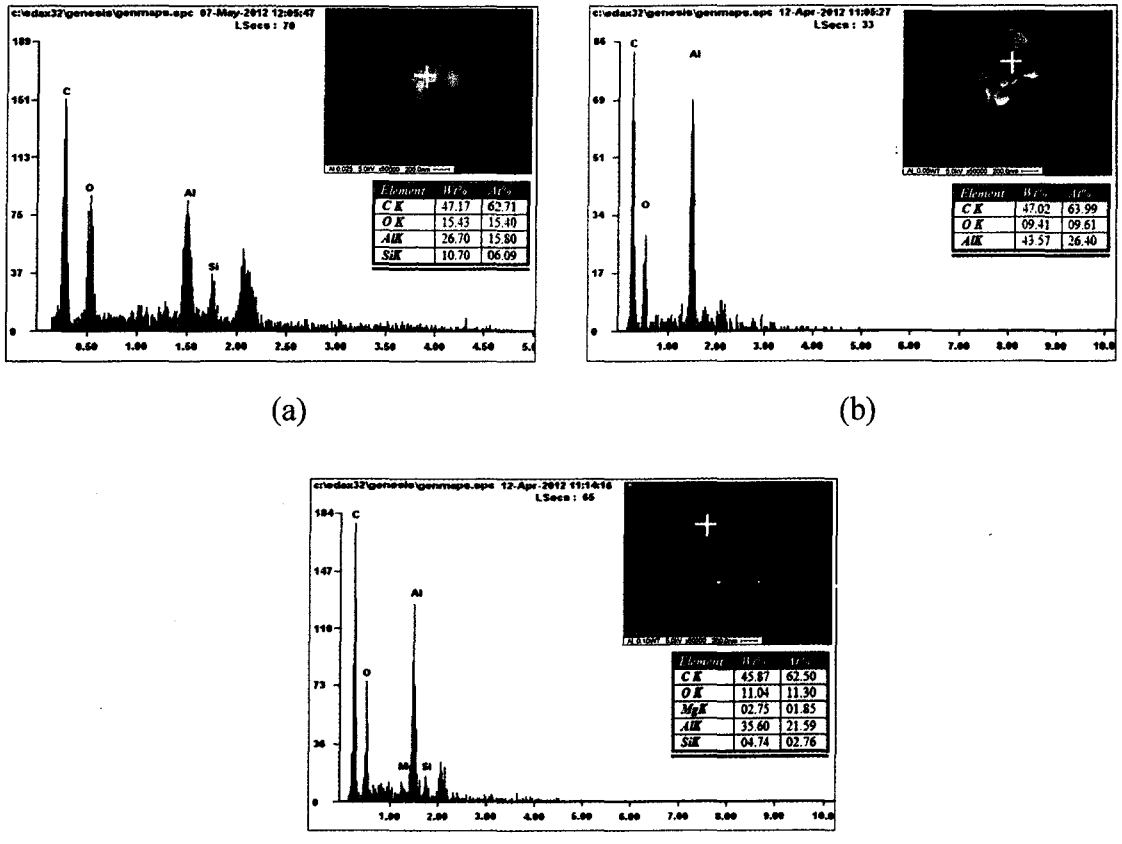

(a) (b)

(c)

Figure 4.8: EDX analysis of samples with 12 mg/ml mixed with different weight percentage of Al nanoparticles. (a) 0.025 wt% (b) 0.050 wt% (c) 0.10 wt%

Figure 4.9 shows the EDX analysis of samples with 12 mg/ml MEH-PPV mixed with different weight percentage of Ag nanoparticles (0.025 wt%, 0.050 wt% and 0.10 wt%). The results of EDX analysis in Figure 4.9 are summarized into Table 4.3. Theoretically, the atomic percentage of Ag should be increased as the weight percentage of Ag nanoparticles used is increased. However, this is not shown in the results. Based on the results, the atomic percentage of Ag is decreased as the weight percentage of Ag nanoparticles is increased from 0.025 wt% to 0.050 wt% and then increased again when the weight percentage of Ag nanoparticles is increased from 0.050 wt% to 0.10 wt%. The reason for this non-linear trend is same as mentioned above.

Table 4.3: Atomic percentage of elements in samples with 12 mg/ml MEH-PPV mixed with different weight percentages of Ag nanoparticles.

Samples	Elements (At %)			
	C	O	Si	Ag
0.025 wt%	53.29	7.49	4.30	34.92
0.050 wt%	68.21	10.58	0.00	21.21
0.100 wt%	69.17	7.69	0.00	23.14

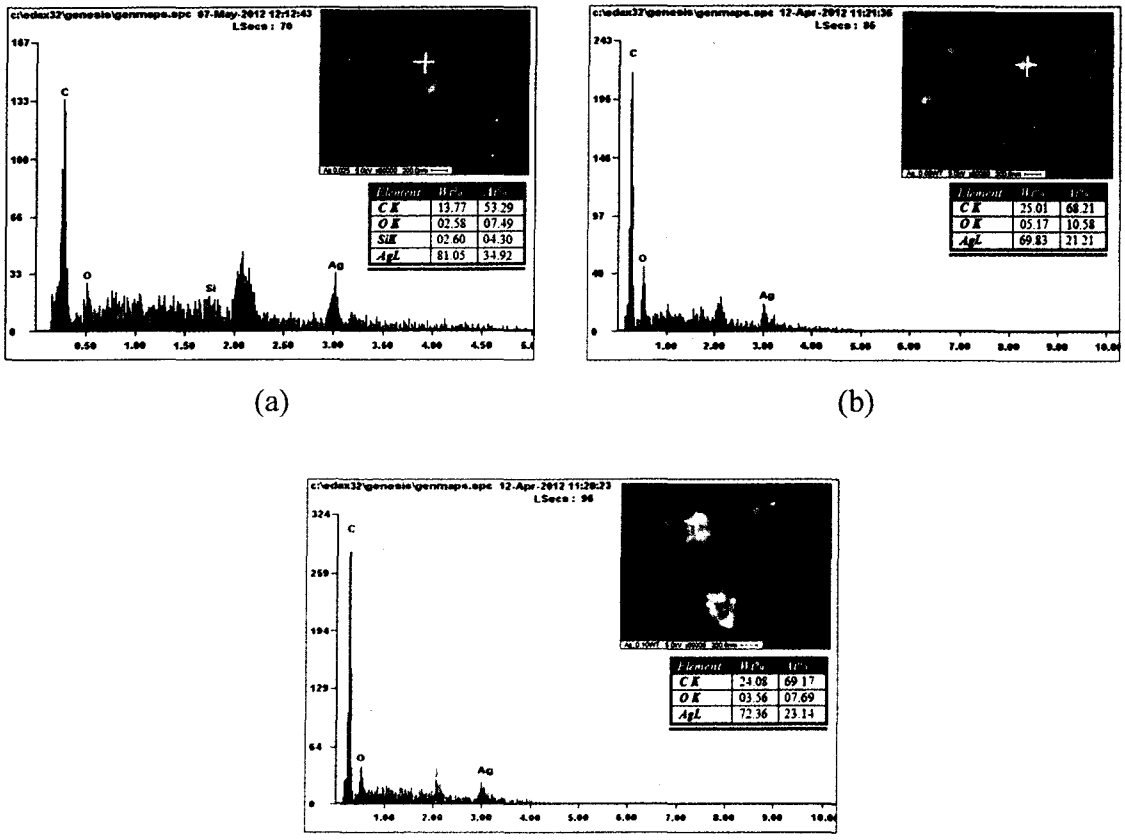

Figure 4.9: EDX analysis of samples with 12 mg/ml mixed with different weight percentages of Ag nanoparticles. (a) 0.025 wt% (b) 0.050 wt% (c) 0.10 wt%

4.3.3 Analysis of AFM

AFM was used to study the morphology of samples with different parameters. In this project, 8 samples were sent to AFM analysis. The samples are 1 empty glass, 1 glass spin-coated with 12 mg/ml MEH-PPV, 6 glasses spin-coated with 12 mg/ml MEH-PPV mixed with different weight percentage of Al and Ag nanoparticles (0.025 wt%, 0.050 wt% and 0.10 wt%). The frames selected for scanning are 5 μm^2 and 10 μm^2. The 3D topography of these samples is shown in Figure 4.10.

Based on Figure 4.10, glass has the smoother surface compared to the other samples. However, there are some peaks observed on the 3D topography of the glass. These peaks are due to the roughness of the glass surface. Compared to glass, sample with 12 mg/ml concentration of MEH-PPV has higher peaks. These peaks are due to the roughness of MEH-PPV layer on the glass substrate.

From Figure 4.10, we found that the peaks in the samples with 12 mg/ml MEH-PPV mixed with different weight percentage of Al nanoparticles are higher compared to those peaks in samples with pure 12 mg/ml MEH-PPV layer. This indicates that the incorporation of Al nanoparticles into MEH-PPV layer has increased the surface roughness of the layer. The Al nanoparticles are agglomerated and hence, increased the surface roughness of the samples.

For samples with 12 mg/ml MEH-PPV mixed with different weight percentage of Ag nanoparticles, we found that the peaks obtained are lower compared to samples with pure MEH-PPV layer. This indicates that the Ag nanoparticles were dispersed more uniform compared to Al nanoparticles. This is because Al nanoparticles supplied

by MTI Corporation have smaller particle size compared to the Ag nanoparticles. As discussed previously in SEM measurement, smaller particles size will lead to higher surface energy which causing the Al nanoparticles to be agglomerated. Hence, the dispersion of Ag nanoparticles in MEH-PPV is more uniform compared to Al nanoparticles.

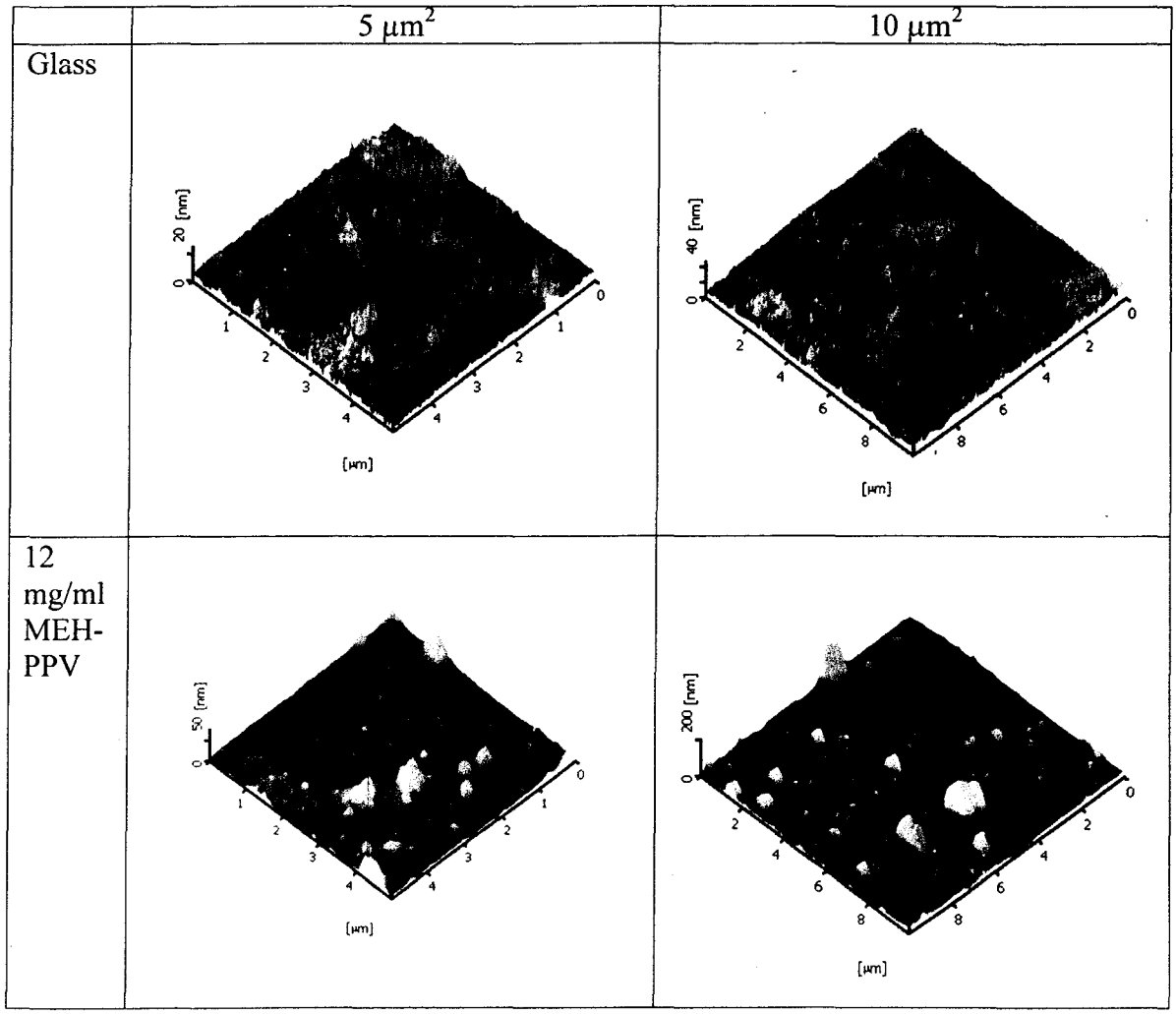

Figure 4.10: 3D topography of glass, samples with 12 mg/ml concentration of MEH-PPV and samples with 12 mg/ml MEH-PPV mixed with different weight percentage of Al and Ag nanoparticles.

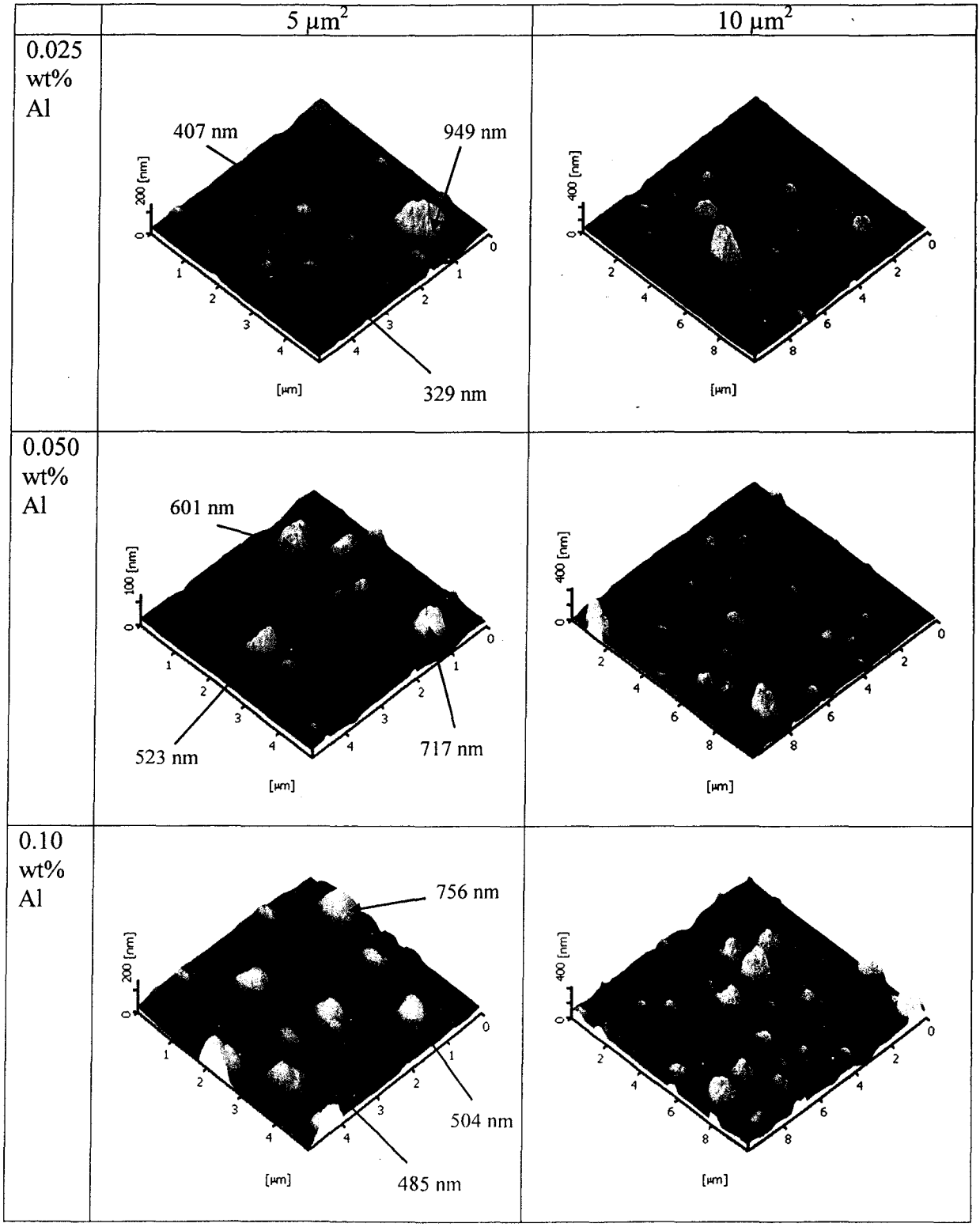

Figure 4.10(continued): 3D topography of glass, samples with 12 mg/ml concentration of MEH-PPV and samples with 12 mg/ml MEH-PPV mixed with different weight percentage of Al and Ag nanoparticles.

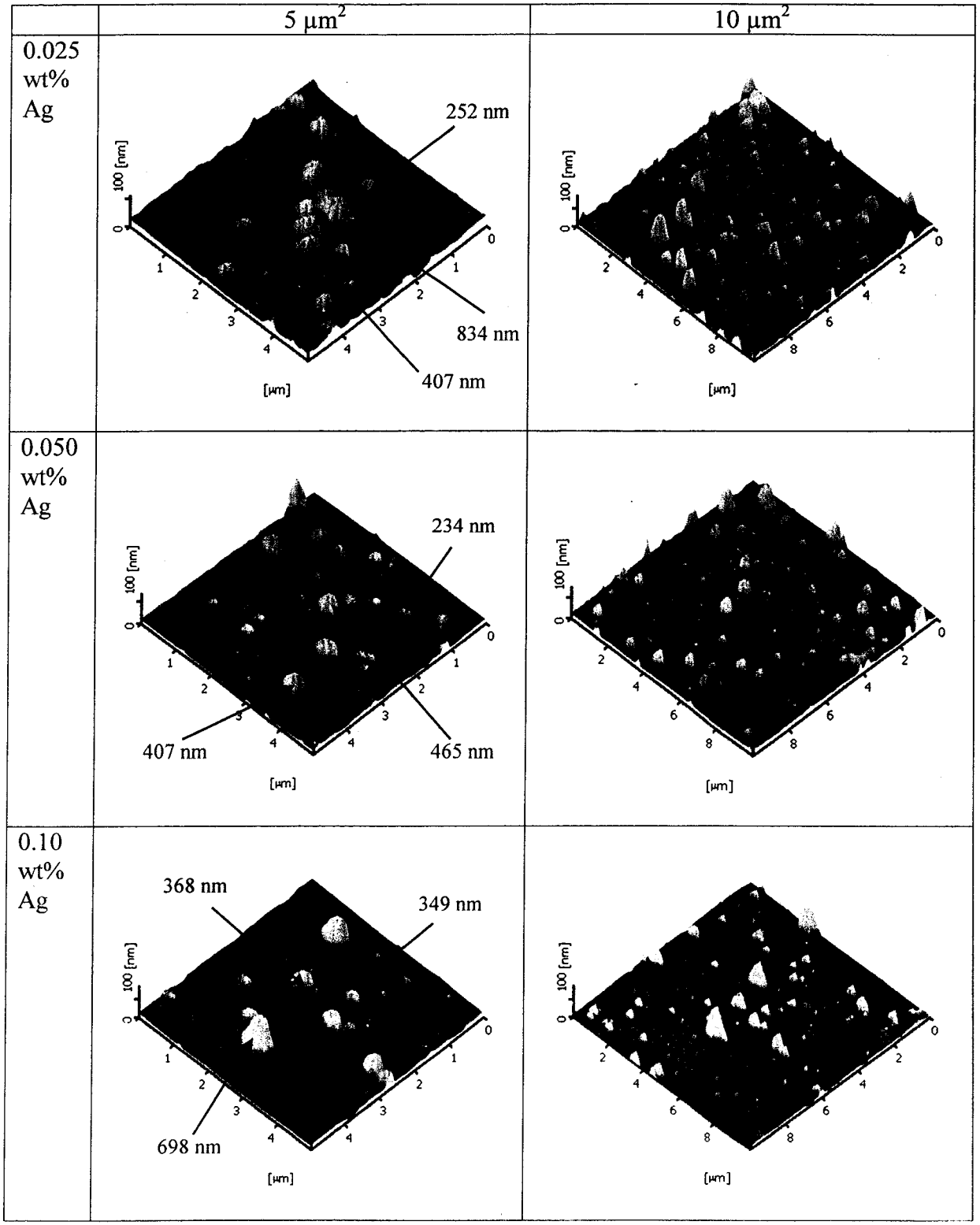

Figure 4.10(continued): 3D topography of glass, samples with 12 mg/ml concentration of MEH-PPV and samples with 12 mg/ml MEH-PPV mixed with different weight percentage of Al and Ag nanoparticles.

Based on Figure 4.10, three peaks were measured for each of the samples added with different weight percentage of Al and Ag nanoparticles. The average size obtained from these peaks is tabulated into Table 4.4 and then, compared with the average size of cluster (Al and Ag nanoparticles) obtained from SEM analysis in Figures 4.5 and 4.6. The purpose of this comparison is to ensure that the peaks found in AFM of these samples are due to the agglomeration of Al and Ag nanoaprticles. No comparison is done for glass and samples with pure MEH-PPV layer because there is no information provided by SEM analysis. Based on Table 4.4, the average size of cluster found in AFM are very close to the measurement obtained from SEM analysis. Hence, it can be said that the peaks in AFM of samples added with different percentage of Al and Ag nanoparticles are due to the agglomeration of these nanoparticles.

Table 4.4: Comparison of average size of cluster (Al and Ag nanopaticles) between AFM and SEM analysis.

Tests	Average Size of Cluster (Agglomerated Nanoparticles)					
	Al (wt%)			Ag (wt%)		
	0.025	0.050	0.10	0.025	0.050	0.10
SEM	659 nm	887 nm	481 nm	309 nm	278 nm	360 nm
AFM	562 nm	614 nm	582 nm	498 nm	369 nm	472 nm

Surface roughness is determined using root-mean-square (RMS). RMS of glass and samples with 12 mg/ml MEH-PPV mixed with different weight percentage of Al and Ag nanoparticles have been tabulated into Table 4.5 and also plotted in Figure 4.11. Based on Table 4.5, it is shown that glass has the lowest RMS value. This indicates that glass has the smoothest surface among the samples. As mentioned earlier, samples with pure 12 mg/ml concentration of MEH-PPV layer (0 wt% of both Al and Ag

nanoparticles) has higher surface roughness compared to glass. Hence, it has higher RMS value compared to glass.

From Table 4.5, RMS values for samples added with different weight percentage of Al nanoparticles are higher than the RMS value of sample with pure MEH-PPV layer. This indicates that the surface of samples added with Al nanoparticles is rougher than the surface of sample with pure MEH-PPV layer. For samples with different weight percentage of Ag nanoaprticles added, the RMS values are lower than sample with pure MEH-PPV layer. This indicates that samples with Ag nanoparticles have smoother surface compared to sample with pure MEH-PPV layer. This is because the dispersion of Ag nanoparticles is more uniform compared to the dispersion of Al nanoparticles. Hence, there is less agglomeration in these samples.

Theoretically, as the weight percentage of nanoparticles added is increased, the RMS value should be increased too. However, this is not shown in Figure 4.11. The RMS value is decreased as the weight percentage of Al nanoparticles added is increased from 0.025 wt% to 0.050 wt%, and then increased again when the weight percentage of Al nanoparticles added increased from 0.050 wt% to 0.10 wt%. The trend was non-linear because the Al nanoparticles were not well-dispersed and only one point was selected for AFM analysis. For samples with Ag nanoparticles added, the RMS value is decreased as the weight percentage of Ag nanoparticles added is increased. This is due to the same reason as mentioned earlier.

Table 4.5: RMS of glass and samples with 12 mg/ml MEH-PPV mixed with different weight percentage of Al and Ag nanoparticles.

Samples	Glass	Al (wt%)				Ag (wt%)			
		0	0.025	0.050	0.10	0	0.025	0.050	0.10
RMS (nm)	2.22	16.43	40.58	33.10	51.71	16.43	16.41	11.87	11.32

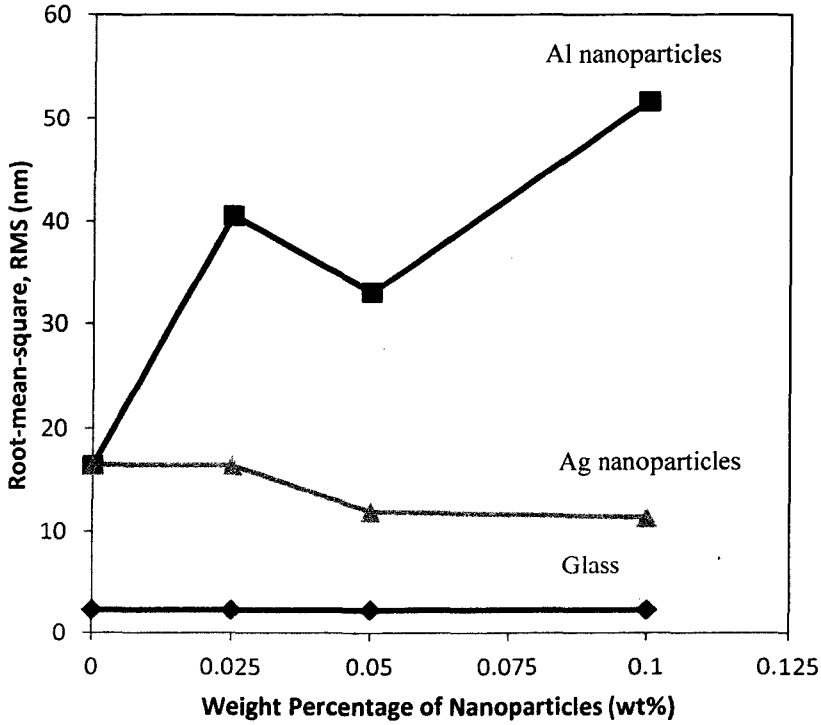

Figure 4.11: Comparison of RMS of glass and samples with 12 mg/ml concentration of MEH-PPV mixed with different weight percentage of Al and Ag nanoparticles.

4.3.4 Analysis of FTIR

In this project, FTIR testing was performed in transmittance mode. Figures 4.12, 4.13, 4.14 and 4.15 show FTIR spectra of MEH-PPV powder, samples with different concentration of MEH-PPV, samples with different weight percentage of Al

nanoparticles and samples with different weight percentage of Ag nanoparticles, respectively.

Figure 4.12 shows the FTIR spectra of MEH-PPV powder. Based on Figure 4.12, the spectra show the bands at 3444 cm^{-1}, 3057 cm^{-1}, 2926 cm^{-1}, 2862 cm^{-1}, 1502 cm^{-1}, 1461 cm^{-1}, 1253 cm^{-1}, 1203 cm^{-1}, 1038 $cm^{-1}$and 966 cm^{-1}. The analysis of these bands is summarized into Table 4.6.

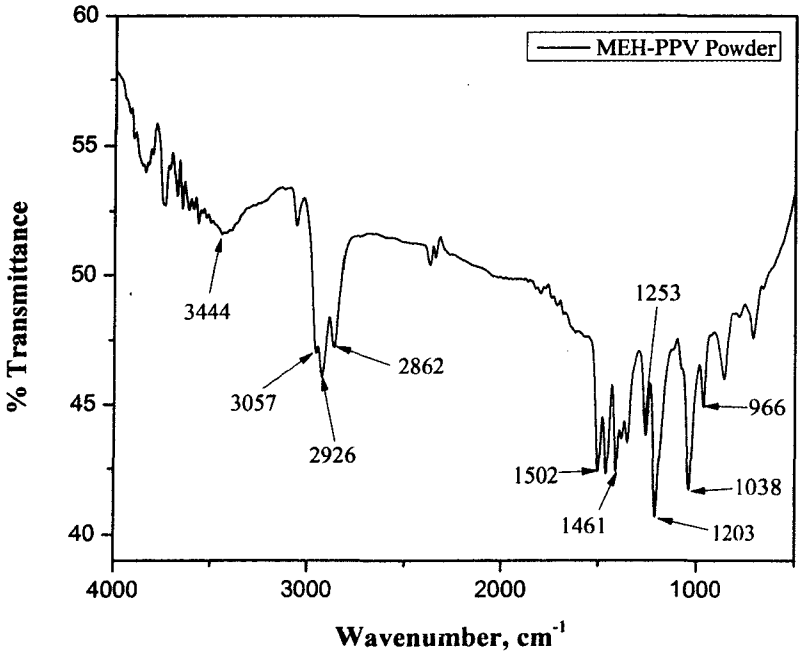

Figure 4.12: FTIR spectra of MEH-PPV powder.

Table 4.6: Analysis of MEH-PPV FTIR spectra (Science-and-fun.de, 2000).

Labels	Infrared band observed in MEH-PPV (cm^{-1})	Assignments
a	3444	O-H stretching vibration
b	3057	=C-H stretching vibration
c	2926	Asymmetric C-H stretching vibration $-CH_2$ group
d	2862	Symmetric CH_3 stretching vibration in $-O-CH_3$ group
e	1502	Symmetric C-H deformation vibration in $-O-CH_2$ group
f	1461	Symmetric CH_2 deformation vibration in $-O-CH_2$ group
g	1253	C-C vibration
h	1203	C-O stretching vibration
i	1038	C-C skeleton vibration
j	966	Vinyl C-Hout-of-plane bend

Based on Table 4.6, the FTIR bands are compared and related to the MEH-PPV structure. The MEH-PPV structure is shown in Figure 4.13. All of the bands obtained are complying with the MEH-PPV vibration modes except for band at 3444 cm^{-1}.

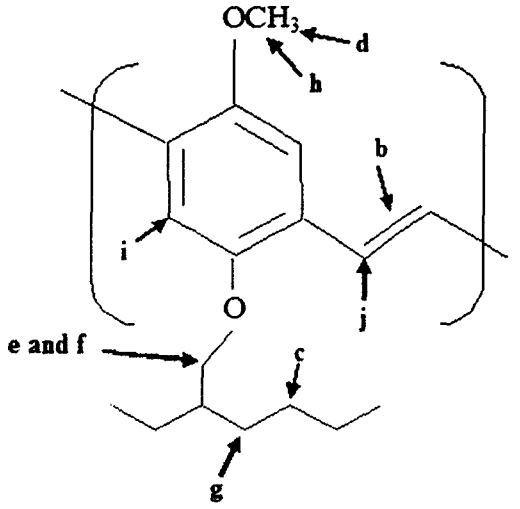

Figure 4.13: Structure of MEH-PPV (Kamarulzaman et al., 2011).

During FTIR analysis, transmittance mode was selected. Based on Figure 4.14, 4.15 and 4.16, the spectra of all of the samples show bands at 3057 cm^{-1}, 2928 cm^{-1} and 2859 cm^{-1} except the spectra of glass. The band at 3057 cm^{-1} is referring to =C-H stretching vibration while the band at 2928 cm^{-1} refers to the C-H stretching vibration in $-CH_2$ group (Science-and-fun.de, 2000). Besides, band at 2859 cm^{-1} is corresponding to the CH_3 stretching vibration in $-O-CH_3$ group (Science-and-fun.de, 2000). Based on Figures 4.15 and 4.16, no information is found for Al and Ag nanoparticles.

Compared to MEH-PPV powder, fewer groups are found in these samples. Only 3 groups are found: group of =C-H stretching vibration, group of C-H stretching vibration and group of CH_3 stretching vibration. This could be due to the thickness of the MEH-PPV layer. The thickness of MEH-PPV layer is very thin if compared to the glass (1 mm thick). Thus, the thickness of MEH-PPV layer could be negligible. When infrared passed through the samples, most of the infrared was transmitted or absorbed by the glass. Therefore, the glass would affect the results obtained as the spectrum produced would be more to the glass rather than MEH-PPV layer. As a result, the groups that found in these samples in Figure 4.14, 4.15 and 4.16 are very weak.

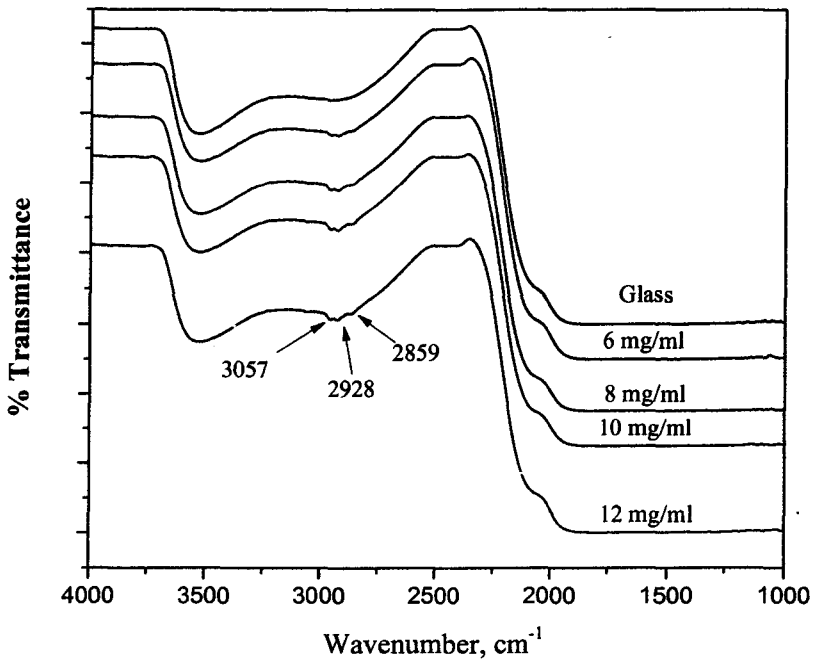

(a)

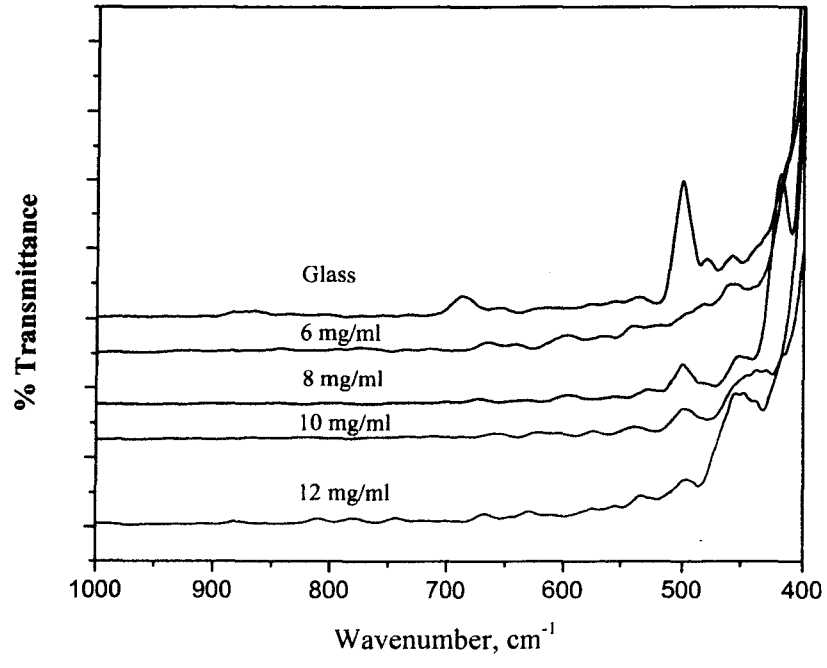

(b)

Figure 4.14: FTIR spectra of glass and samples with different concentration of MEH-PPV at wavenumber (a) 1000 cm^{-1} to 4000 cm^{-1} (b) 400 cm^{-1} to 1000 cm^{-1}.

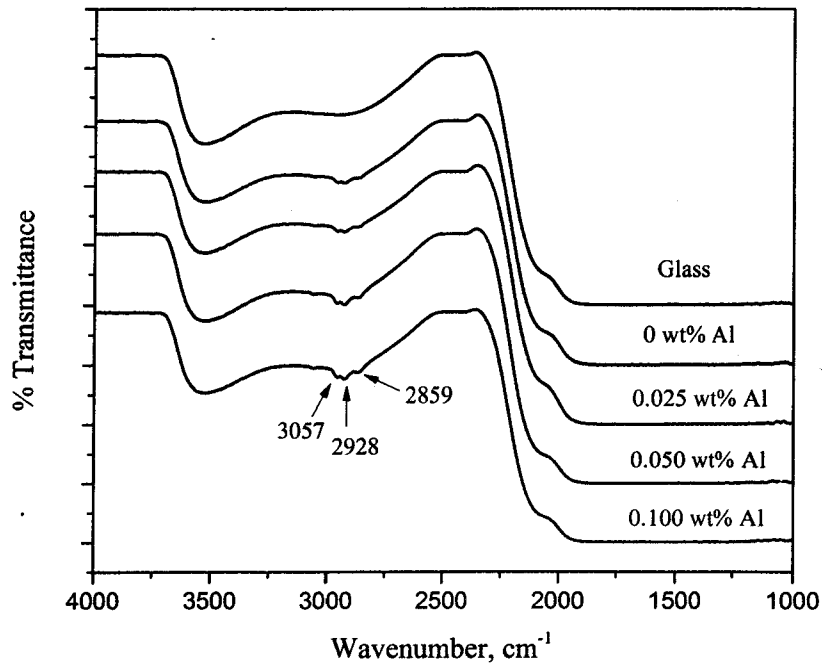

(a)

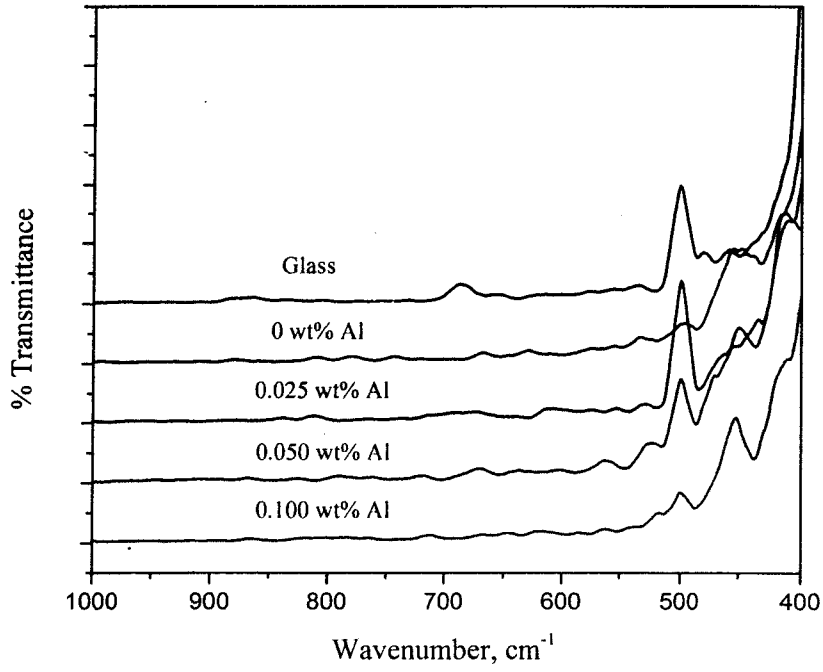

(b)

Figure 4.15: FTIR spectra of glass and samples added with different weight percentage of Al nanoparticles at wavenumber (a) 1000 cm^{-1} to 4000 cm^{-1} (b) 400 cm^{-1} to 1000 cm^{-1}.

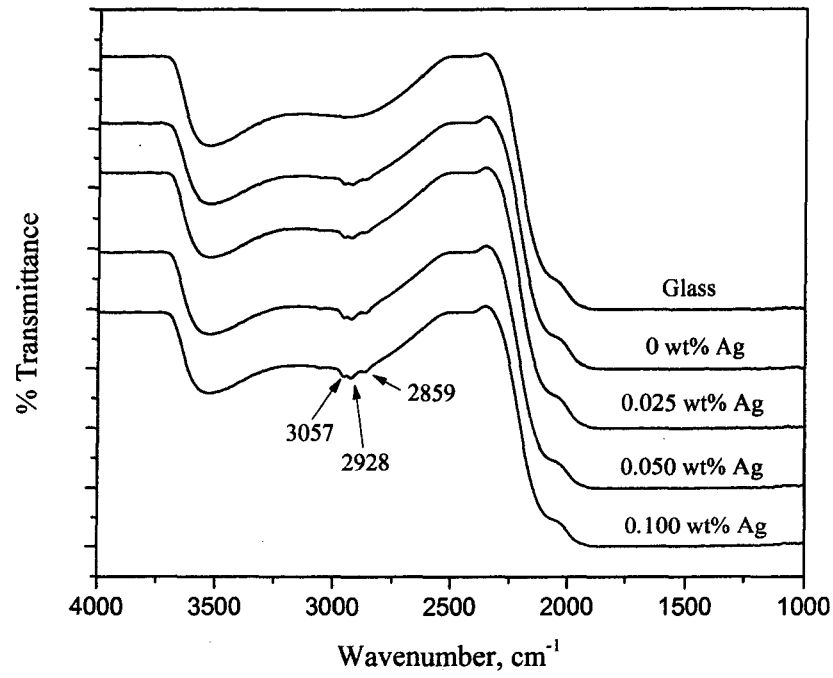

(a)

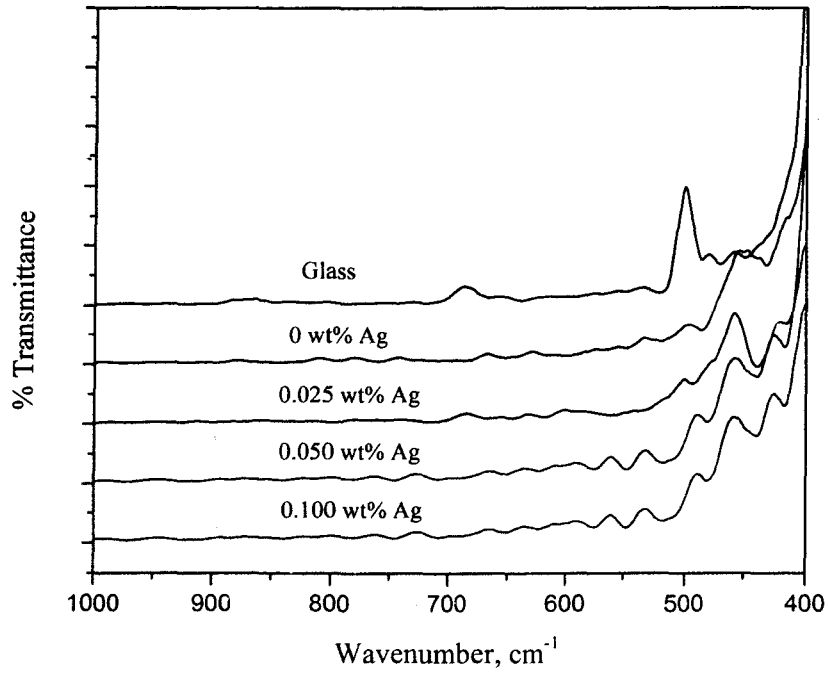

(b)

Figure 4.16: FTIR spectra of glass and samples added with different weight percentage of Ag nanoparticles at wavenumber (a) 1000 cm^{-1} to 4000 cm^{-1} (b) 400 cm^{-1} to 1000 cm^{-1}.

4.4 Electrical Characterization

Electrical characterization was used to investigate electrical properties of the samples. In electrical characterization, I-V measurement was carried out to determine I-V characteristics of the samples.

4.4.1 Analysis for I-V Measurement

I-V measurement had been performed on the samples to investigate their electrical properties. For the second part of this project, 4 samples with different concentration of MEH-PPV (6 mg/ml, 8 mg/ml, 10 mg/ml and 12 mg/ml) were measured. By using Sigma Plot 10, the obtained I-V results were then converted into log I-V curve, as shown in Figure 4.17.

Based on Figure 4.17, current is increased as the concentration of MEH-PPV is increased. This indicates that current output could be increased by increasing the concentration of MEH-PPV. This is because polymers are composed of polycrystalline and amorphous phases. The amorphous phases of polymers will limit the carrier mobility because the hoping process in this disorder region is difficult (Li et al., 2011). As the concentration of MEH-PPV is increased, the crystalline phase in MEH-PPV will be increased too. Hence, the current output of MEH-PPV will be increased. Based on Figure 4.17, sample with 12 mg/ml concentration of MEH-PPV has the highest current output and better performance compared to other concentration of MEH-PPV.

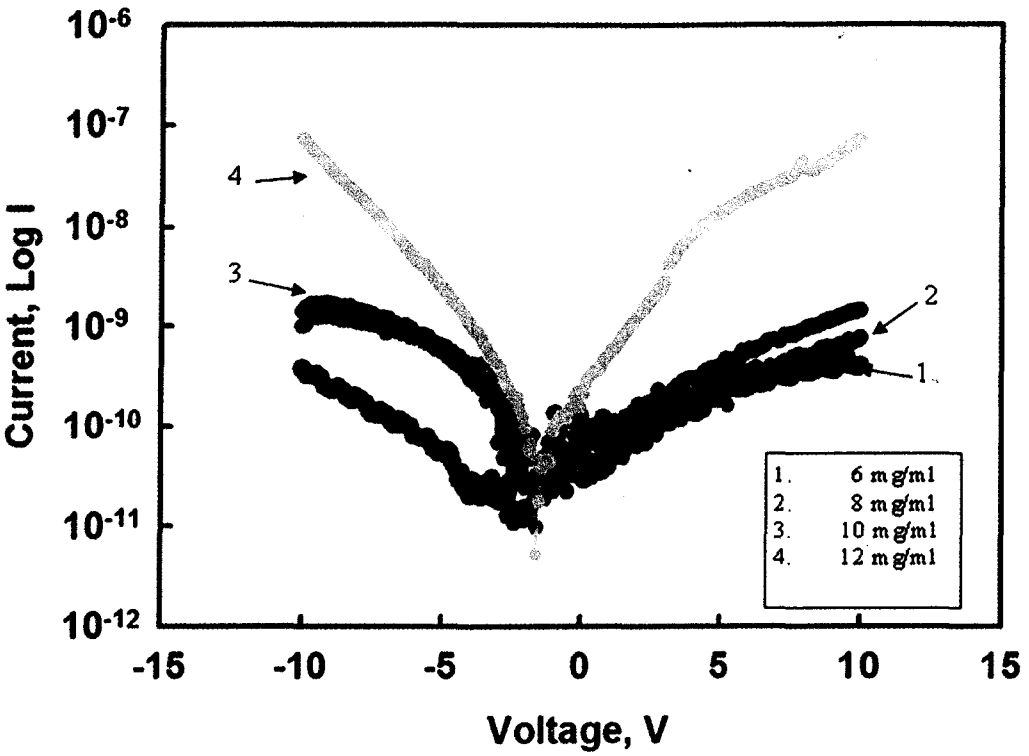

Figure 4.17: Current-voltage plots of samples with different concentration of MEH-PPV.

12 mg/ml concentration of MEH-PPV was chosen to proceed to next parameters (incorporation of Al and Ag nanoparticles). The reason to choose concentration of 12 mg/ml is due to the better electrical properties compared to other concentration of MEH-PPV. Different weight percentage of Al and Ag nanoparticles (0.025 wt%, 0.050 wt% and 0.10 wt%) were added into 12 mg/ml MEH-PPV and then spin-coated on substrate. Based on Figure 4.18, the conductivity of samples with different weight percentage of Al and Ag nanoparticles added are different from the sample with pure MEH-PPV. This indicates that the incorporation of Al and Ag nanoparticles will alter the electrical properties of devices. Theoretically, the incorporation of these metallic (Al and Ag) nanoparticles should enhance the current output of devices. This is because the surface plasmonic resonance able to enhance the electric field around the metal nanoparticles (Samoc et al., 2011). However, this is not up to expectation for some parameters due to the agglomeration of nanoparticles.

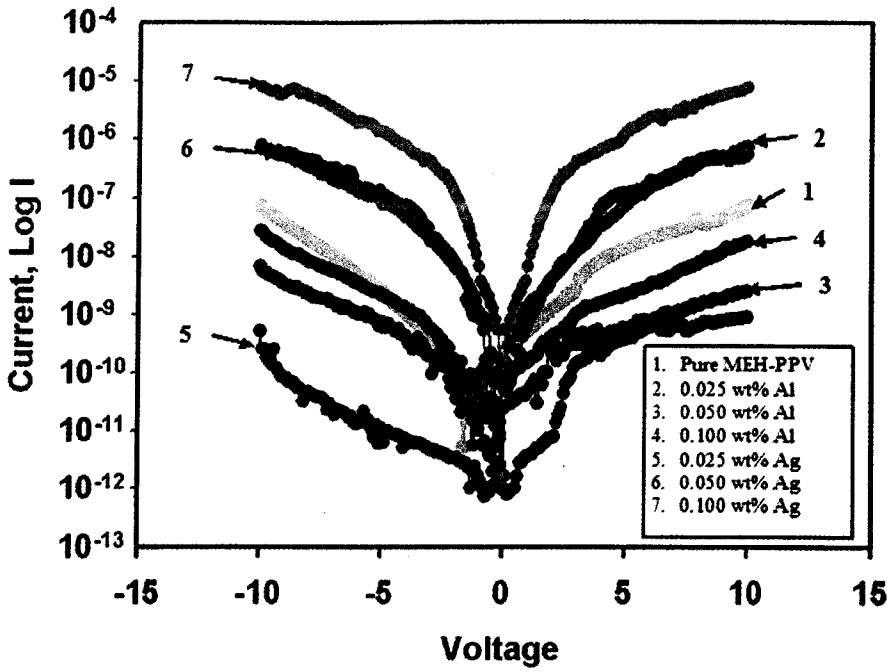

Figure 4.18: Current-voltage plots of samples with different weight percentage of Al and Ag nanoparticles added.

For samples with different weight percentage of Al nanoparticles added, we expect that the current output should be higher than sample with pure MEH-PPV, and increased as the weight percentage of Al nanoparticles added is increased. However, this is not shown in Figure 4.18. Based on Figure 4.18, only sample added with 0.025 wt% Al nanoparticles shows the improved current output. The samples added with 0.050 wt% and 0.10 wt% of Al nanoparticles show lower current output compared to pure MEH-PPV. The lower performance of these samples is mainly due to the agglomeration of nanoparticles in MEH-PPV. This is shown in the AFM analysis as the RMS value of sample added with different weight percentage of Al nanoparticles is higher compared to sample with pure MEH-PPV. The agglomeration will induced inhomogeneous distributions of nanoparticles in the polymer, hence affecting electrical conductivity of the samples (Mariatti et al., 2010).

For samples with different weight percentage of Ag nanoparticles added, the current output is increased as the weight percentage of Ag nanoparticles added is increased. However, the sample with 0.025 wt% Ag nanoparticles added has lower current output than sample with pure MEH-PPV. This is because this sample has lower filling factor compared to the samples added with 0.050 wt% and 0.10 wt% Ag nanoparticles. For nanocomposites consisting of metallic nanoparticles and polymer matrix, the electrical properties of such composites are depending on the filling factor (Faupel et al., 2008). At high volume fractions of metal nanoparticles, a 3D conducting network can be developed in the matrix and hence, the electrical conductivity can be increased (Filpo et al., 2010). At lower filling factor of Ag nanoparticles, polymer matrix will be the dominant phase in the nanocomposites and this will increase the resistivity (Mariatti et al., 2011).

Overall, incorporation of Ag nanoparticles into MEH-PPV will give a better enhancement on the performance of devices compared to Al nanoparticles. This is because the dispersion of Ag nanoparticles is more uniform compared to Al nanoparticles, as discussed previously in SEM analysis and AFM analysis. There are more thin spaces between well-dispersed Ag nanoparticles and hence, less electron trap sites as the electron hopping between the nanoparticles become favorable (Yoon et al., 2004; Xie et al., 2011).

4.5 Porphyrin and Cu-Porphyrin

4.5.1 Electrical Properties

Fig. 4.19 shows I-V test results on different concentration of Cu-porphyrin and porphyrin with gap distance of 630 μm and 160 μm respectively. Both solutions with

the concentration of 0.5 mg/ml gave the highest current value at the voltage of 5V. However, the current values of porphyrin devices are much lower compared with the Cu-porphyrin devices.

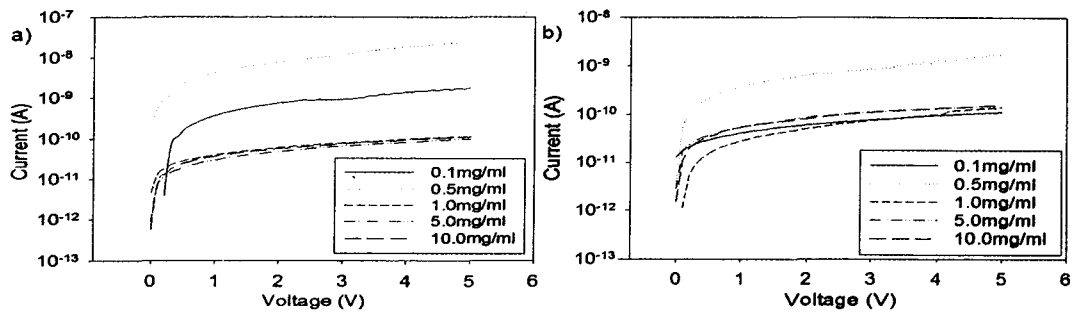

Fig.4.19 I-V curves of a) Cu-porphyrin with gap distance of 0.63 mm, and b) porphyrin with the gap size of 0.16 mm.

Fig. 4.20 revealed the overall electrical results of Cu-porphyrin and porphyrin devices drop casted using 0.5 mg/ml solution with varying gap distances. The gap distance between source and drain varied from 160 μm to 700 μm. The results proved that Cu-porphyrin with gap distance of 630 μm and porphyrin with gap distance of 160 μm, show the highest current value at 5V as to compare with the rest of the gap distances. Cu-porphyrin devices with larger gap distance (Fig. 4.20a) showed a better electrical result. However, the current values of the electrical result for gap distance 0.16 mm until 0.56 mm are close compared to the electrical value for gap distance 0.63 mm and 0.70 mm. Drop casting method is not easy to fabricate a uniform thin film. Therefore, this incident happened. Fig. 4.20b with the 0.5 mg/ml porphyrin devices shows the devices with 0.16mm gap distance have much higher current value. The current value rest of the devices with different gap distance, from 0.25mm until 0.70mm remain almost the same. This also might due to the non-uniformity of the organic thin film. This proves that the gap distance of the device does not affect much towards the electrical properties of the device.

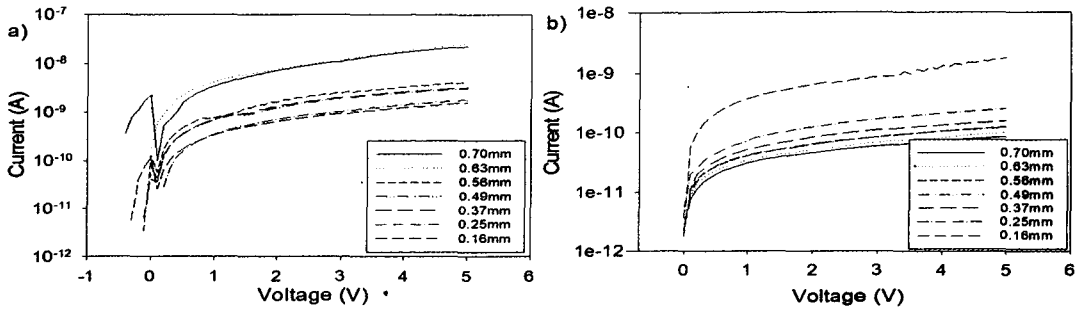

Fig. 4.20 I-V curves of a) 0.5 mg/ml Cu-porphyrin, and b) 0.5 mg/ml porphyrin

The current value for both Cu-porphyrin and porphyrin devices with the fixed gap distance of 630 μm and 160 μm respectively at the operating voltage of 5 V are summarized at Table 4.7. From the table, the devices casted with Cu-porphyrin have higher conductivity compare to the devices casted with the solution of porphyrin. The current value drop as the drop casting solution concentration increase to above 0.5 mg/ml and the current value for both solutions remain almost the same as the drop casted solution with the concentration of 1.0 mg/ml to 10.0 mg/ml. This is caused by the arrangement of the organic molecules which have sufficient time to rearrange themselves accordingly and form as organic thin film with high degree of crsytallinity before the solution drying up [Mittal et al., 2012].

Table 4.7 Current value of Cu-porphyrin and porphyrin at varying concentration with the specific gap distances and operating voltage of 5V.

Concentration (mg/ml) / Sample	0.1	0.5	1.0	5.0	10.0
	Current Value, I (A)				
Cu-porphyrin ***Gap distance = 630 μm**	1.82×10^{-09}	2.53×10^{-08}	1.17×10^{-10}	1.01×10^{-10}	1.15×10^{-10}
Porphyrin ***Gap distance = 160 μm**	8.66×10^{-11}	1.75×10^{-9}	1.39×10^{-10}	1.55×10^{-10}	1.56×10^{-10}

Fig.4.21 showing the bar charts of I-V test results for both porphyrin with varying organic concentration and gap distance at the voltage of 5 V. As refer to Fig. 4.21a, Cu-porphyrin with the concentration of 0.1 and 0.5 mg/ml give a more significant value of current compared to the others concentration. The reason is the Cu-porphyrin has good intermolecule interaction where contact resistance was found higher with thicker film [Boudinet et al, 2010]. As a result, the current value decreased. However, the uppermost current value falls at the concentration of 0.5 mg/ml with the gap distance of 630 μm. Cu-porphyrin devices which casted with concentration of 0.1 mg/ml produced results which explained the effect of gap distance and current value at the early stage. This proved that the larger the gap distance between source and drain, the higher the current value. However, the current values of the devices drop when the gap distance value greater than 490 μm. Based on research done by Gupta and Hong [9] using pentacene, the mobility drop when the thickness of the pentacene layer was above 35 nm. Furthermore, Cu-porphyrin devices drop casted with the concentration of 0.5 mg/ml having constantly increasing current value with increasing gap distance up to 630 μm. The Cu-porphyrin devices with the concentration above 1.0 mg/ml shows low current value as compare to 0.1 mg/ml and 0.5 mg/ml. At low solution concentration, these macromolecules able arrange accordingly more freely and form a better crystallinity thin film. As portrayed in Fig. 4.22b, the highest current value is obtained for porphyrin devices drop casted with concentration of 0.5 mg/ml with the gap distance of 160 μm. In addition, porphyrin devices also contribute to the high current value when the devices are drop casted with the concentration of 5.0 mg/ml. As a comparison for both of these porphyrin drop casted devices, Cu-porphyrin devices exhibit a higher current value as compare to metal-free porphyrin, due to the metal-to-ligand charge

transfer [Maldotti et al., 1993]. By referring to Fig. 4.21, the gap distance does not contribute much effect towards the electrical properties of the organic devices, however, the concentration of the solutions play a major role to the electrical properties of the devices due to the crystal formation of the organic thin film. The reason is the lower the solution concentration, the longer the drying time and the organic molecules will have enough time to arrange to form a better crystal thin film.

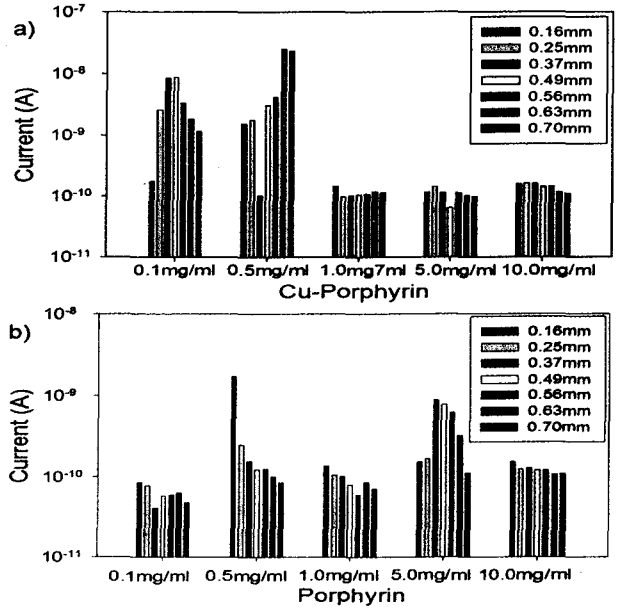

Fig. 4.21 Bar chart showing the I-V results for different concentration of a) Cu-Porphyrin and b) Porphyrin solution at 5 V.

4.5.2 Surface Morphology

With refer to SEM image in Fig.4.22, the circular shape constituents are the Cu-porphyrin. The amount of the constituents increased proportionally with the concentration of the Cu-porphyrin thin film. The higher the concentration of the organic solution, the amount of constituents seen is more. From Fig. 4.22a, it shows that Cu-porphyrin is well coated on the surface of the glass substrate. Through observation using SEM, there are very few small rings shape constituents present, which identified

as the crystal Cu-porphyrin, which formed during drop casting process. At low concentration, the droplet of the drop casting solution will have longer time to dry up as compare to the solution with higher concentration. This will further allow the organic materials to arrange themselves and form into a better quality of crystalline thin film [Kymissis et al, 2008 and Miyamoto et al., 1994]. As the concentration increased from 0.1 mg/ml to 0.5 mg/ml, Fig. 4.22b shows that the amount of small crystal ring formation present on top of the glass substrate is a lot more and well dispersed compare with the crystal ring formation as shown in Fig. 4a. Therefore, Cu-porphyrin thin film form through 0.5 mg/ml solution concentration does show better electrical properties as compare to Cu-porphyrin thin film form through 0.1 mg/ml solution concentration. With refer to Fig. 4.22c, the flakes growing bigger as compare to the flakes show in Fig. 4.22b. The number of flakes reduces as the concentration of the drop casted solution increase to 1.0 mg/ml. This condition is more obvious when the drop casted solution concentration increase to 5.0 mg/ml where the number of flakes present is lessen (Fig. 4.22c). Meanwhile, there are crystals which present in rod shape as concentration of the drop casting Cu-porphyrin solution increased. This happened due to many possible reasons such as strong electrostatic forces between the porphyrins molecules, hydrogen bonding, van der Waals, axial coordination, and other weak intermolecular interactions [Lee et al., 2011]. Fig.4.22a shows the current value of the organic device started to drop when the device are drop-casted at concentration higher than 0.5 mg/ml. This important finding proves that the performance of the device reduced due to poor thin film formation [Amato et al., 2009]. This indicates that the Cu-porphyrin have stronger interaction between molecules itself.

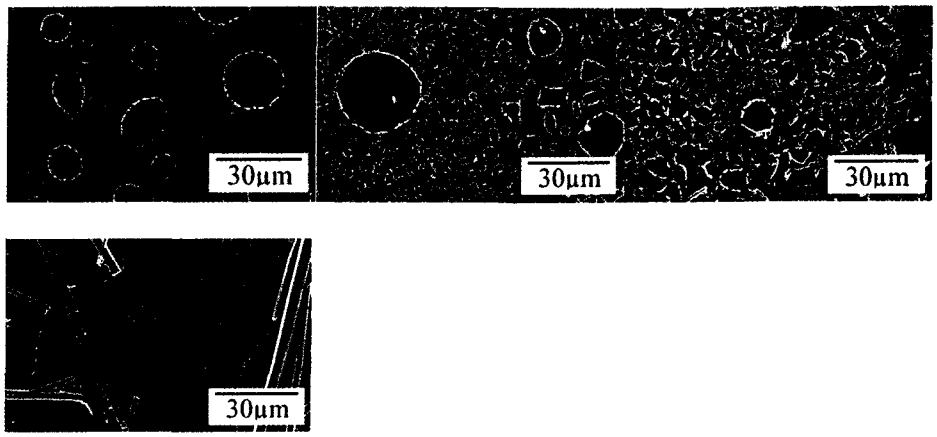

Fig. 4.22 SEM image shows Cu- porphyrin with the concentration of a) 0.1 mg/ml; b) 0.5 mg/ml; c) 1.0 mg/ml and d) 5.0 mg/ml was dropped casted on top of a glass substrate.

Porphyrin has strong conjugated π-system which may cause this macromolecule to aggregate [Gburek et al., 2010]. Fig. 4.23 indicates that the formation of these flakes become larger as the concentration of the drop casted solution increases. As the comparison between Fig. 4.23c and Fig. 4.23c, porphyrin tends to form a larger piece of crystal as compare with Cu-porphyrin. Therefore, it reveals that porphyrin conductivity keep on increasing as the concentration of the drop casted solution increase until reaching 5.0 mg/ml. However, Cu-porphyrin conductivity decreases as the drop casted solution increase to above 0.5 mg/ml. Cu-porphyrin devices have higher conductivity as a result of the present of copper atom at the centre of the porphyrin core structure. In order for these organic materials to have higher electrical conductivity, it must have better crystal packing and better alignment [Ma et al., 2010].

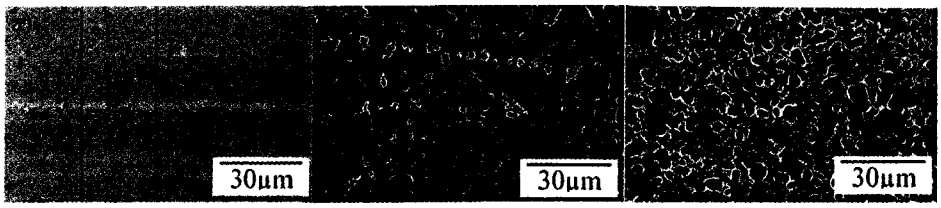

Fig.4.23 SEM image showing porphyrin with the concentration of a) 0.1 mg/ml; b) 0.5 mg/ml and c) 1.0 mg/ml was dropped casted on top of a glass substrate.

4.6 bis{2-alkyl-(S)-(+)-2-(6-[4-4-decyloxyphenylazo)-benzoyloxy]-2-naphthyl)propinate} (azo)

This study is about investigating the transporting characteristic of azo as semiconductor. 7 azo and 9 azo had been selected for electrical transporting characteristic due to their crystallization formation are much better compare to the rest of the azo had been synthesize. Azo possesses properties of n-type or p-type semiconductors. The samples are prepared in 3 different parameters, (a) 0.02 ml of 9 azo solution dropped cast on dielectric layer, (b) 0.04 ml of 9 azo solution dropped cast on dielectric layer, and 0.02 ml of 7 azo solution dropped cast on dielectric layer. The samples were measured and are showed in Fig. 4.24 to 35.

(a) 0.02 ml 9azo

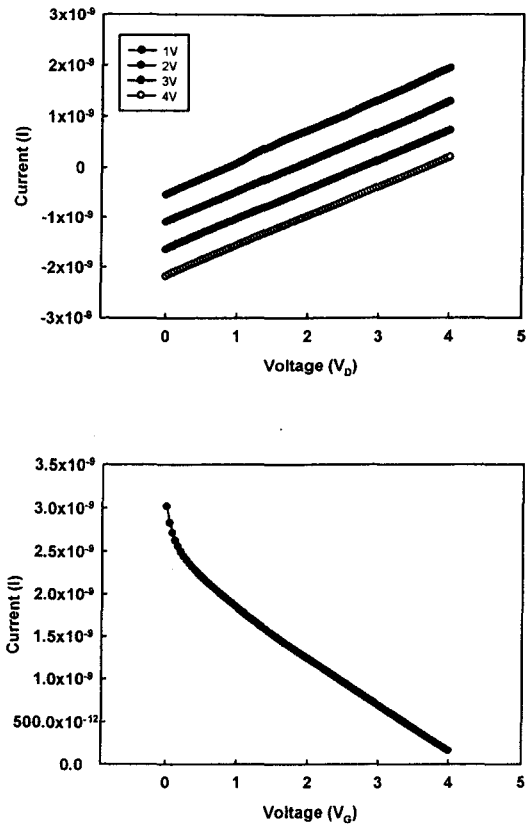

(a) (b)

Figure 4.24: N-type measurement (a) output characteristic of 0.02 ml 9azo-based OFET (V_G = 1 to 4 V) and (b) transfer characteristic of 0.02 ml 9azo-based OFET (V_D = 4 V).

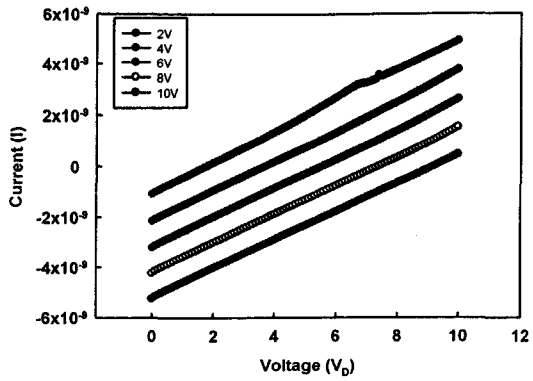

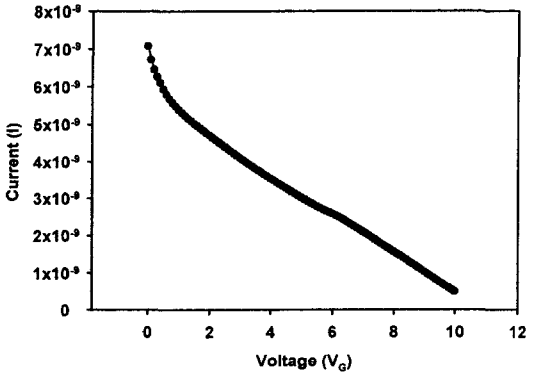

(a) (b)

Figure 4.25: N-type measurement (a) output characteristic of 0.02 ml 9azo-based OFET (V_G = 2 to 10 V) and (b) transfer characteristic of 0.02 ml 9azo-based OFET (V_D = 10 V).

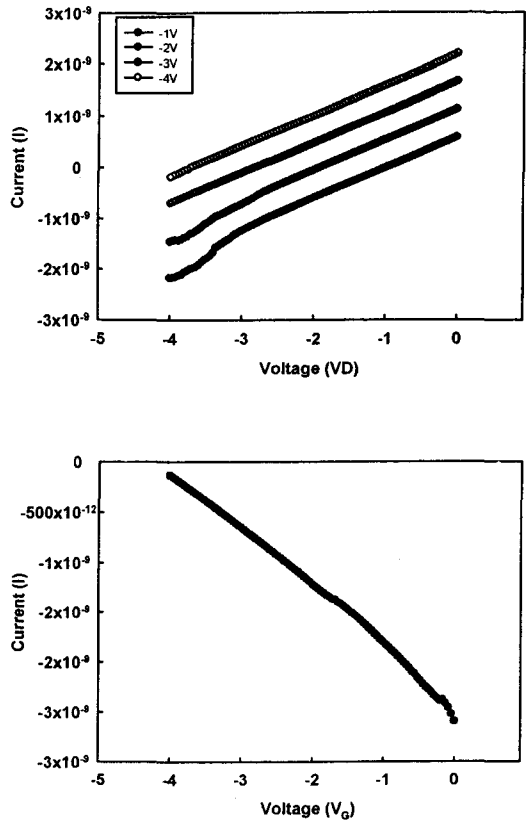

(a) (b)

Figure 4.26: P-type measurement (a) output characteristic of 0.02 ml 9azo-based OFET (V_G = -1 to -4 V) and (b) transfer characteristic of 0.02 ml 9 azo-based OFET (V_D = -4 V).

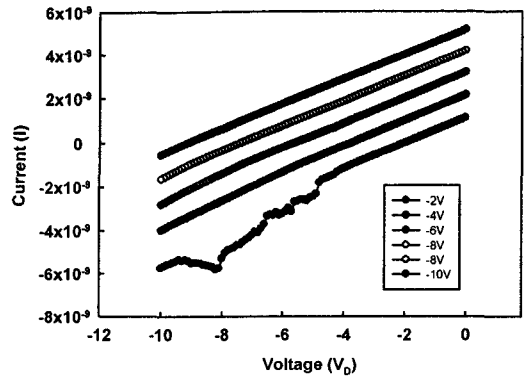

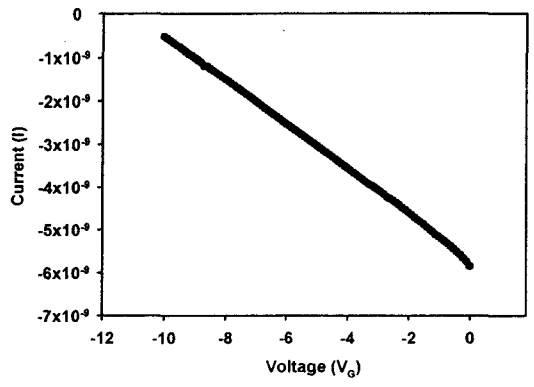

(a) (b)

Figure 4.27: P-type measurement (a) output characteristic of 0.02 ml 9 azo-based OFET (V_G = -2 to -10 V) and (b) transfer characteristic of 0.02 ml 9 azo-based OFET (V_D = -10 V).

(b) 0.04 ml 9azo

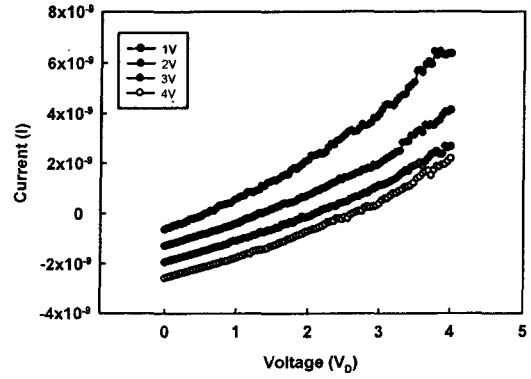

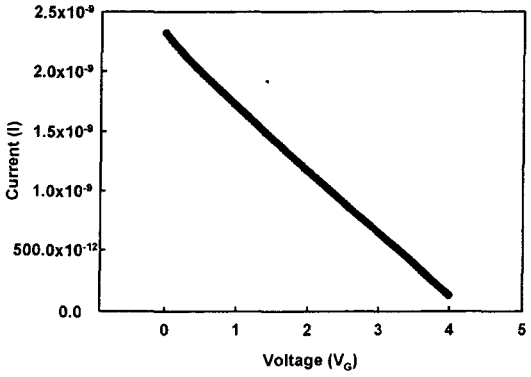

(a) (b)

Figure 4.28: N-type measurement (a) output characteristic of 0.04 ml azo-based OFET (V_G = 1 to 4 V) and (b) transfer characteristic of 0.04 ml 9azo-based OFET (V_D = 4 V).

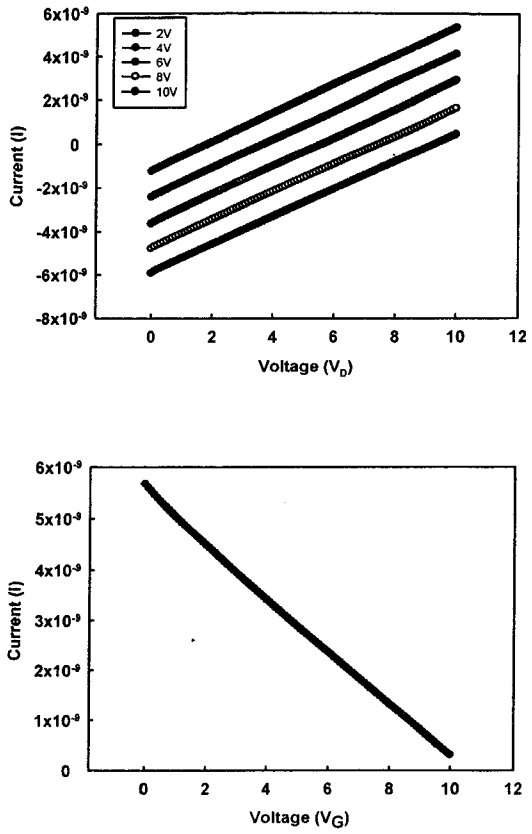

(a) (b)

Figure 4.29: N-type measurement (a) output characteristic of 0.04 ml 9azo-based OFET (V_G = 2 to 10 V) and (b) transfer characteristic of 0.04 ml 9azo-based OFET (V_D = 10 V).

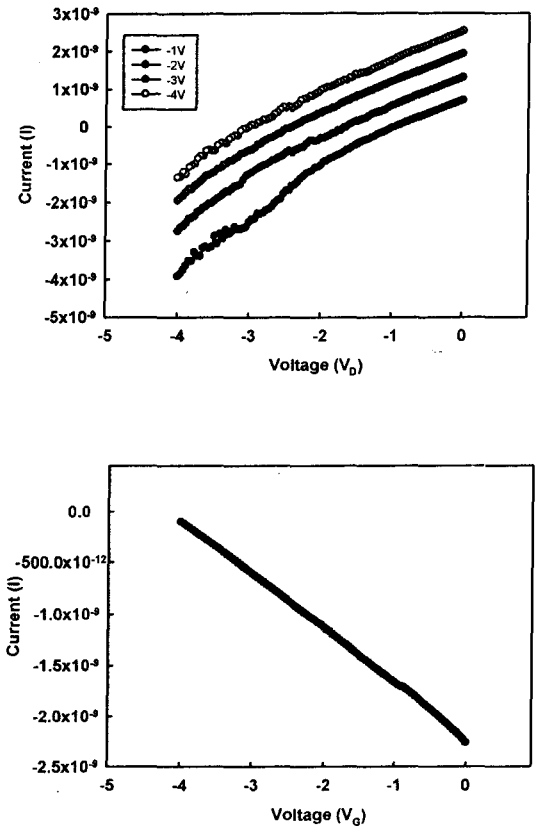

(a) (b)

Figure 4.30: P-type measurement (a) output characteristic of 0.04 ml 9azo-based OFET (V_G = -1 to -4 V) and (b) transfer characteristic of 0.04 ml 9azo-based OFET (V_D = -4 V).

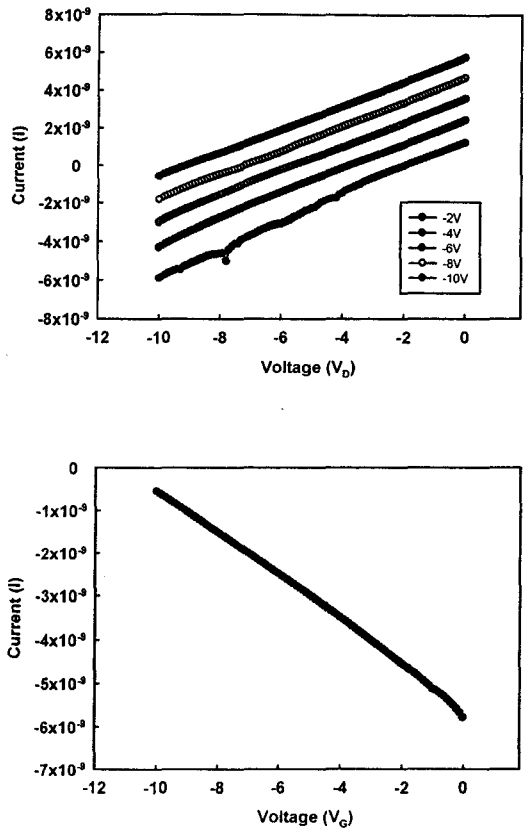

(a) (b)

Figure 4.31: P-type measurement (a) output characteristic of 0.04 ml 9azo-based OFET (V_G = -2 to -10 V) and (b) transfer characteristic of 0.04 ml 9azo-based OFET (V_D = -10 V).

(C) 0.02 ml 7azo

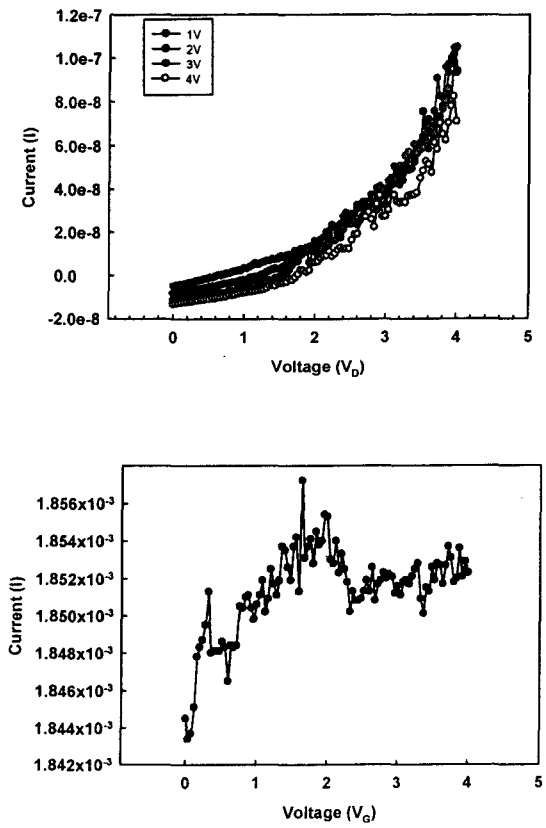

(a) (b)

Figure 4.32: N-type measurement (a) output characteristic of 0.02 ml 7azo-based OFET (V_G = 1 to 4 V) and (b) transfer characteristic of 0.02 ml 7azo-based OFET (V_D = 4 V).

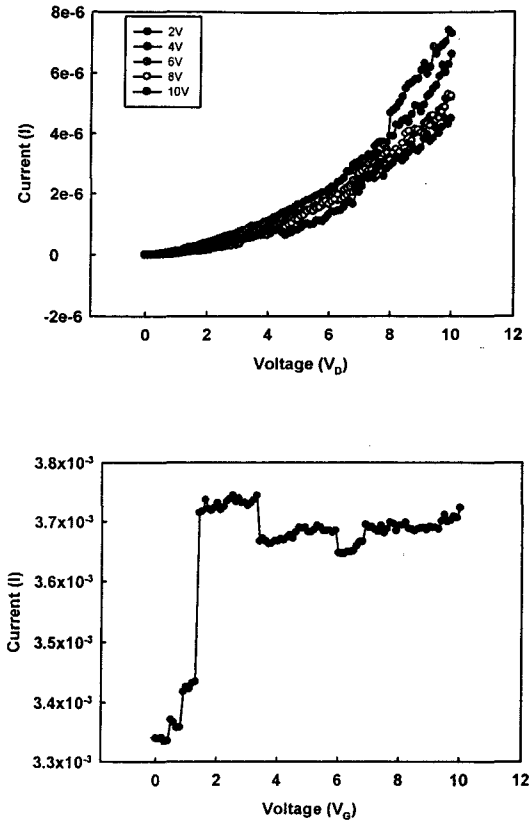

(a) (b)

Figure 4.33: N-type measurement (a) output characteristic of 0.02 ml 7azo-based OFET (V_G = 2 to 10 V) and (b) transfer characteristic of 0.02 ml 7azo-based OFET (V_D = 10 V).

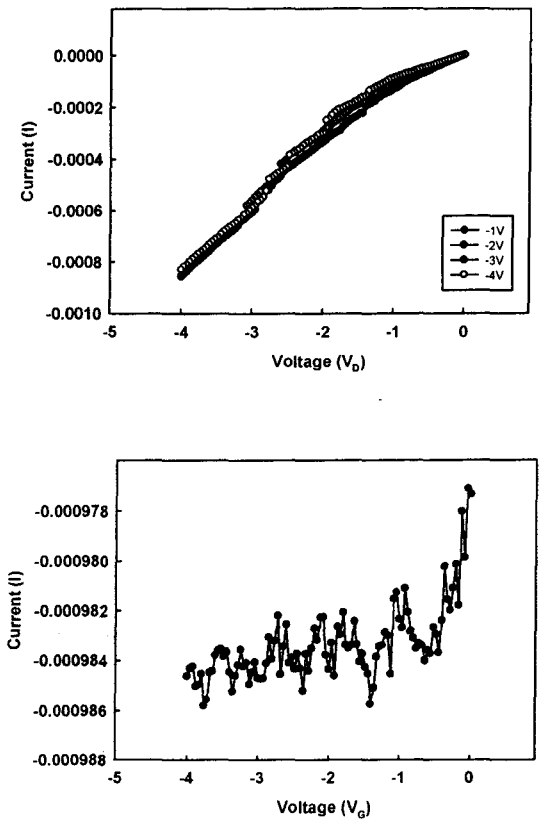

(a) (b)

Figure 4.34: P-type measurement (a) output characteristic of 0.02 ml 7azo-based OFET (V_G = -1 to -4 V) and (b) transfer characteristic of 0.02 ml 7azo-based OFET (V_D = -4 V).

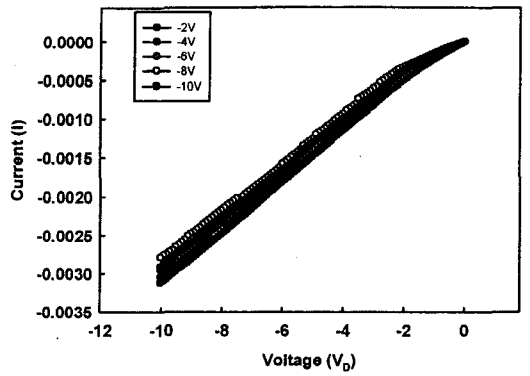

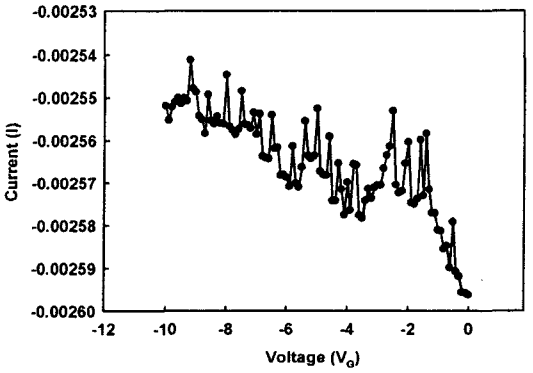

(a) (b)

Figure 4.35: P-type measurement (a) output characteristic of 0.02 ml 7 azo-based OFET (V_G = -2 to -10 V) and (b) transfer characteristic of 0.02 ml 7azo-based OFET (V_D = -10 V).

In this study, both p-type and n-type semiconductors characteristics are not available. The results did not show an output characteristic and transfer characteristics of an OFET device, but showing a dielectric characteristic. This explained that azo material is not a semiconductor material but a dielectric material. From the results obtained, 9 azo will be more suitable to act as dielectric materials than 7 azo because of the length of the spacer which plays an important role in determining the arrangement of these macromolecules.

4.7 Fullerene (C60)

Previous work demonstrated that natural Aloe vera paste is a suitable natural material for dielectric application. This work further fabricated an OFET as test structure to investigate the workability of the natural material as gate dielectric. However, the study shows C_{60} and natural Aloe vera layers are incompatible due to their large different of surface energy ($\Delta\gamma$ = -23.6%); with C_{60} and natural Aloe vera layers respectively having surface energy of 43.8 mJ/m^2 and 57.3 mJ/m^2. Here, $\Delta\gamma = \gamma s - \gamma d$; where γs is the surface energy of C_{60} and γd is the surface energy of dielectric layer. To further enhance the compatibility of the natural Aloe vera and C_{60} layers, 1.5 wt% of SiO_2 NPs was blended into the natural Aloe vera paste. The surface energy of the blended dielectric layer has been reduced from 57.3 mJ/m^2 to 38.9 mJ/m^2. With the combination of C_{60} layer deposited on the blended dielectric, the magnitude of $\Delta\gamma$ (= +11.2%) has been reduced more than 50% and the surface energy of blended dielectric layer is lower than that of C_{60}. The reduction of the surface energy is due to the interactions of natural Aloe vera molecules with SiO_2 NPs molecules. The addition of SiO_2 NPs tend to weaken the intermolecular bond among the Aloe vera molecules [Tang et al., 2009 and Gunko et al, 2007] by creating the strong hydrogen bond between the Aloe vera molecules and SiO_2 NPs molecules [Tang et al., 2009]. There are two advantages of this design. Firstly, it is predicted that the formation of C_{60} layer is following Volmer-Weber mode with initially island of C_{60} being formed and later a continuous layer would be achieved with relatively thick dimension [Venables et al, 2000]. The thicker the organic semiconductor (C_{60}) layer, the higher the probability of charges can be transported due to efficient conducting pathways [Yang et al., 2006]. Hence, increases the mobility of an OFET [Yang et al., 2006]. It has been reported that typical thickness of C_{60} in OFETs is in the range of 50 to 300 nm, with thicker the

thickness; higher the mobility [Zhang et al., 2007, Ullah et al., 2009, and Yang et al., 2005]. Therefore, the thickness (250 nm) of C_{60} being used in this work is acceptable and justifiable. Secondly, the molecular structures of C_{60} are being preserved without much distortion during the deposition as the cohesion force of those molecules within C_{60} is able to withhold the structures together. If the cohesion force is extremely large, it is impossible to establish bondings between C_{60} and the blended dielectric layer [Melzer and Seggern, 2010 and Qi et al., 2010]. In order to solve this adhesion issue, balance of force between cohesion and adhesion must be achieved. One of the indicators is from $\Delta\gamma$. It is preferable to have a positive value of $\Delta\gamma$ as what has been explained earlier. In order to achieve balance of force, the positive value of $\Delta\gamma$ must be as low as possible but not equal to zero or lower than that [Gao et al., 2009 and Wang et al., 2009]. This has been achieved by combining the blended (1.5 wt% of SiO_2 NPs) dielectric with C_{60} layers. As the loading of SiO_2 NPs in the dielectric is reducing from 1.5 wt% to 0 wt%, a significant increment of γd has been recorded. It shifted $\Delta\gamma$ to negative values. In contrast, as the loading increases beyond 1.5 wt%, value of γd is reducing monotonically. As a result, the $\Delta\gamma$ value increases positively. Besides, natural Aloe vera blended with 1.5 wt% of SiO_2 NPs layer have displayed better dielectric properties; i.e., lower leakage current density and higher dielectric constant than natural Aloe vera without SiO_2 NPs [Khor and Cheong, 2013]. Therefore, in this work, the optimum loading of 1.5 wt% of SiO_2 NPs has been used as the gate dielectric for the C_{60}-based OFET.

Previous research works on OFET device have reported that result of effective mobility, threshold voltage, on/off current ratio, and sub-threshold swing were affected when the device was exposure to atmospheric conditions [Li et al., 2011]. To

investigate the OFET performance in atmospheric conditions, in this work, the output and transfer characteristics were measured twice. One measurement was done immediately after the OFET was fabricated and the other measurement was done on the same test structure using similar measurement set up after it was exposure to atmospheric condition for 14 days. During the 14 days, the device was kept in a clean container to prevent contamination onto the device. The output characteristics of those two measurements are shown in Fig. 4.36. Based on the results, the device shows n-type output characteristics even though it was measured in open air without any encapsulation or passivation. The test structure measured at 14^{th} day shows a minor shift with decreasing of current in a range of 9.3% to 94.8% with the increment of gate voltage from 0 V to 40 V (Table 4.8) when compared to the measurement recorded on the as-fabricated test structure.

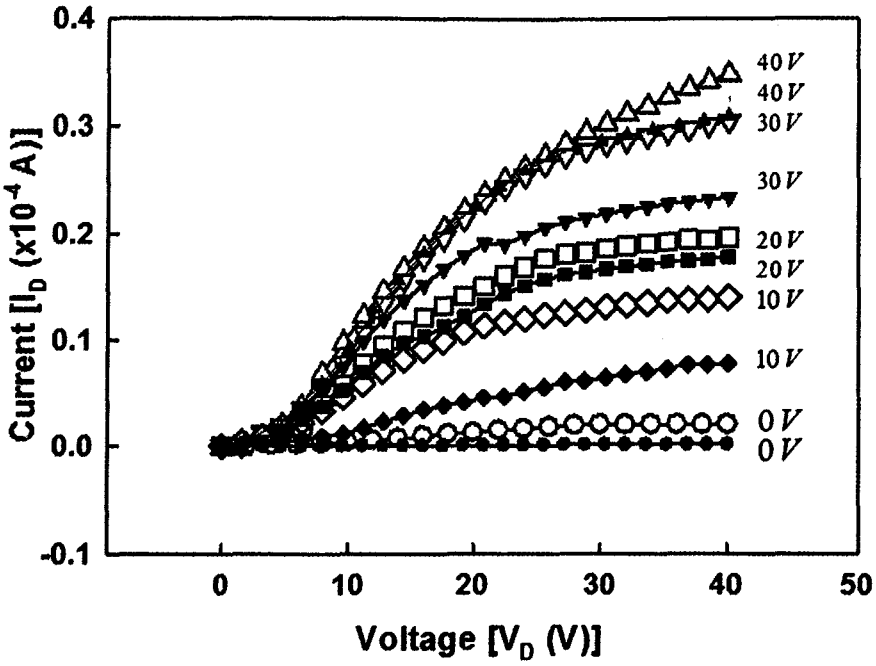

Fig. 4.36. Output Characteristic of C_{60}-based OFET (open symbols indicates measurement performed on as-fabricated test structure and closed symbol indicates measurement obtained after 14^{th} day).

Table 4.8. Comparison of output current measured from as-fabricated OFET (1^{st} day) and OFET exposure to open air for 14^{th} days.

Gate voltage	Output current (A)		Different	Percent %
	1^{st} day	14^{th} day		
40 V	3.47×10^{-5}	3.09×10^{-5}	3.80×10^{-6}	11.0
30 V	3.04×10^{-5}	2.34×10^{-6}	2.81×10^{-5}	92.4
20 V	1.96×10^{-5}	1.78×10^{-5}	1.80×10^{-6}	9.2
10 V	1.40×10^{-5}	7.80×10^{-6}	6.20×10^{-6}	44.3
0 V	2.00×10^{-6}	1.04×10^{-7}	1.90×10^{-6}	95.0

To further establish performance of the OFET, effective mobility (μ), threshold voltage (V_T), on/off current ratio (I_{on}/I_{off}), and sub-threshold swing (S) in the saturation regime of the transfer characteristics (Figs. 4.37 and 4.38) from the two measurements were extracted. Effective mobility of the OFET was calculated by fitting the data into Equation 1,

$$I_D = 1/2\ (W/L)\ \mu C\ (V_G - V_T)^2 \qquad (1)$$

where I_D is the drain current, V_G is the gate voltage, and C is the capacitance per unit area. Capacitance of the dielectric was measured from a capacitor with an Al/natural Aloe vera blended with 1.5 wt% of SiO_2 NPs/Al structure, and found to be ~ 6.86 pF/cm^2 at 1.2 kHz (Fig. 4.39). The extracted parameters of the OFET with two measurements performed at different time are summarized in Table 4.9.

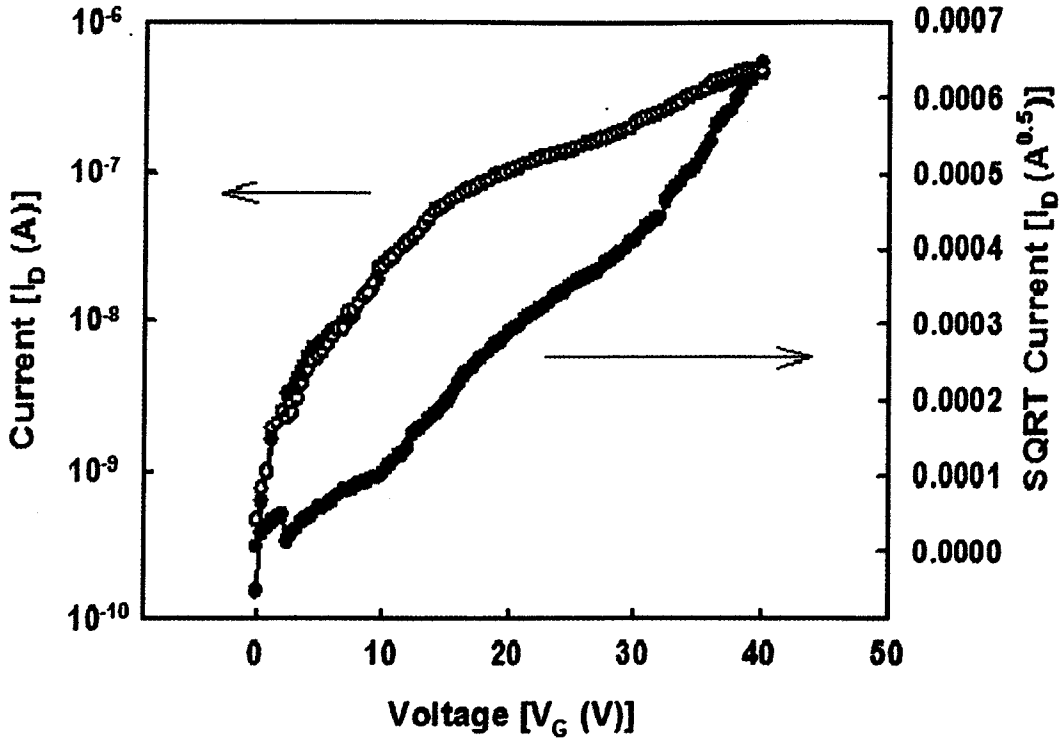

Fig. 4.37. Transfer characteristic of C_{60}-based OFET with V_{DS} = 40 V, measured on as-fabricated test structure.

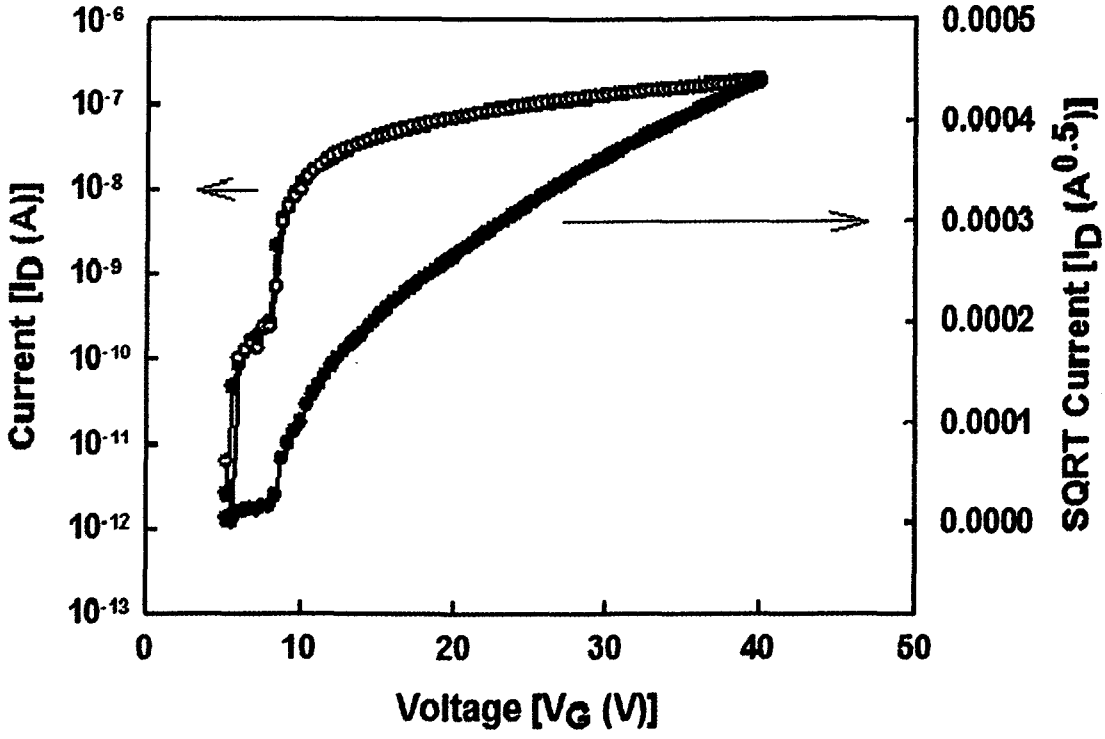

Fig. 4.38. Transfer characteristic of C_{60}-based OFET with V_{DS} = 40 V, measured at 14th day.

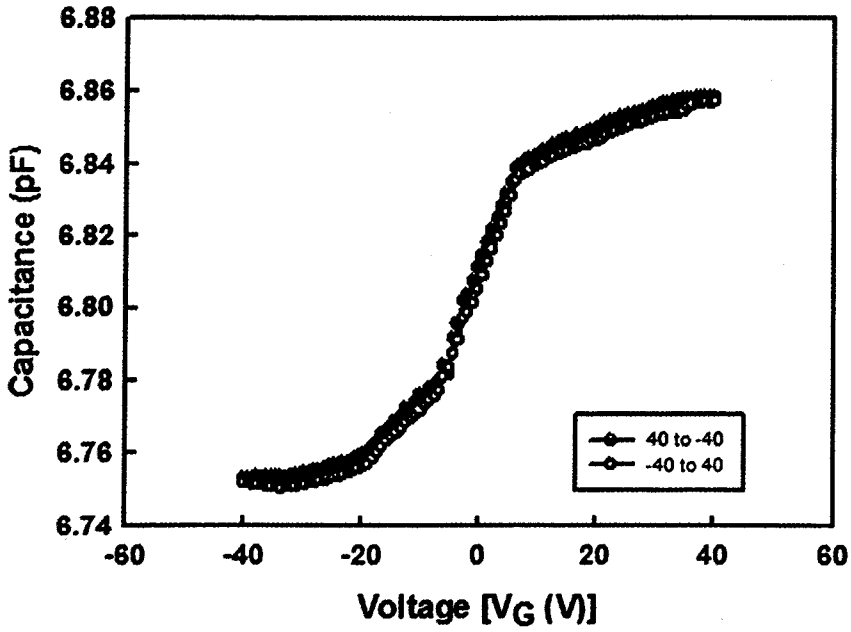

Fig. 4.39. Capacitance (*C*) measured at 1.2 kHz, sweeping gate voltage from 40 V to -40 V and then from -40 V to 40 V.

Table 4.9. Summary of the electrical parameters measured from as-fabricated OFET (1st day) and OFET exposure to open air for 14th days.

Properties	**1st day**	**14th day**
Effective mobility, μ (cm^2/Vs)	1.110	0.669
Threshold voltage, V_T (V)	0	7
Current on/off ratio, $I_{on/off}$	10^3	10^4
Sub-threshold swing, S (V/decade)	4.56	1.31

The effective mobility measured on as-fabricated test structure is 1.110 cm^2/Vs but after 14^{th} days the mobility has dropped approximately 40% to 0.669 cm^2/Vs. But these values are still much higher than that being reported previously using albumen as gate dielectric (0.13 cm^2/Vs) [Chang et al., 2011]. Albumen sample has lower mobility, this may due to the k value of albumen sample (k = ~5.3 - 6.1) [Chang et al., 2011] which is higher than natural Aloe vera samples (k = 3.9) [Khor and Cheong 2013]. High-k dielectric layer may enhance charge carrier localization in semiconductor layer; [Tan et al., 2009, Houili et al., 206, Deman and Tarby 2006, Sakai et al., 2009] in contrast low-k value in dielectric may reduce charge carrier localization in semiconductor layer, i.e., at the interface between layers of organic dielectric and semiconductor interface and may lead to high mobility [Tan et al., 2009, Kanbur et al., 2012, James et al., 2012, Stadlober et al., 2005]. Besides, the threshold voltage has been increased from 0 V to 7 V after 14^{th} days of exposure. The value measured from as-fabricated test structure is comparable to the value reported in Ref. [Chang et al., 2011] (1.5 V). The values of threshold voltage and effective mobility are degraded over time due to increment of electron being trapped in either C_{60} or interface of C_{60} and dielectric; as the test structure is being exposure to open air, moisture or oxygen molecules can be easily diffused [Gao et al., 2009]. The oxygen molecules from the moisture act as traps that decreased the mobility and as electron acceptors that increase the threshold voltage [Sakanoue et al., 2008]. Moreover, a large number of experiments have found that oxygen molecules which act as electron traps/electron acceptors thereby directly degraded the mobility of the samples [Ono et al., 2010, Chen et al., 2011, Chen et al., 2012]. With this trapping of electron, values of current on/off ratio and sub-threshold swing are actually improved over time. The former parameter increases an order of magnitude, which is preferable for organic memory application [Chen et al., 2012]. The

much reduction of sub-threshold swing value indicates the reduction of interface trap density between C_{60} and dielectric. With these, it has been demonstrated that natural Aloe vera blended with SiO_2 NPs has huge potential to be used as gate dielectric in OFET.

Chapter 5

CONCLUSIONS& RECOMMENDATIONS

5.0 Poly[2-methoxy-5-(2'-ethylhexyloxy)-1,4-phenylenevinylene] (MEH-PPV)

5.1 Conclusions

After completing this project, two objectives of this project have been achieved. Capacitor test structures have been successfully fabricated by coating of organic material (MEH-PPV) on glass substrates. The effect of different weight percentage of aluminum (Al) and silver (Ag) nanopartucles (0.025 wt%, 0.050 wt% and 0.10 wt%) on current-voltage characteristics of the organic devices has been successfully studied.

In this project, samples with different weight percentage of Al and Ag nanoparticles were spin-coated on glass substrates. Based on SEM results, it is found that dispersion of 0.025 wt%, 0.050 wt% and 0.10 wt% Al and Ag nanoparticles on glass substrates are acceptable and can be adapted to final device fabrication. Samples with different concentration of MEH-PPV (6 mg/ml, 8 mg/ml, 10 mg/ml and 12 mg/ml) were fabricated and sent to current-voltage (I-V) measurement. Based on the results, 12 mg/ml concentration of MEH-PPV has the best electrical properties. Hence, different weight percentage of Al and Ag nanoparticles (0.025 wt%, 0.050 wt% and 0.10 wt%) were incorporated into 12 mg/ml concentration of MEH-PPV to form composites layers.The effect of type of nanoparticles and their composition on the devices were studied in terms of film morphology and electrical properties.

Based on SEM results, dispersion of Al and Ag nanoparticles in MEH-PPV matrix can be observed and the cluster size of Al and Ag nanoparticles can be measured.

From EDX analysis, the presence of elements such as carbon, oxygen, sodium, magnesium, silicon, aluminum and silver are detected. From AFM results, it is found that samples added with different weight percentage of Al nanoparticles have higher RMS values. This is due to the agglomeration of Al nanoparticles inside MEH-PPV matrix. According to FTIR analysis, it is found that all the samples (with different concentration of MEH-PPV and different weight percentage of Al and Ag nanoparticles added) consist of =C-H stretching vibration, C-H stretching vibration in $-CH_2$ group and CH_3 stretching vibration in –O–CH3 group. Lastly, I-V measurement showed that by incorporation of Al and Ag nanoparticles, the electrical properties of the devices have been studied. Overall, incorporation of Ag nanoparticles gave better enhancement on current output compared to Al nanoparticles. This is because dispersion of Ag nanoparticles is more uniform compared to Al nanoparticles.

5.2 Recommendations

During the progress of this project, some problems were found. There are some suggestions to improve the research. The suggestions are listed as below.

i. In this project, inhomegeneity related to the dispersion of nanoparticles is the main problem. Agglomeration of nanoparticles will affect lower the performance of devices. Hence, the sonication time should be lengthened in order to disperse the nanoparticles more uniformly.

ii. Nanoparticles have very large surface area and hence, very high surface energy. Therefore, nanoparticles will tend to be agglomerated. In order to prevent the agglomeration, the surface of nanoparticles can be modified using organic layer to make them more hydrophobic for organic media. For example, silver

nanoparticles can be surface functionalized with polylactic acid in order to prevent agglomeration. These organic layers canimprove the stability of nanoparticles by forming a physical or electrostatic barrier against agglomeration.

iii. The time for electrode coating should be controlled properly. This is because the heat generated during thermal evaporation will destroy the structure of MEH-PPV layer. This will lead to inaccuracy I-V measurement. The timing should be optimized in order to get sufficient thickness of electrode without damaging the MEH-PPV layer.

5.3 Porphyrin and Cu-Porphyrin

The effects of Cu in porphyrin thin film, concentration of the organic materials on surface morphology and leakage current have been studied. Cu-porphyrin and porphyrin at concentration of 0.5 mg/ml showed the highest current value at 5 V with gap distance of 630 μm and 160 μm, respectively. Current value for both Cu-porphyrin and porphyrin were 2.53x10-8 A and 1.75x10-9 A, correspondingly. Cu-porphyrin is a better choice to be used as the organic thin film because it enhanced the electrical properties of the device as compare to metal free porphyrin. The reason is Cu-poprhyrin thin film drop casted with low solution concentration is able to form a better crystal thin film due to the strong metal-ligand interaction in between the organic molecule and the metalloporphyrin will normally have better charge transfer as compare with metal-free porphyrin crystal formation of the Cu-porphyrin thin film.

5.4 bis{2-alkyl-(S)-(+)-2-(6-[4-4-decyloxyphenylazo)-benzoyloxy]-2-naphthyl)propinate} (azo)

The azo materials synthesized are not suitable for the application for semiconductor in organic transistor application. The reason behind is with regard to the structure design of the organic materials. The spacer materials might not suitable to use as semiconductor materials. In further research, thiophene will be added to the synthesized organic materials. Macromolecular with π-conjugated backbone will be synthesized as core structure organic materials. Organic materials with thiophene exhibits well balanced ambipolar organic field-effect transistor performance; this will indirectly enhance the mobility of the organic materials as semiconductor materials for organic transistor. The macromolecures with π-conjugated backbone are normally acted as conducting polymers, owing to their unique electric and electronic properties. Electron from the core structure can be redrawing with the present of alkyl side group. This side group will able to form link in between two or more macromolecule. Therefore, the conductivities and Fermi levels of the macromolecule can be controllably changed by chemical and electrochemical doping methods

5.5 Fullerene (C60)

This work had utilized natural Aloe vera blended with 1.5 wt% of SiO_2 NPs as a dielectric layer in C_{60}-based n-type OFETs. The blended dielectric layer was screen-printed on a glass substrate followed by thermally deposition of C_{60} as a semiconductor layer with bottom-gate and top-contact structure. The OFET characteristics had been studied at atmospheric condition. The design of C_{60} and blended dielectric layers in the

OFET had been justified using surface energy concept. The produced OFET revealed an effective mobility of 1.110 cm^2/Vs with zero threshold voltage. After 14 days of exposure in an open air, the parameters reduced but on/off current ratio and sub-threshold swing had improved significantly.

5.6 Future works

There are a lot of factors affecting the performance of the device. In order to optimize the performance of device, more parameters should be controlled properly. Suggestions for future works are:

i. Investigation on the effect of solvent type to the performance of organic device.

ii. Investigation on the effect of nanoparticles size to the performance of organic device.

iii. Investigation on the effect of surface-modifying nanoparticles to the performance of organic device.

REFERENCES

Agostiano, A., Petrella, A., Cozzoli, P.D., Curi, M.L., Striccoli, M., Cosma, P., Farinola, G.M., Babudri, F., Naso, F.(2004).TiO_2nanocrystals- MEH-PPV composite thin films as photoactive material. *Thin Solid Films*, 451-452, pp. 64-68.

Aleshin, A.N., Shcherbakov, I.P., Petrov, V.N., Titkov, A.N.(2011). Solution-processed polyfluorene-ZnO nanoparticles ambipolar light-emitting field-effect transistor.*Organic Electronics*, 12, pp. 1285-1292.

Arnautov, S.A., Nechvolodova, E.M., Bakulin, A.A., Elizarov, S.G., Khodarev, A.N., Martyanov, D.S., Paraschuk, D.Y.(2004).Properties of MEH-PPV films prepared by slow solvent evaporation.*Synthetic Metals*, 147, pp. 287-291.

Aw, K.C., Lee, K.W., Wong, H.Y.(2011). Non-volatile memory with zinc oxide nanoparticles embedded in a hybrid polymethylsilsesquioxane layer. *Microelectronic Engineering*, 88, pp. 2837-2839.

Barford, W. (2005).Electronic and Optical Properties of Conjugated Polymers. New York: Oxford University Press Inc, pp. 1-16.

Berger, P.R., Yoon, W.J., Jung, K.Y., Liu, J.W., Duraisamy, T., Revur, R., Teixeira, F.L., Sengupta, S.(2010). Plasmon-enhanced optical absorption and photocurrent in organic bulk heterojunction photovoltaic devices using self-assembled layer of silver nanoparticles. *Solar Energy Materials & Solar Cells*, 94, pp. 128-132.

Bernius, M., Inbasekaran, M., Brien, J.O., Wu, W. (2000).Progress with Light-Emitting Polymers.*Adv. Mater*, 12, pp.1737-1750.

Bochwitz, J.(2001). Organic Light-Emitting Diodes with Doped Charge Transport Layer.*Institute for Applied Photophysics*, pp. 7-114.

Bredas, J. and Silbey, R. (1991).Conjugated Polymer: The Novel Science and Technology of Highly Conducting and Nonlinear Optically Active Materials. Dordrecht: Kluwer Academic Publishers, pp.229-231.

Bredol, M., Matras, K., Szatkowski, A., Sanetra, J., Anna, P.S.(2009). P3HT/ZnS: A new hybrid bulk heterojunction photovoltaic system with very high open circuit voltage. *Solar Energy Materials & Solar Cells*, 93, pp. 662-666.

Brutting, W., Berleb, S., Muckl, A.G. (2000). Device Physics of Organic Light Emitting Diodes Based on Molecular Materials. *Organic Electronics*, 2, pp. 1-36.

Campbell, I.H., Crone, B.K., Smith, D.L. (2007). Physics of Organic Light-Emitting Diodes.*Semiconducting Polymers: Chemistry, Physics and Engineering*, vol 2, pp. 421-520.

Cao, G. and Wang, Y. (2012) *NANOSTRUCTURES AND NANOMATERIALS: Synthesis, Properties, and Applications*. 2nd ed. USA: World Scientific Publishing Co., pp.19-57.

Carter, S.A., Scott, J.C., Brock, P.J.(1997). Enhanced luminance in polymer composite light emitting devices. *Appl.PhysLett.*, 71, pp. 1145-1147.

Carter, S.A., Arango, A.C., Brock, P.J.(1999). Charge transfer in photovoltaics consisting of interpenetrating networks of conjugated polymer and TiO_2 nanoparticles. *Applied Physics Letters*, 74, pp.1698-1700.

Cheng, G.,Tang, E., Ma, X., Pang, X., Zhao, Q. (2006).Surface modification of zinc oxide nanoparticle by PMAA and its dispersion in aqueous system.*Applied Surface Science*, 252,pp.5227-5232.

Chin, B.D., Park, M., Yu, J.W., Chun, M.S., Han, S.H.(2008). Enhanced photocurrent and efficiency of poly(3-hexylthiophene)/fullerence photovoltaic devices by the incorporation of gold nanoparticles. *Journal of Industrial and Engineering Chemistry*, 14, pp. 382-386.

Colegrove, J. (2010).OLED Display and OLED Lighting Technology and Market Forecast.*OLEDs World Submit 2010*, pp.1-28.

Cosma, P., Petrella, A., Tamborra, M., Curri, M.L., Striccoli, M., Comparelli, R.,Agostiano, A.(2008). Photocurrent generation in a CdSnanocrystals/poly[2-methoxy-5-(2'-ethyl-exyloxy)phenylenevinylene] electrochemical cell. *Thin Solid Films*, 516, pp. 5010-5015.

Cui, T. H., Liu, Y.(2008). Organic/Polymer Field-Effect Transistors and Their Applications.*Handbook of Organic Electronics and Photonics*, vol 1, pp. 263-303.

Cumings, J., Huang, J., Hines, D.R., Jung, B.J., Bronsgeest, M.S., Tunnell, A., Ballarotto, V., Katz, H.E., Fuhrer, M.S., Williams, E.D.(2011). Polymeric semiconductor/graphene hybrid field-effect transistors. *Organic Electronics*, 12, pp. 1471-1476

Cuong, T.T., Phillips, M.R., Nguyen, T.P.(2008). Blue Shift in the luminescence spectra of MEH-PPV films containing ZnOparticles.*Journal of Luminescence*, 128, pp. 2031-2034.

Das, N.C., Sokol, P.E.(2010).Hybrid photovoltaic devices from regioregularpolythiophene and ZnO nanoparticles composites.*Renewable Enegry*, 35, pp. 2683-2688.

Edn.com (2005).OLEDs Replacing LCDs in Mobile Phones - 2005-04-07 13:00:00 | EDN. [online] Available at: http://www.edn.com/article/468587-OLEDs_Replacing_LCDs_in_Mobile_Phones.php [Accessed: 13 May 2012].

Friend[a], R.,Burroughhes, J., Shimoda, T. (1999).Laser and Optics: Polymer diodes. *Physic World*, pp. 35-39.

Friend[b], R., Gymer, R.W., Burroughes, J.H., Marks, R.N., Taliani, C., Bradley, D.D.C., Dos Santos, D.A., Bredas, J.L., Logdlund, M., Salaneck, W.R.(1999). Electroluminescence in conjugated polymers.*NATURE*, 397 pp. 121-129.

Heflin, J. (2004).Organic Optoelectronic Nanostructures.*Introduction to Nanoscale Science and Technology*, pp. 487-507.

Hou, Y.B., Li, Y., Hui, J., Shi, Q.M., Wang, Y., Feng, Z.H.(2008). Photovoltaic properties of MEH-PPV/TiO_2. Chinese Science Bulletin, 53, pp. 2743-2747.

Huang, Z., Jiang, ., Yang, P., Chen, J., Xin, Y., Xu, J.(2008). High PL-efficiency ZnOnanocrystalline/PPV composite nanofibers.*Computar Science and Technology*, 68, pp. 3240-3244.

Huang, Z., Chen, J., Yang, P., Wang, C., Zhan, S., Zhang, L., Li, W., Wang, C., Jiang, Z., Shao, C.(2011).Ag nanoparticles/PPV composite nanofibers with high and sensitive opto-electronic response.*Nanoscale Research Letters 2011*, 6, pp. 121-125.

Inpor, K.,Meeyoo, V., Thanachayanont, C.(2011). Enhancement of photovoltaic performance using hybrid CdSnanorods and MEH-PPV active layer in ITO/TiO_2/MEH-PPV:CdS/Au devices. *Current Applied Physics*, 11, pp. S171-S174.

Kafafi, Z. (2005).*Organic Electroluminescene*. New York: CRC Press Taylor and Francis Group.

Kamarulzaman, N., Abdul Aziz, N.D., Subban, R.H.Y., Hamza, A.S., Ahmed, A.Z., Osman, Z., Rusdi, R., Kamarudin, N., Jumali, N.S., Shaameri, Z. (2011) Poly[2-Methoxy-5-(2'-Ethylhexyloxy)-(p- Phenylenevinylene)] (MEH-PPV) Synthesized via a Modified Gilch Method and the Electrical Conductivities of MEH-PPV/MCMB Films. *2011 3rd International Symposium & Exhibition in Sustainable Energy & Environment*, 1-3 pp. 63-68.

Khan, Rizwan U. A., Hunziker, C., Ulbricht, R., Tapponnier, A., Gunter, P.(2008).Organic Semiconducting Thin Films.Handbook of Organic Electronics and Photonics, vol 2, pp. 33-79.

Kim, Y.K., Lee, K.Y., Kwon, O.K., Shin, D.M., Sohn, B.C., Choi, J.H.(2000). Size dependence of electroluminescence of nanoparticle (rutile-TiO_2) dispersed MEH-PPV films. *Synthetic Metals*, 111-112, pp. 207-211.

Kim, D.Y., Nah, Y.C., Kim, S.S., Park, J.H., Park, H.J., Jo, J.(2007). Enhanced electrochromic absorption in Ag nanoparticle embedded conjugated polymer composite films. *Electrochemistry Communications*, 9, pp. 1542-1546

Kline, R.J., McGehee, M.D.(2008). Charge Transport and Morphology in Conjugated Polymers. *Handbook of Organic Electronics and Photonics*, vol 1, pp. 85-112.

Kochergin, V., Neely, L., Jao, C.Y., Robinson, H.D.(2011).Aluminum plasmonic nanostructures for improved absorption in organic photovoltaic devices.*Applied Physics Letters*, 98, 133305, pp. 1-5.

Kymakis, E., Spyropoulos, G.D., Stylianakis, M., Stratakis, E.(2011).Plasmonic organic photovoltaics doped with metal nanoparticles. *Photonics and Nanostructures-Fundamentals and Applications*, 9, pp. 184-189.

Ltaief, A., Bouazizi, A., Davenas. J. (2009). Charge Transport in Carbon Nanotubes-Polymer Composite Photovoltaic Cells. *Materials*, 2, pp. 710-718.

Lee[a], K.W., Mo, K.H., Jang, J.W., Kim, N.K., Lee, W., Kim, I.M., Lee, C.E.(2009). Charge transport in low-concentration MEH-PPV conjugated polymer/fullerence composites. *Current Applied Physics*, 9, pp. 1315-1317.

Lee[b], T., Cho, B., Kim, T.W., Choe, M., Wang, G., Song, S.(2009). Unipolar nonvolatile memory devices with composites of poly(9-vinylcarbazole) and titanium dioxide nanoparticles. *Organic Electronics*, 10, pp.473-477.

Lee, H.H., Kim, H.J., Jung, S.M., Kim, Y.H., Kim, B.J., Ha, S., Kim, Y.S., Yoon, T.S.(2011). Characterization of gold nanoparticle pentacene memory device with polymer dielectric layer.*Thin solid films*, 519, pp.6140-6143.

Li, Z. and Meng, H. (2007).Organic Light-Emitting Materials and Devices. New York: CRC Press Taylor and Francis Group.

Li, F.M., Nathan, A., Wu, Y., Ong, B.S. (2011). Organic Thin Film Transistor Integration: A Hybrid Approach, *vol 1*, pp. 1-12.

Lian, T., Anderson, N.A., Hao, E., Ai, X., Hastings, G.(2002).Subpicosecondphotoinduced electron transfer from a conjugated polymer to SnO_2 semiconductor nanocrystals.*Physica E*, 14, pp. 215-218.

Liu, J., Shi, Y., Yang, Y. (2001). Solvation-induced morphology effects on the performance of polymer-based photovoltaic devices. *Adv.Funct.Mater.*, 11, pp.1-6.

Macbrook, M.F., Pearson, C., Kolb, D., ZeZe, D.A., Petty, M.C.(2008). Memory effects in hybrid silicon-metallic nanoparticle-organic thin film structures. *Organic Electronics*, 9, pp.816-820.

Mariatti, M., Chan, K.L., Lockman, Z. (2010).Effect of ultrasonication medium on the properties of copper nanoparticle-filled epoxy composite for electrical conductive adhesive (ECA) application.*J Mater Sci: Mater Electron*, 21, pp. 772-778.

Mariatti, M., Chan, K.L., Lockman, Z., Sim, L.C. (2011).Effects of the Size and Filler Loading on the Properties of Copper- and Silver-Nanoparticle-Filled Epoxy Composites.*Journal of Applied Polymer Science*, 121 pp.3145-3152.

Murray, M.M., Holmes, A.B. (2000). Poly(acrylenevinylene)s Synthesis and Applications in Semiconductor Devices. *Semiconducting Polymers*, Chapter 1, pp. 1-32.

Navan, R.R., Panigrahy, B., Baghini, M.S., Bahadur, D., Rao, V.R.(2011). Mobility enhancement of solution-processed Poly(3-Hexylthiophene) based organic transistor using zinc oxide nanostructures. *Composite: Part B*, xxx, pp. xxx-xxx.

Nguyen, T.P., Jolinat, P. (2008). Physics and Technology of Organic Light Emitting Diodes.*Handbook of Organic Electronics and Photonics*, vol 3, pp. 245-311.

Nguyen, T.P., Musa, I., Massuyeau, F., Faulques, E.(2012).Investigations of optical properties of MEH-PPV/ZnOnanocomposites by photoluminescence spectroscopy.*Synthetic Metals*, xxx, pp. xxx-xxx.

Oled-info.com (2009).OLED lighting - OLED light bulb. [online] Available at: http://www.oled-info.com/oled-light [Accessed: 13 May 2012].

Oled-info.com (2010). Samsung announces Super AMOLED plus displays. [online] Available at: http://www.oled-info.com/samsung-announces-super-amoled-plus-displays [Accessed: 13 May 2012].

Oled-display.net (2012).OLED lighting. [online] Available at: http://www.oled-display.net/oled-lighting/ [Accessed: 13 May 2012].

Park, O.O., Lim, Y.T., Lee, T.W., Lee, H.C.(2002). Enhanced photo-stability of conjugated polymer nanocomposites doped with functionalized nanoparticles. *Optical Materials*, 21, pp.585-589.

Park, O.O., Park, J.H., Park, S.I., Kim, T.H.(2007). Enhanced electroluminescence in emissive polymer/CdSe double-layer films.*Thin Solid Films*, 515, pp.3085-3089.

Park, H.H., Lee, C.Y., Choi, Y.J., Yoon, S.(2010). Effect of Ag nanoparticles on the electron energy stucture and electrical properties of poly(p-phenylenevinylene) (PPV). *Synthetic Metals*, 160, pp. 621-624.

Park, H.H., Choi, Y.J., Golledge, S., Johnson, D.C.(2011). A study on the incorporation of ZnO nanoparticles into MEH-PPV based organic-inorganic hybrid solar cells. *Ceramics International*, xxx, pp., xxx-xxx.

Periyayya, U., Kang, J.H., Ryu, J.H., Hong, C.H.(2011). Synthesis and improved luminescence properties of OLED/ZnO hybrid materials. *Vacuum*, 86, pp. 254-260

Qian, J., Qiao, L., Wang, D., Zuo, L., Ye, Y., Chen, H., He, S.(2011). Localized surface resonance enhanced organic solar cell with gold nanospheres. *Applied Energy*, 88, pp. 848-852.

Reyes,R., M., Avila-Nino, J.A., Segura-Cardenas, E., Sustaita, A.O.,Cruz-Cruz, I., Lopez-Sandoval, R.(2011). Nonvolatile write-once-read-many-times memory device with functionalized-nanoshells/PEDOT:PSSnanocomposites. *Materials Science and Engineering B*, 176, pp. 462-466.

Riman, R., Vasiliev, A.N., Gulliver, E.A., Khinast, J.G., (2009).Highly dispersible polymer-coated silver Nanoparticles.*Surface & Coatings Technology*, 203, pp.2841-2844.

Samoc, M., Szeremeta, J., Nyk, M., Chyla, A., Strek, W.(2011).Enhancement of photoconduction in a conjugated polymer through doping with copper nanoparticles.*Optical Materials*, 33, pp. 1372-1376.

Scott, J.C., Malliaras, G.G. (2000). The Chemistry, Physics and Engineering of Organic Light-Emitting Diodes.*Semiconducting Polymers Chemistry, Physics and Engineering, 1*, pp. 411-457.

Shukla, M., Brahme, N.(2011). Improved efficiency of MEH-PPV:PCBM solar cells by the use of ZnSnano-particles. *Poly. Bull.*, 67, pp. 709.718.

Sirringhaus, H., Chang, J.F., Breiby, D.W., Nilsen, M.M., Solling, T.I., McCulloch, I. (2004). Enhanced mobility of poly(3-hexylthiophene) transistors by spin coating from high-boiling-point solvents. *Chem.Mater.*, 16, pp. 4772-4776.

Su, W.F., Zeng, T.W., Lo, H.H., Chang, C.H., Lin, Y.Y., Chen, C.W.(2009). Hybrid poly(3-hexylthiophene)/titanium dioxide nanorods material for solar cell applications. *Solar Energy Materials & Solar Cells*, 93, pp. 952-957.

Tibtech.com (2011).Conductive Materials or Metal Conductivity - *TIBTECH innovations* -. [online] Available at: http://www.tibtech.com/conductivity.php [Accessed: 29 March 2012].

Urbanek, P., Kuritka, I., Krcmar, P.(2011). The influence of ZnO content on optoelectronic properties of films from MEH-PPV/ZnO.*Composite. Mathematical Methods and Techniques in Engineering and Environmental Science*, 1, pp. 411-414.

Uthirakumar, P., Lee, Y.S., Suh, E.K., Hong, C.H.(2008). Hybrid fluorescent polymer-zinc oxide nanoparticles: Improved efficiency for luminescence conversion LED. *Journal of Luminescence*, 128, pp. 287-296.

Varlikli, C., Saygili, G., Ozsoy, C., Oner, I., Zafer, C., Icli, S.(2011). Enhanced electroluminescence from MEH-PPV-POSS:$CuInS_2$Nanocomposite based organic light emitting diode. *Synthetic Metals*, 161, pp. 196-202.

Wang, L., Li, B., Kang, B., Wang, P., Qiu, Y. (2005). Improvement of photovoltaic performance of solid-state dye-sensitized solar cells by iodine doping in conjugated polymer. *Journal of Photochemistry and Photobiology A: Chemistry*, 172 ,pp. 135-139.

Wang, X., Wang, M.(2008). PPV/TiO2 hybrid composites prepared from PPV precursor reaction in aqueous media and their application in solar cell. *Polymer*, 49, pp. 1587-1593.

Wang, M.T., Geng, H.W., Han, S.K., Peng, R.X.(2010). Enhanced performance of hybrid photovoltaic devices via surface-modifying metal oxides with conjugated polymer. *Solar Energy Materials & Solar Cells*, 94, pp. 547-553.

Wen, T.C., Hsieh, S.N., Guo, T.F.(2007). Polymer/gold nanoparticles light emitting diodes utilizing high work function metal cathodes. *Materials Chemistry and Physics*, 101, pp. 383-386.

Wiederrecht, G. (2010).*Handbook of Nanoscale Optics and Electronics*. Amsterdam: Elsevier B.V., p.107-108.

Wolff, K., Hilleringmannm U.(2012). Inverter circuits on glass substrates based on ZnO-nanoparticle thin-film transistors. *Solid-state Electronics*, 67, pp.11-16.

Xie, Z., Shao, S., Liu, F., Fang, G., Zhang, B., Wang, L.(2011). Enhanced performances of hybrid polymer solar cells with p-methoxybenzoic acid modified zinc oxide nanoparticles as electron acceptor. *Organic Electronics*, 12, pp. 641-647.

Yang, Y., Cheng, F.C., Xu, Q. (2004).Enhanced efficiency of plastic photovoltaic devices by blending with ionic solid electrolytes.*APPLIED PHYSICS LETTERS*, 84 p.pp. 3181-3183.

Yang, S.H., Nguyen, T.P., Rendu, P.L., Hsu, C.S. (2005).Optical and electrical properties of PPV/SiO_2 and PPV/TiO_2 composite materials.*Composite Part A: Applied Science and Manufacturing*, 36, pp. 509-513.

Yang, Y., Lin, J.J., Prakash, A., Ouyang, J.(2006).Polymer memory device based on conjugated polymer and gold nanoparticles.*Journal of Applied Physics*, 100, pp. 1-5.

Yang, S.H., Rendu, P.L., Nguyen, T.P., Hsu, C.S.(2007). Fabrication of MEH-PPV/SiO2 and MEH-PPV/TiO_2Nanocomposites with enhanced luminescent stabilities. *Rev.Adv.Mater.Sci.*, 15, pp. 144-149.

Yang, F.Y., Hse, M.Y., Hwang, G.W., Chang, K.J.(2010). High-perfomancepoly(3-hexylthiophene) top-gate transistors incorporating TiO_2nanocomposite dielectrics. *Organic Electronics*, 11, pp.81-88.

Yang, S.F., Zhang, W.F., Xu, Y., Wang, H.T., Xu, C.H.(2011). Fe3O4 nanoparticles induced magnetic field effect on efficiency enhancement of P3HT:PCBM bulk heterojunction polymer solar cells. *Solar Energy Materials & Solar Cells*, 95, pp. 2880-2885.

Yoon[a], K.H., Park, S.B., Yang, B.D.(2004). Size effect of nanoparticles on the conjugated polymer in PPV/SiO_2nanocomposites.*Materials Chemistry and Physics*, 87, pp. 39-43.

Yoon[b], K.H., Yang, B.D., Chung, K.W.(2004). Dispersion effect of nanoparticles on the conjugated polymer-inorganic nanocomposites.*Materials Chemistry and Physics*, 83, pp. 334-339.

Yoon[c], K.H., Yang, B.D.(2004). Effect of nanoparticles on the conjugated polymer in the PPV/TiO_2nanocomposites.*Synthetic Metals*, 142, pp. 21-24.

Zeng, T.W., Lin, Y.Y., Lo, H.H., Chen, C.W., Chen, C.H., Liou, S.C., Huang, H.Y., Su, W.F.(2006).A large interconnecting network within hybrid MEH-PPV/TiO_2nanorod photovoltaic devices. *Nanotechnology*, 17, pp. 5387-5392.

Zhang, J., Ju, X., Wang, B.J., Li, Q.S., Liu, T., Hu, T.D.(2001). Study on the optical properties of PPV/TiO_2nanocomposites. *Synthetic Metals*, 118, pp. 181-185.

APPENDICES

Appendix 1: Review studies on the effect of nanoparticles on the performance of organic devices.

Reference	Device					Nanoparticles															Effects							
	PLED	OFET	LE-OFET	Solar Cell	Memory	SiO_2	TiO_2	ZnO	SnO_2	Fe_3O_4	C	Fullerence	Graphene	ZnS	CdS	CdSe	Ag	Au	Al	Cu	Electrical	Luminance	Absorption	PL Intensity	FTIR	Raman	Stability	Mobility
Carter et. al., 1997	√					√	√														√	√						
Carter et. al., 1999				√			√														√							
Yang et. al., 2001				√								√									√							
Kim et. al., 2000	√						√														√	√						
Zhang et. al., 2001	√						√																√	√				
Lian et. al., 2002				√					√												√							√
Park et. al., 2002	√					√												√			√	√						
Agostiano et. al., 2004				√			√														√		√	√				
Yoon et. al., 2004	√					√															√				√	√		
Yoon et. al., 2004	√						√																√	√	√			
Yoon et. al., 2004	√						√														√			√	√			
Yang et. al., 2005	√					√	√														√			√	√	√		
Yang et. al., 2006					√													√			√							
Zeng et. al., 2006				√			√														√		√					
Kim et. al., 2007				√													√						√					
Park et. al., 2007	√															√					√	√		√				
Wen et. al., 2007	√																	√			√	√		√				
Yang et. al., 2007	√					√	√																√			√	√	
Chin et. al., 2008				√														√			√		√					
Cosma et. al., 2008				√											√						√		√	√				
Cuong et. al., 2008				√				√																√		√		

Appendix 1(continued): Review studies on the effect of nanoparticles on the performance of organic devices.

Reference	Device					Nanoparticles															Effects							
	PLED	OFET	LE-OFET	Solar Cell	Memory	SiO_2	TiO_2	ZnO	SnO_2	Fe_3O_4	C	Fullerence	Graphene	ZnS	CdS	CdSe	Ag	Au	Al	Cu	Electrical	Luminance	Absorption	PL Intensity	FTIR	Raman	Stability	Mobility
Huang et. al., 2008								√																√	√			
Hou et. al., 2008				√			√														√		√					
Mabrook et. al., 2008					√													√			√						√	
Uthirakumar et. al., 2008	√							√														√		√			√	
Wang et. al., 2008				√			√																√	√				
Bredol et. al., 2009				√										√							√							
Lee et. al., 2009				√								√																√
Lee et. al., 2009					√		√														√							
Su et. al., 2009				√			√														√		√					
Berger et. al., 2010				√													√				√		√					
Das et. al., 2010				√				√													√		√	√				
Park et. al., 2010	√																√				√		√					
Wang et. al., 2010				√			√														√				√			
Yang et. al., 2010		√					√														√						√	
Aleshin et. al., 2011			√					√													√	√	√					
AW et. al., 2011					√			√													√							√
Cumings et. al., 2011		√											√								√							√
Huang et. al., 2011																	√				√			√	√			
Inpor et. al., 2011				√			√														√		√					
Kochergin et. al., 2011				√													√	√	√				√					
Kymakis et. al., 2011				√													√	√			√							
Lee et. al., 2011					√													√			√							

Appendix 1(continued): Review studies on the effect of nanoparticles on the performance of organic devices.

Reference	Device					Nanoparticles															Effects							
	PLED	OFET	LE-OFET	Solar Cell	Memory	SiO_2	TiO_2	ZnO	SnO_2	Fe_3O_4	C	Fullerence	Graphene	ZnS	CdS	CdSe	Ag	Au	Al	Cu	Electrical	Luminance	Absorption	PL Intensity	FTIR	Raman	Stability	Mobility
Navan et. al., 2011		√						√													√							√
Park et. al., 2011				√				√													√		√					
Periyayya et. al., 2011	√							√															√	√				
Qian et. al., 2011				√														√			√		√					
Reyes et.al., 2011					√						√										√				√			
Shukla et. al., 2011				√										√							√		√	√				
Samoc et. al., 2011				√																√	√		√					
Urbanek et. al., 2011	√							√															√	√				
Xie et. al., 2011				√				√													√				√			
Yang et. al., 2011				√						√											√							
Nguyen et. al., 2012	√							√															√	√			√	
Wolff et. al., 2012		√						√													√							

Appendix 2: Review studies on the effect of nanoparticles on the performance of polymer light emitting diodes.

Reference	Nanoparticles						Device Active Layer							Solvent				Process		Effects						
	SiO_2	TiO2	ZnO	CdSe	Au	Ag	PPV	HV-PPV	MEH-PPV	MEH-PPV-POSS	P3HT	FTBT	PCBM	p-xylene	Chloroform	Benzene	Toluene	Spin Cast	Drop Cast	Electrical	Luminance	Absorption	PL Intensity	FTIR	Raman	Stability
Carter et. al., 1997	√	√							√					√				√		√	√					
Kim et. al., 2000		√									√				√			√		√	√					
Zhang et. al., 2001		√					√											√				√	√			
Park et. al., 2002	√				√		√											√		√	√					
Yoon et. al., 2004	√						√													√				√	√	
Yoon et. al., 2004		√					√															√	√	√		
Yoon et. al., 2004		√					√													√			√	√		
Yang et. al., 2005	√	√					√											√		√			√	√	√	
Park et. al., 2007				√					√							√		√		√	√		√			
Wen et. al., 2007					√			√									√	√		√	√		√			
Yang et. al., 2007	√	√							√					√				√				√			√	√
Uthirakumar et. al., 2008			√									√									√		√			√
Park et. al., 2010						√	√											√		√		√				
Periyayya et. al., 2011			√										√		√			√				√	√			
Urbanek et. al., 2011			√						√						√		√		√			√	√			
Nguyen et. al., 2012			√						√								√	√				√	√			√